NASA TECHNICAL NOTE

LOW-SPEED WIND-TUNNEL TESTS OF 1/9-SCALE MODEL OF A VARIABLE-SWEEP SUPERSONIC CRUISE AIRCRAFT

H. Clyde McLemore, Lysle P. Parlett, and William G. Sewall

Langley Research Center
Hampton, Va. 23665

NATIONAL AERONAUTICS AND SPACE ADMINISTRATION • WASHINGTON, D. C. • JUNE 1977

1. Report No.	2. Government Accession No.	
NASA TN D-8380		

4. Title and Subtitle

LOW-SPEED WIND-TUNNEL TESTS OF 1/9-SCALE MODEL OF A VARIABLE-SWEEP SUPERSONIC CRUISE AIRCRAFT

5. Report Date: June 1977

6. Performing Organization Code:

7. Author(s)

H. Clyde McLemore, Lysle P. Parlett, and William G. Sewall

8. Performing Organization Report No.: L-11149

10. Work Unit No.: 743-04-12-02

9. Performing Organization Name and Address

NASA Langley Research Center
Hampton, VA 23665

11. Contract or Grant No.:

13. Type of Report and Period Covered: Technical Note

12. Sponsoring Agency Name and Address

National Aeronautics and Space Administration
Washington, DC 20546

14. Sponsoring Agency Code:

15. Supplementary Notes

16. Abstract

Tests have been conducted in the Langley full-scale tunnel to determine the aerodynamic characteristics at low subsonic speeds of a 1/9-scale model of a variable-sweep supersonic cruise aircraft. The model configurations investigated were the basic unflapped arrangement, a take-off flap arrangement, and a landing flap arrangement with several strake leading-edge flow control devices. The tests were conducted at angles of attack from about -5° to 36°, sideslip angles from -5° to 10°, and Reynolds numbers from 3.92×10^{6} to 5.95×10^{6} corresponding to test velocities of about 54.5 to 81.7 knots.

17. Key Words (Suggested by Author(s))

Aerodynamics
Low-speed stability and control
Supersonic cruise aircraft
Variable sweep

18. Distribution Statement

Unclassified - Unlimited

Subject Category 01

19. Security Classif. (of this report)	20. Security Classif. (of this page)	21. No. of Pages	22. Price*
Unclassified	Unclassified	79	$5.00

* For sale by the National Technical Information Service, Springfield, Virginia 22161

LOW-SPEED WIND-TUNNEL TESTS OF 1/9-SCALE MODEL OF A VARIABLE-SWEEP SUPERSONIC CRUISE AIRCRAFT

H. Clyde McLemore, Lysle P. Parlett,
and William G. Sewall
Langley Research Center

SUMMARY

Low-speed tests have been conducted in the Langley full-scale tunnel to determine the force and moment characteristics of a 1/9-scale model of a variable-sweep supersonic cruise aircraft.

The model, with or without flaps deflected, had a pitch-up characteristic in the moderate to high angle-of-attack range. The pitch-up appeared to be caused mainly by the wing strake; deflecting the whole strake in incidence or modifying the leading edge of the strake by drooping it or by adding a slat provided a small improvement in longitudinal stability. The slatted-strake landing or take-off configuration with T-tail provided longitudinal stability to angles of attack of 12° to 15°. Above these angles of attack the T-tail resulted in a severe pitch-up. In general, the complete model had good lateral and directional stability characteristics to about 15° angle of attack, after which the stability deteriorated rapidly with increasing angle of attack and instability occurred near maximum lift.

INTRODUCTION

The present study is part of an overall effort by the National Aeronautics and Space Administration to provide the technology base for the development of supersonic cruise vehicles. The configuration concept which is the subject of this paper is a derivative of one studied in the National SST (supersonic transport) program (refs. 1 and 2), and traces its ancestry to the SCAT 16 configuration of the SCAT (supersonic commercial air transport) studies (ref. 3). As studied in the SST program, the concept exhibited one of the highest ratios of payload to gross weight of all those submitted for evaluation.

The dominant feature of the configuration is the nonintegrated variable-sweep wing. The variable-sweep feature was utilized to provide high levels of low-speed lift, good subsonic flight efficiency, and good supersonic cruise efficiency with a relatively small highly loaded wing which would involve less structural design uncertainty than would the lightly loaded large wings of competing concepts.

The nonintegrated variable-sweep concept was abandoned during its development primarily because of a conflict between longitudinal stability criteria that existed at that time and because of effects of the engine exhaust on the

horizontal tail. Placement of the horizontal tail in a high, or T-tail, position would have eliminated adverse thermal and acoustic effects of the jet on the tail and would have prevented a venturilike suckdown of the horizontal tail as the exhaust jet streamed between it and the ground during take-off rotation, both of which were problems for a low-tail configuration. However, a T-tail was generally known to produce a deep stall problem as the tail dropped into the wake of the stalled wing and became ineffective. Because "stick-pusher" or attitude-limiting systems, which are dependent upon attitude and pitch-rate sensing, were not considered permissible at that time in commercial aircraft, the contractor conducting the SST study ultimately took the alternate route of integrating the wing and horizontal tail and suspending the engine nacelles from the latter before abandoning the variable-sweep approach altogether. Since that time, developments in stability criteria and in aeroelectronic technology and an increased emphasis on CCV (control-configured vehicles) have opened the path to serious study of a T-tail solution to the problems of the variable-sweep SST.

The purposes of the subject tests were (1) to establish a comprehensive matrix of aerodynamic data from which the development of acceptable operating procedures in the critical low-speed regime could be explored, and thus take advantage of new criteria and develop propulsion and aeroelectronic technologies and (2) to explore means of alleviating those aerodynamic characteristics of the configuration that most adversely affect interdisciplinary trades. One of the problems associated with configurations similar to the test model is pitch-up at moderate angles of attack. This problem is studied in some detail and means of alleviating the pitch-up are discussed.

The present investigation consisted of low-speed wind-tunnel tests to determine the static longitudinal, lateral, and directional stability characteristics of a 1/9-scale model of a variable-sweep supersonic cruise aircraft. The tests were conducted in the Langley full-scale tunnel at Reynolds numbers from 3.92×10^6 to 5.95×10^6 (corresponding to test velocities from about 54.5 knots to 81.7 knots), angles of attack from about -5° to 36°, and angles of sideslip from -5° to 10°. The model variables were flap, slat, strake, strake leading-edge devices, sweep angle, low-tail and T-tail arrangements, and straight and drooped fuselage noses.

SYMBOLS

The data are referred to the stability system of axes. (See fig. 1.) The origin of the axes corresponds to the model center of gravity which is at 50 percent of the mean aerodynamic chord of the 72° swept-wing configuration. (See fig 2.)

b reference wing span ($\Lambda = 72^\circ$), 3.34 m

C_D drag coefficient, $\frac{\text{Drag}}{qS}$

C_L lift coefficient, $\frac{\text{Lift}}{qS}$

C_l rolling-moment coefficient, $\frac{\text{Rolling moment}}{qSb}$

C_{l_β} rate of change C_l with β for $\beta = 5^\circ$ to -5°

C_m pitching-moment coefficient, $\frac{\text{Pitching moment}}{qS\bar{c}}$

C_n yawing-moment coefficient, $\frac{\text{Yawing moment}}{qSb}$

C_{n_β} rate of change of C_n with β for $\beta = 5^\circ$ to -5°

C_Y side-force coefficient, $\frac{\text{Side force}}{qS}$

C_{Y_β} rate of change of C_Y with β for $\beta = 5^\circ$ to -5°

c wing chord, m

$\bar{c}$ reference mean aerodynamic chord ($\Lambda = 72^\circ$), 2.03 m

i_s strake incidence angle, deg (nose-down, negative)

i_t horizontal-tail incidence angle, deg (nose-up, positive)

L/D lift-drag ratio

q free-stream dynamic pressure, Pa

S wing reference area ($\Lambda = 72^\circ$), 5.77 m^2

V free-stream velocity, m/sec

X,Y,Z body reference axes (fig. 1)

α angle of attack, deg

β angle of sideslip, deg

$\delta_{f,te}$ flap deflection, deg

$\delta_{s,le}$ strake leading-edge deflection, deg

Λ wing leading-edge sweep angle, deg

Abbreviations:

H.R.L. horizontal reference line

L.E. leading edge

T.E. trailing edge

MODEL

Drawings of the 1/9-scale model are shown in figures 2, 3, 4, and 5, and additional dimensional characteristics are given in table I. Photographs of the 1/9-scale model mounted for tests in the Langley full-scale tunnel and of a 1/135-scale model (1/15-scale of larger model) mounted in a 1/15-scale model of the full-scale tunnel are presented as figures 6, 7, and 8. The 1/9-scale model was constructed of wood and fiber glass over an aluminum frame and was considered to be rigid for these low-speed tests. The models were constructed to simulate the shape of the elastic airplane with the 20° swept wing in 1g flight.

The model had a variable-sweep wing with outboard pivots, a single vertical tail, and an interchangeable horizontal tail (low tail and T-tail (high tail)). The horizontal tail was all-movable for incidence angles from -20° to 5°. The wing pivot was 5.378 m behind the undrooped fuselage nose at span station 0.70 m. The wing sweep could be varied from 20° to 72° for the unflapped wing and from 20° to 30° for the take-off flap arrangement and could be set only at 20° for the landing flap arrangement. The take-off flap arrangement (designated 14°/28° and shown in fig. 3) consisted of an intermediate large forward section (0.20c) deflected 14° and a smaller aft section (0.12c) deflected 28°. The landing arrangement (designated 30°/50° and shown in fig. 3) consisted of an intermediate large forward section (0.20c) deflected 30° and a smaller aft section (0.12c) deflected 50°. The wing outboard of the pivot had a leading-edge slat (0.135c) deflected 10° for the take-off flap arrangement ($\delta_{f,te}$ = 14°/28°) and 30° for the landing flap arrangement ($\delta_{f,te}$ = 30°/50°). The center of gravity of the model was assumed to be 0.50$\bar{c}$ or 5.210 m behind the undrooped fuselage nose. The model was unpowered but was equipped with flow-through nacelles having equal inlet and exit areas. Several devices were used on the wing strake for delaying the formation of leading-edge vortex, namely, a leading-edge slat, leading-edge droop, and deflection of the whole strake (nose downward). The geometric characteristics and angular deflections of these devices are shown in figures 4 and 5.

TESTS AND CORRECTIONS

The 1/9-scale model was tested in the Langley full-scale tunnel; a 1/135-scale model (1/15-scale of larger model) was tested in both the Langley

full-scale tunnel and a 1/15-scale model of the full-scale tunnel. Force tests were conducted at Reynolds numbers, based on a mean aerodynamic chord of 2.03 m, from 3.92×10^6 to 5.95×10^6 (corresponding to velocities of about 54.5 knots to 81.7 knots) with most of the tests conducted at the lower value. Angles of attack ranged from about -5° to 36° and sidelsip angles ranged from -5° to 10°. The model configuration variables are given in table II.

Wool tufts were attached to the upper surface of the wing, fuselage, horizontal tail, and vertical tail to aid in the interpretation of force test results.

The test data have been corrected for tunnel airflow angularity, buoyancy, and strut tares. Wall corrections were found by theory and by experiment on the 1/135-scale model to be negligible and were not incorporated into the data. (Theory of ref. 4 showed an angularity of 0.35° and a dynamic pressure correction of 0.75 percent at a lift coefficient of 1.0.)

PRESENTATION OF DATA

In a few instances it was desirable to compare longitudinal data for the slatted-strake take-off flap arrangement at $\beta = 0^\circ$ with data for other configurations, but these particular data at $\beta = 0^\circ$ were not obtained. Upon examination of the data at $\beta = -5^\circ$ to 5°, however, it was determined that $\beta = 5^\circ$ had very little effect on the longitudinal data; therefore, data for the take-off flap arrangement with slatted strake at $\beta = -5^\circ$ were used in place of data at $\beta = 0^\circ$ in figures 18, 19, and 21.

RESULTS AND DISCUSSION

Longitudinal Aerodynamic Characteristics

The configurations with a low tail were tested only as a basis for comparison and not as an acceptable alternate tail position. This is because of the aforementioned excessive tail temperatures due to the engine exhaust and because of the suckdown of the horizontal tail when in proximity to the ground. Therefore, the analysis of the data in this report is mainly for the configurations with the T-tail. The data are generally analyzed with regard to the achievement of high lift and adequate stability and control for angles of attack up to the angle at which the outboard wing panels stall. This angle of attack seems to be the maximum usable angle of attack because stall of the outboard panels normally indicates loss of damping in roll, loss of lateral control, and excessive buffeting.

Tuft studies.- As an aid to interpreting the fo ce and moment characteristics, flow studies were made by observing and photographing wool tufts that were attached to the surfaces of the wings, fuselage, and tail for a few selected configurations with 20° wing sweep. The clarity of the photographs was quite poor; therefore, the flow patterns were diagramed and are presented in figures 9 to 12 to illustrate the general airflow characteristics of the model.

In general, the strake tufts show smooth unstalled flow throughout the angle-of-attack range, but the presence of a leading-edge vortex is evident. Modifications to the strake (i.e., slats, drooped leading edge, or strake incidence) reduced the intensity of the leading-edge vortex. The outboard wing panels are seen to be stalled at high angles of attack for all configurations, but the flaps remain unstalled. This stall of the outboard wing panels is important in the analysis of the force test data because although the outboard wing panels begin to stall at angles of attack between 18° and 22° and are usually completely stalled at an angle of attack of 26°, the force data (figs. 13 to 26) show that the lift coefficients continue to rise to higher angles of attack. These greater values of lift coefficient are evidently the result of increased vortex lift on the wing strake and would probably not be considered usable lift for an operational aircraft because, as pointed out previously, the prior outboard wing stall would probably have already resulted in loss of damping in roll, inadequate lateral control, and excessive buffeting.

The wing slat did not function as well as expected, and it is believed that modifications to the slat deflection angle and slot geometry would have improved the airflow over the outboard wing for angles of attack greater than 22°. The tuft test data also showed that sideslipping the model in general caused the flow to deteriorate earlier over the advancing wing.

Reynolds number.- At the outset of the program, tests were conducted on the flapped configuration for a range of wind-tunnel speeds to determine whether there were appreciable effects of Reynolds number and to determine whether tests at speeds lower than maximum tunnel speed would be acceptable. These effects of Reynolds number are shown in figure 13 where variations in Reynolds number in the range from 3.92×10^6 to 5.95×10^6 were shown to have

little effect on the aerodynamic characteristics, particularly to angles of attack of about 20°. Above this angle, maximum C_L was increased a small amount with increasing Reynolds number. The difference was considered to be negligible, however, for the purposes of the present investigation; and since the test program could be expedited by using the lower velocity, the remaining tests were conducted at a Reynolds number of 3.92×10^6 (test velocity of about 54.5 knots).

Wing sweep.- The effects of wing leading-edge sweep on the aerodynamic characteristics of the clean wing configuration with and without the T-tail and the low-tail arrangements are shown in figures 14 and 15. Increasing wing-sweep angle decreased lift and lift-curve slope in the angle-of-attack range to about 15°. The pitch-up that began at about 7° angle of attack for the 20° sweep condition for either horizontal-tail arrangement was also alleviated slightly by increasing wing-sweep angle.

High-lift devices.- One point that should be noted at the beginning of this discussion of the high-lift devices is that the lift coefficients of the present investigation for a particular angle of attack appear to be unusually low. The reason for this characteristic is the manner in which C_L is defined. The fully swept planform area was selected as the reference area since this was the area used by previous investigators (governmental and industrial) concerned with the variable-sweep concept. The lift coefficients of the present investigation would be increased by about 50 percent if the reference area had been that of the 20° swept-wing configuration (the area being based on that described by extending the leading and trailing edge of the variable-sweep panels to the aircraft center line).

The effects of wing high-lift devices (flaps and slats) on the aerodynamic characteristics for the basic strake and the slatted strake are shown in figures 16 and 17 for the two tail arrangements. The lift coefficient at all angles of attack increased considerably by the addition of flaps and slats, and the longitudinal stability characteristics for the T-tail arrangement were about the same as for the undeflected flap condition, except that the onset of pitch-up was delayed from an angle of attack of about 7° for the clean configuration to about 10° for the flap-down configurations with the T-tail. The model, with or without flaps deflected, had a pitch-up characteristic in the moderate to high angle-of-attack range. The pitch characteristics for the slatted-strake configuration are shown in figure 18. The slatted strake was considered to be part of the basic high-lift system since it had been identified in reference 5 as a recommended feature. The data of figure 18 show that for both configurations ($\delta_{f,te}$ = 14°/28° and 30°/50°), use of the slatted strake provided an improvement in longitudinal stability. The pitch-up for the flap-down T-tail configurations was delayed to an angle of attack of 12° to 15° (as compared with about 10° for the basic-strake configuration) and was somewhat less severe than that of the basic-strake configuration at higher angles of attack. Hence, the slatted strake was considerably better than the basic strake in providing high usable lift values for the take-off and for the landing flap arrangements. Even with the slatted strake, however, the longitudinal instability was quite severe at the angle of attack at which the outboard wing panels stalled approximately 22°; therefore, it would probably not be posssible

to use all the high lift coefficient that would be available from the standpoint of wing stall.

Strake modifications.- The tuft studies of figures 9 to 12, as well as past experience with strakes similar to those of the present model (ref. 5), have indicated that the pitch-up is associated with the loading of the strake. Hence, the effect of removing the slatted strake for the landing and take-off flap arrangements was investigated and the results are shown in figure 19. The effects of removing the strake were an increase in longitudinal stability, a marked delay in the onset of and reduction in severity of the pitch-up, and a loss of lift. Since the slatted strake had resulted in improved longitudinal stability and increased maximum usable lift coefficient when compared with the basic strake, alternate strake modifications were investigated to determine whether other ways of controlling strake flow would be perhaps more effective or more simple than the use of the slat.

The effect of drooping the leading edge of the strake is shown in figures 20 and 21. Figure 20 shows that increasing the droop angle beyond 30° did not have any significant effect on longitudinal stability, lift, or drag. Figure 21 shows a comparison of the aerodynamic characteristics for the 30° droop condition, the basic strake, and the slatted strake. These data show that the drooped leading edge was as effective as the strake slat in delaying the onset of as well as reducing the severity of the pitch-up.

It was reasoned further that if the strake was causing a large positive pitching moment at high angles of attack, then deflecting the whole strake (nose downward) should relieve the pitch-up caused by the strake lift and should improve the longitudinal stability by improving the flow over the wing behind the strake. The effect of deflecting the whole strake to $i_s = -15^\circ$ for the landing flap arrangement is shown in figure 22. These data show that increasing the incidence of the strake delayed the onset of the pitch-up. The lift was virtually unaffected for angles of attack below 25°, and the drag reduced significantly at the higher angles of attack. The data suggest the possibility of programing the strake incidence to vary on a one-to-one basis with angle of attack in order to delay the onset of pitch-up to at least $\alpha = 15^\circ$, and probably further with higher ratios of strake incidence angle to angle of attack.

The overall effect of the various strake arrangements for the take-off flap arrangement is shown in figure 23. The whole strake was deflected only 5° for this flap arrangement, and from the higher strake incidence data of figure 22, it appears that larger strake incidence angles would have increased the longitudinal stability of the take-off flap arrangement and would probably have delayed the pitch-up. Of the strake arrangements investigated, however, the slatted strake appears to be the best arrangement for the take-off flap configuration.

None of the strake modifications had a significant effect on the maximum lift coefficient or on the maximum usable C_L, and none of the modifications allowed the use of the maximum lift that would be available if it were not for the pitch-up. The significance of these data is that the pitch-up appeared to

be caused mainly by the wing strake, and deflecting the whole strake in incidence or modifying the leading edge of the strake by drooping it or by adding a slat provided a small improvement in the longitudinal stability. Because of the strong influence of the strake arrangement on the longitudional stability, this wing apex area should be the area for concentrated study to determine means of improving the longitudinal stability characteristics of the variable sweep supersonic cruise aircraft in its landing and take-off modes.

Effect of horizontal tail incidence.- The effect on the aerodynamic characteristics of horizontal tail incidence is shown in figures 24 to 26. The horizontal tail is quite effective in providing longitudinal trim throughout the angle-of-attack range for either the T-tail or the low-tail arrangement.

Lateral-Directional Aerodynamic Characteristics

The lateral-directional aerodynamic characteristics of the model with and without the tail installed are shown in figures 27 to 33 for several values of wing leading-edge sweep and for several wing configurations. The comparable stability derivatives are shown in figures 34 to 36. The derivatives were obtained by determining the incremental change in the lateral-directional characteristics caused by a 10° change in sideslip angle ($+5^{\circ}$ to -5°).

In general, the complete model had good lateral-directional characteristics to about 15° angle of attack, after which the stability deteriorated very rapidly and instability occurred at about 20° angle of attack (near maximum C_L).

CONCLUSIONS

The results of force tests in the Langley full-scale tunnel on a 1/9-scale model of a variable-sweep supersonic cruise aircraft show the following conclusions:

1. The model, with or without flaps deflected, had a pitch-up characteristic in the moderate to high angle-of-attack range. The pitch-up appeared to be caused mainly by the wing strake, and deflecting the whole strake in incidence or modifying the strake leading edge by drooping it or by adding a slat provided a small improvement in longitudinal stability.

2. The slatted-strake landing or take-off flap arrangement with T-tail provided longitudinal stability to angles of attack of 12° to 15°. Above these angles of attack, however, the T-tail resulted in a severe pitch-up.

3. Both the T-tail and low-tail arrangements provided good longitudinal control effectiveness throughout the angle-of-attack range.

4. In general, the complete model had good lateral-directional stability characteristics to about 15° angle of attack, after which the stability decreased very rapidly with increasing angle of attack and instability occurred near maximum lift.

Langley Research Center
National Aeronautics and Space Administration
Hampton, VA 23665
April 7, 1977

REFERENCES

1. Commercial Supersonic Transport Program. Phase II-A Comprehensive Report. D6-8680 (Contract No. FA-SS-64-4), Boeing Co., Nov. 1, 1964.

2. Commercial Supersonic Transport Program. Phase II-C Interim Aircraft Performance Assessment Report. D6-19910 (Contract FA-SS-66-5), Boeing Co., Nov. 15, 1965.

3. Proceedings of NASA Conference on Supersonic-Transport Feasibility Studies and Supporting Research - September 17-19, 1963. NASA TM X-905, 1963.

4. Heyson, Harry H.: Use of Superposition in Digital Computers To Obtain Wind-Tunnel Interference Factors for Arbitrary Configurations, With Particular Reference to V/STOL Models. NASA TR R-302, 1969.

5. Freeman, Delma C., Jr.: Low Subsonic Flight and Force Investigation of a Supersonic Transport Model With a Variable-Sweep Wing. NASA TN D-4726, 1968.

TABLE I.- MODEL DIMENSIONS

Wing (all wing dimensions refer to the 72° swept-wing configuration):		
Area, m^2		5.77
Span, m		3.34
Aspect ratio		1.93
Mean aerodynamic chord, m		2.03
Root chord, m		4.13
Sweep of wing leading edge, deg		20 to 72
Geometric twist (referenced to H.R.L.) at -		
Root, deg		-1.33
Tip (80-percent semispan, parallel to fuselage center line), deg		-5.52
Moment reference:		
Longitudinal distance from undrooped nose, m		5.21
Vertical distance above H.R.L., m		0.063
	T-tail	Low tail
Horizontal tail:		
Area, m^2	0.651	1.036
Span, m	1.42	1.65
Mean aerodynamic chord, m	0.50	0.64
Incidence, deg	-20 to 5	-20 to 5
Dihedral, deg	10	-10
Vertical tail:		
Area, m^2	0.823	0.509
Span, m	0.76	0.72
Sweep angle for -		
Leading edge, deg	37	34
Trailing edge, deg	30	20
Root chord, m	1.90	1.67
Tip chord, m	0.64	0.27
	Inboard	Outboard
Engines[a] (flow-through nacelles only):		
Spanwise location of engines (to front of inlets), m	2.54	5.46
Location relative to H.R.L., deg	-5.75	-4.25

[a]Engines are skewed 1.5° from X-axis with exhaust nozzles pointing outward.

TABLE II.- MODEL CONFIGURATION VARIABLES

Λ, deg	Strake	Wing slat deflection, deg	Wing flap deflection, deg	Tail
Clean wing configuration				
20, 30, 42, and 72	Off and on	Retracted	0	Off, T, and low
Take-off flap arrangement				
20 and 30	Off and on; incidence, 0°, -5°, -10°, and -15°; L.E. devices, slat and drooped L.E. of 0°, 30°, 60°, and 90°	10	14/28	Off, T, and low; incidence, 5°, 0°, -5°, -10°, and -20°
Landing flap arrangement				
20	Off and on; incidence, 0°, -5°, -10°, and -15°; L.E. devices, slat and drooped L.E. of 0°, 30°, 60°, and 90°	30	30/50	Off, T, and low; incidence, 5°, 0°, -5°, -10°, and -20°

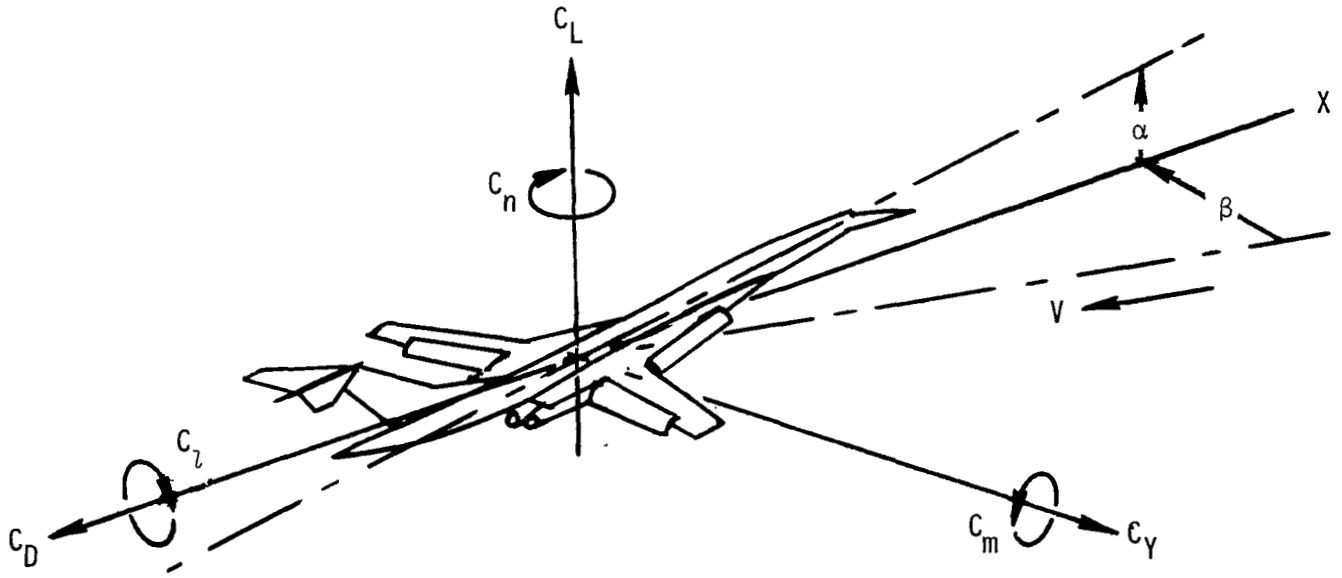

Figure 1.- Stability system of axes and positive sense of angles, forces, and moments.

Wing reference dimensions:

Area	5.77 m^2
Aspect ratio	1.93
Mean aerodynamic chord	2.03 m
Spanwise location of $\bar{c}$	0.383 b/2 (0.64 m)
Span	3.34 m
Incidence at -	
Root	-1°20'
0.80 b/2	-5°31'

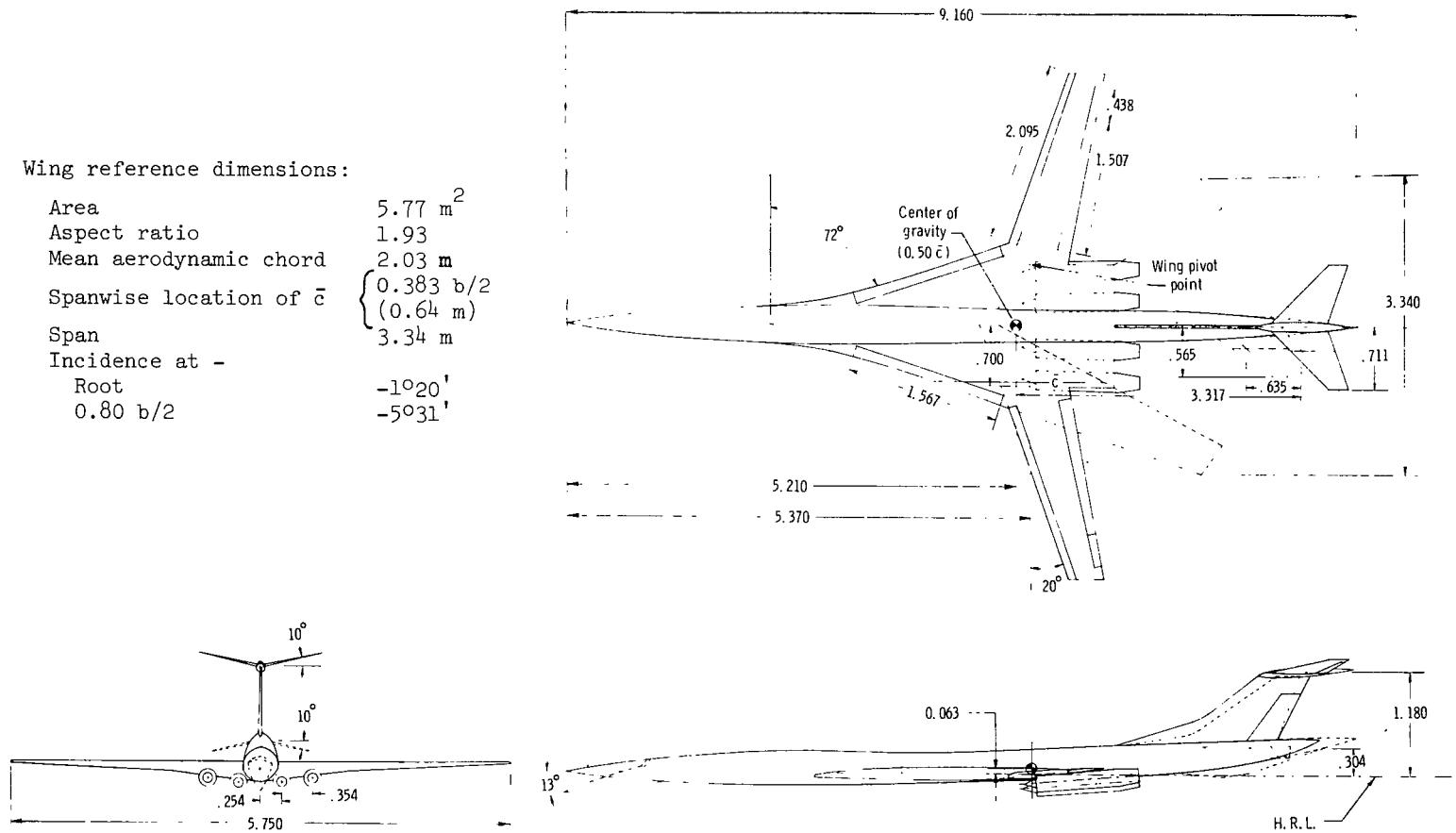

Figure 2.- Geometric characteristics of 1/9-scale model of variable-sweep supersonic cruise aircraft. All dimensions are in meters.

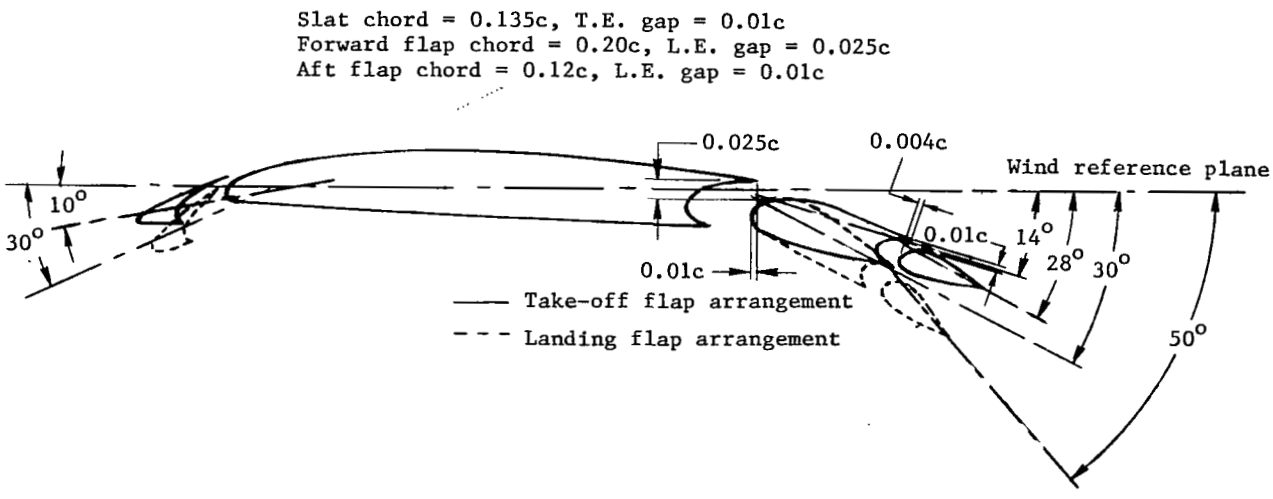

Figure 3.- Landing and take-off flap arrangements and slat for 20° swept-wing configurations. Streamwise section at spanwise station 1.2 m.

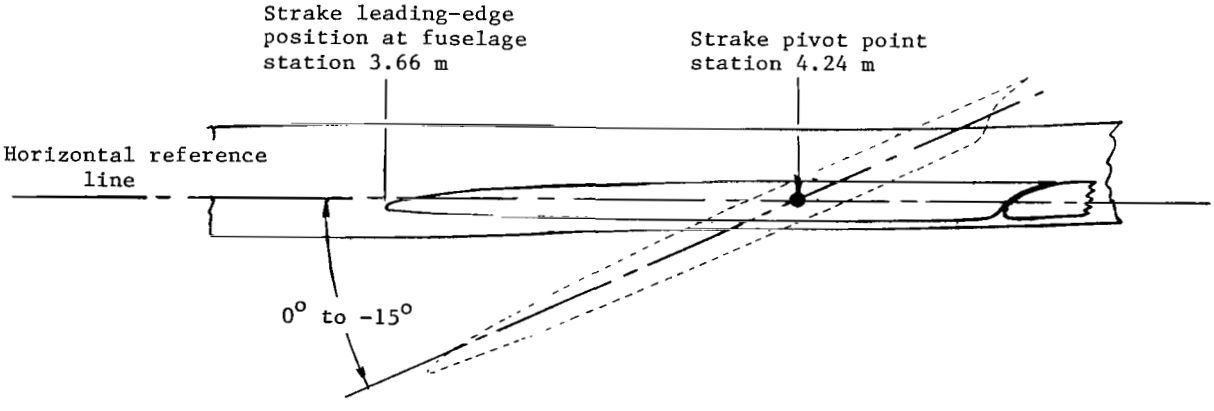

Figure 4.- Wing strake with pivot at station 4.24 m from undrooped nose of model. Streamwise section at spanwise station 0.44 m.

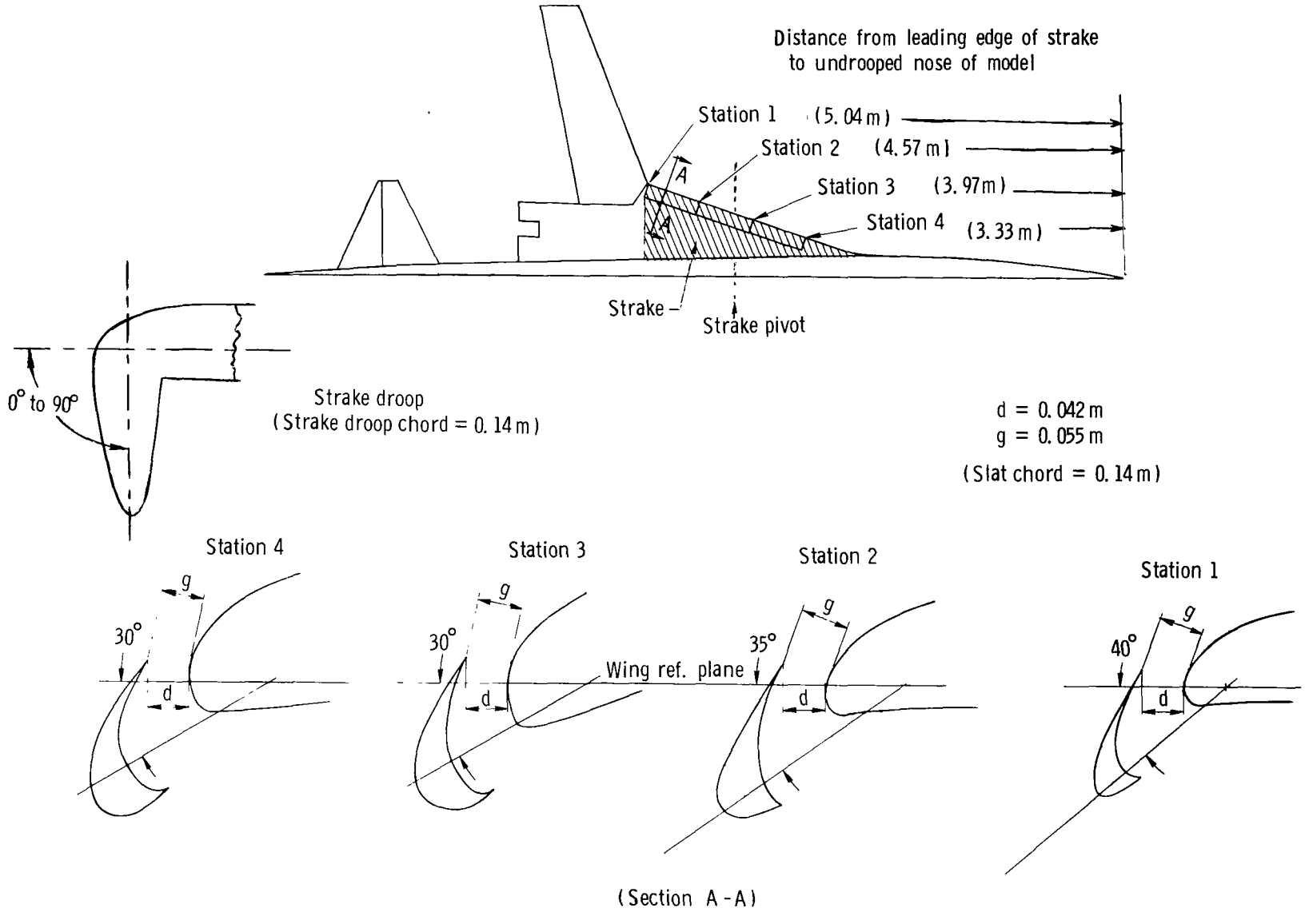

Figure 5.- Wing strake slat and droop. Sectional views are normal to strake leading edge.

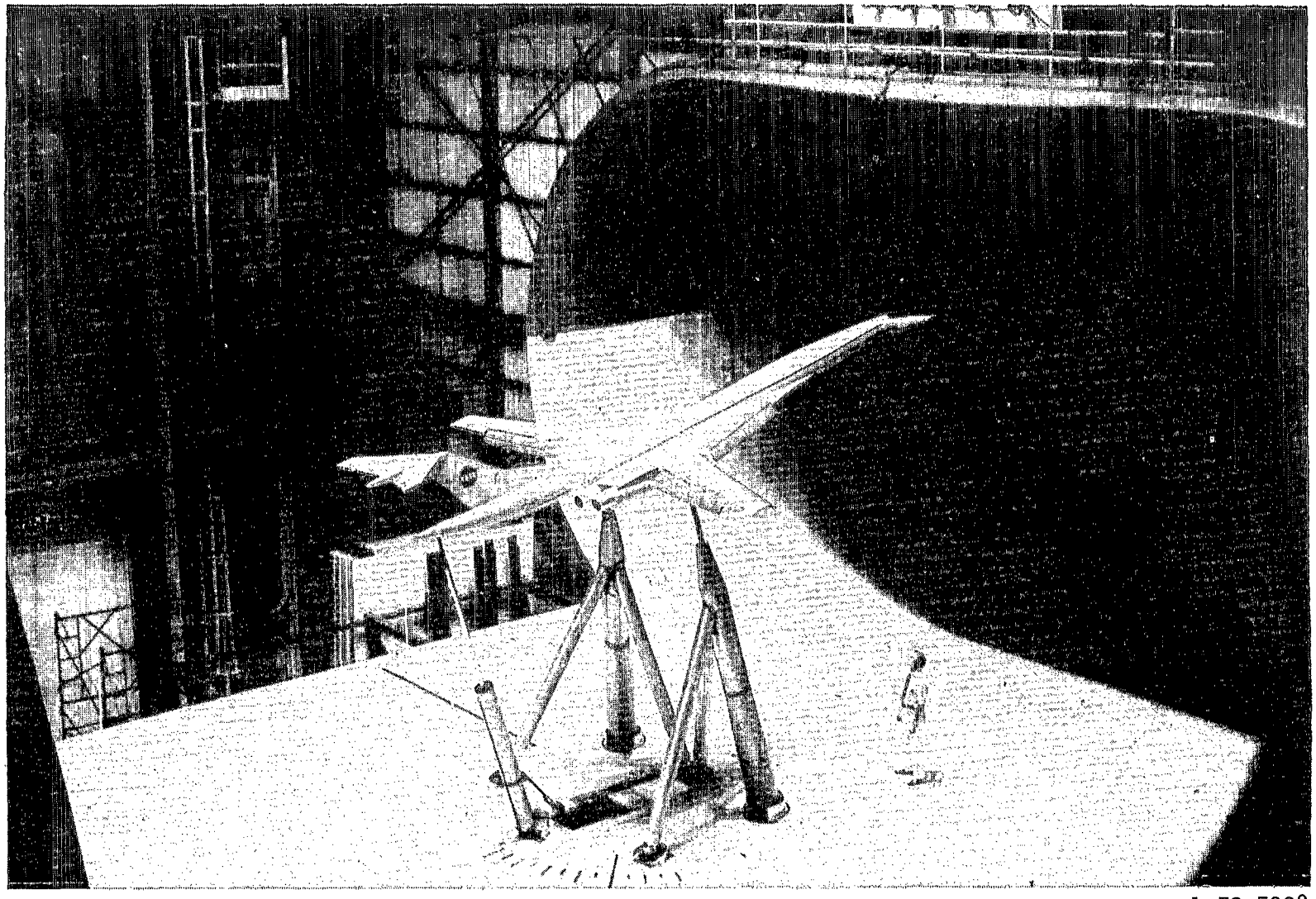

L-73-5028

Figure 6.- Three-quarter rear view of 1/9-scale model mounted for tests in Langley full-scale tunnel.

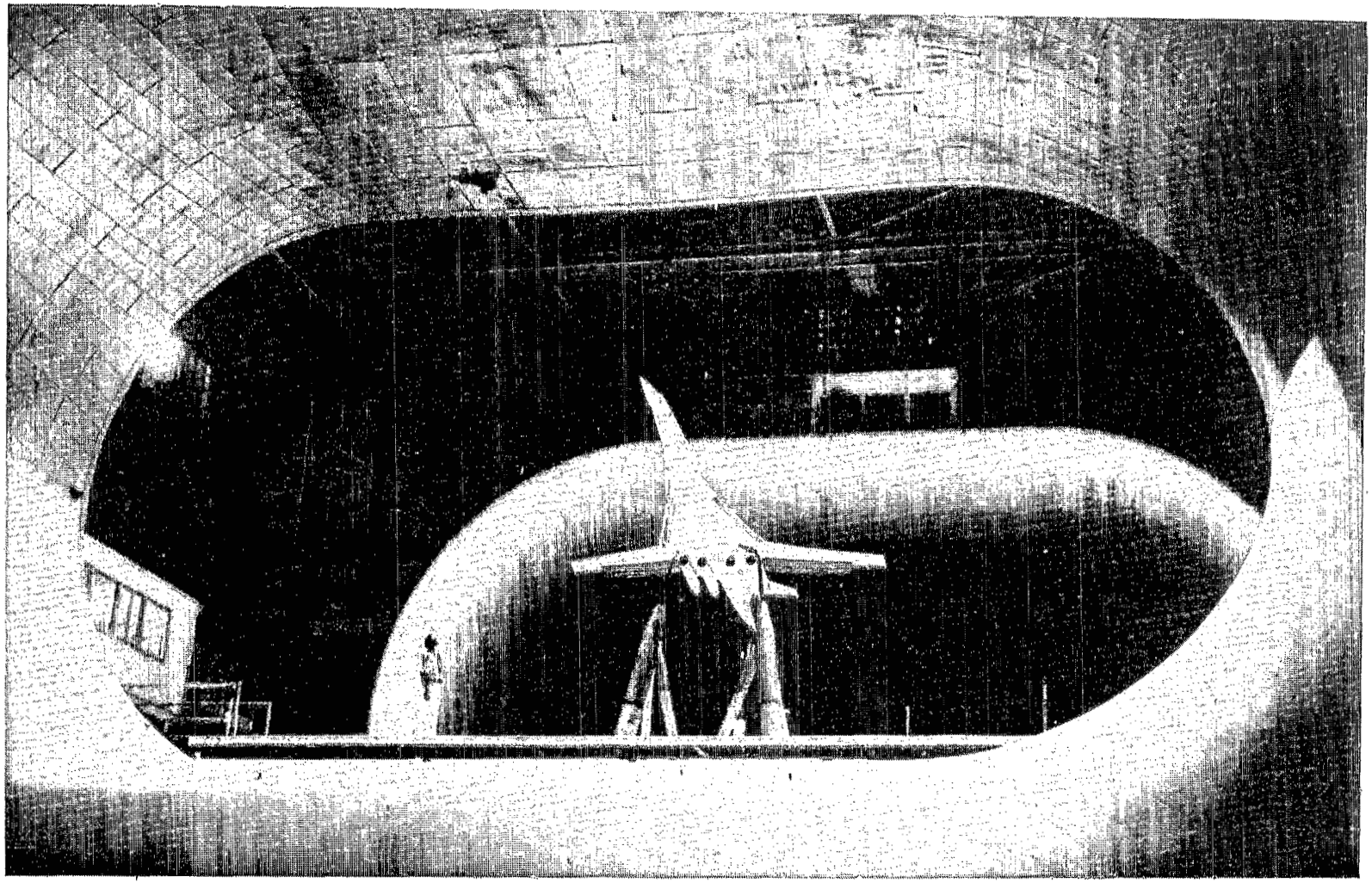

L-73-5026

Figure 7.- Bottom front view of 1/9-scale model mounted for tests in Langley full-scale tunnel.

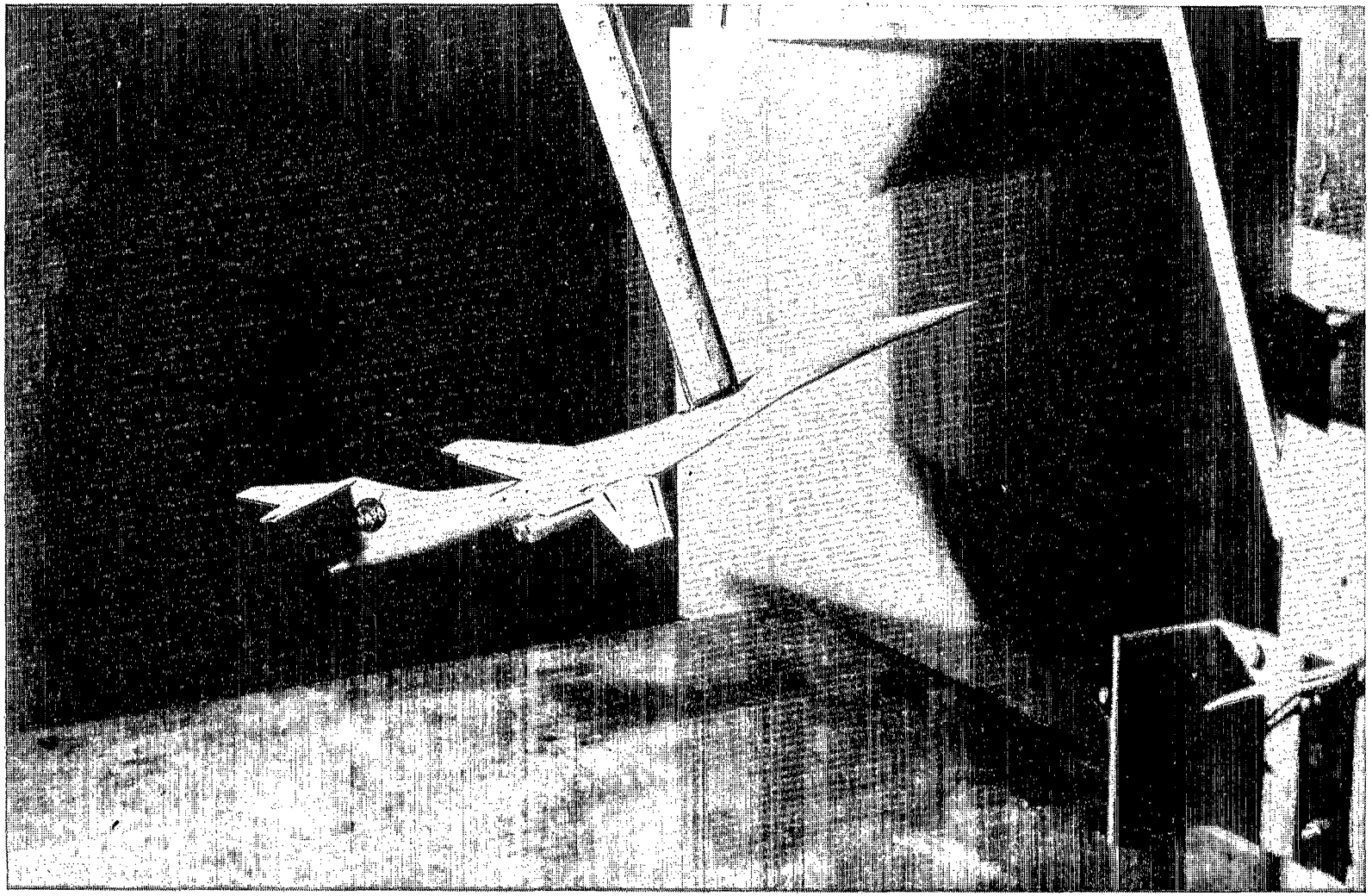

L-73-5024

Figure 8.- Three-quarter rear view of 1/135-scale model in a 1/15-scale model of Langley full-scale tunnel.

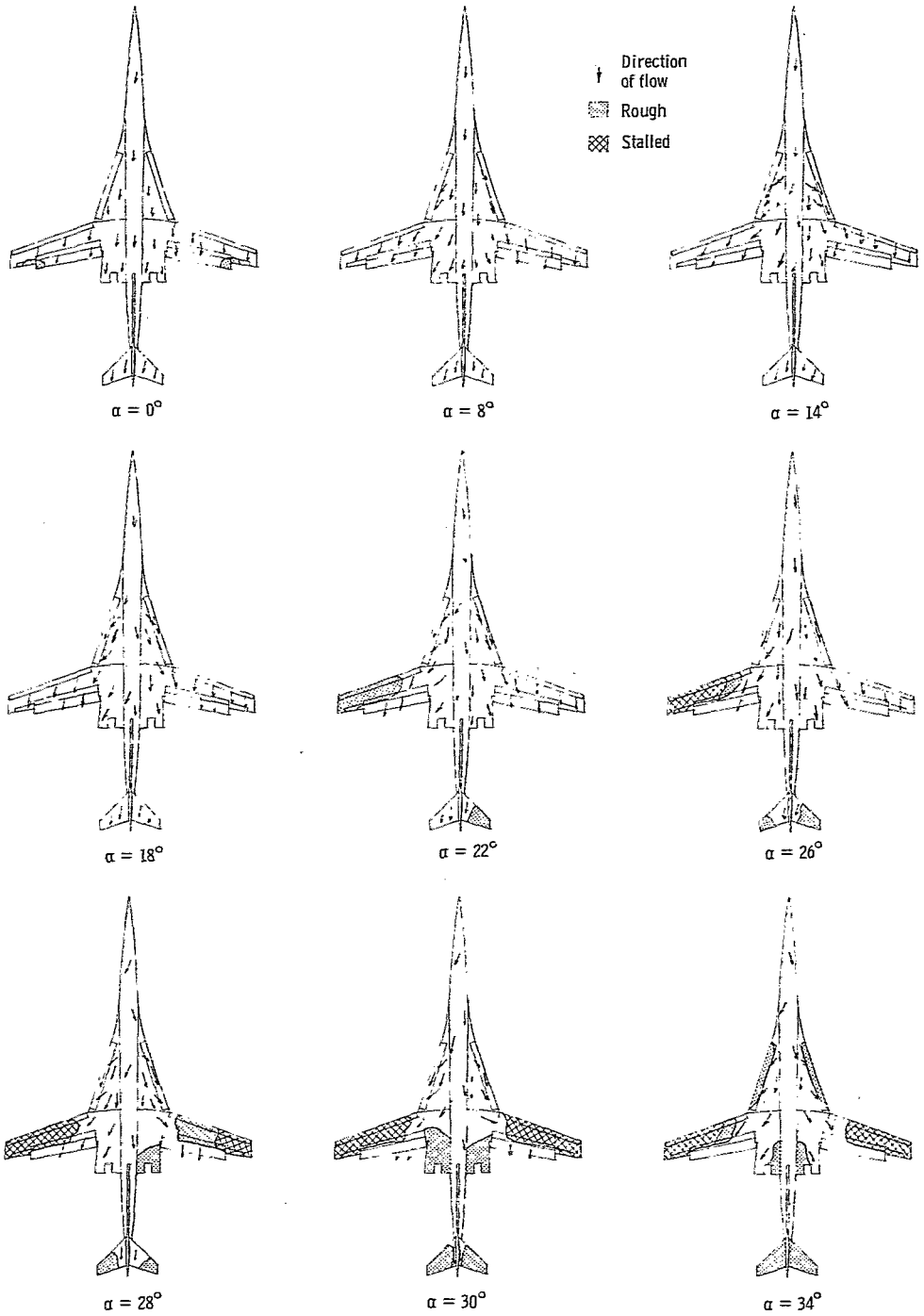

(a) $i_s = 0°$.

Figure 9.- Airflow patterns with strake incidence varied. $\delta_{f,te} = 30°/50°$; $\delta_{s,le} = 0°$; T-tail; $i_t = 0°$; $\Lambda = 20°$; $\beta = 0°$.

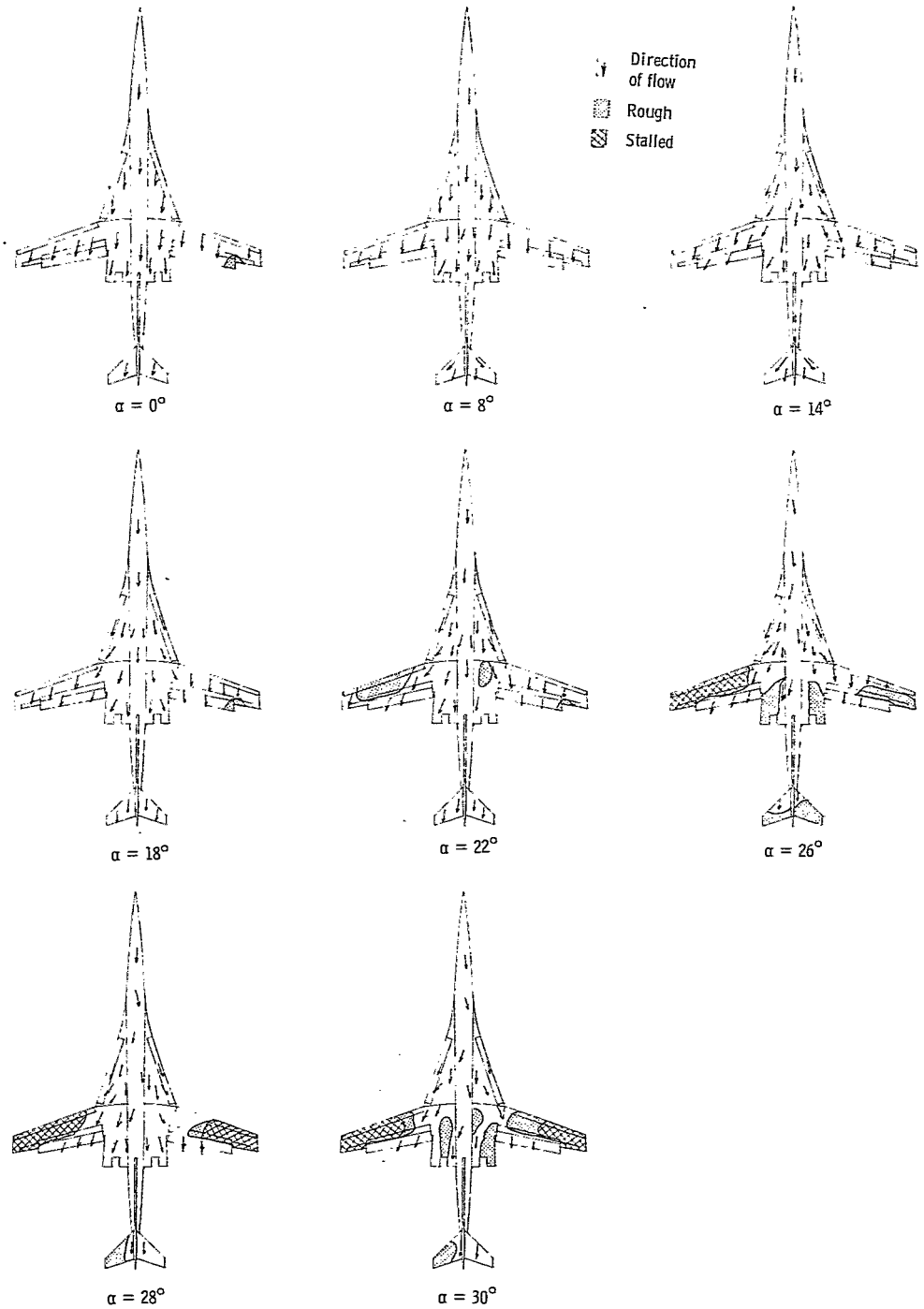

(b) $i_s = -5^o$.

Figure 9.- Continued.

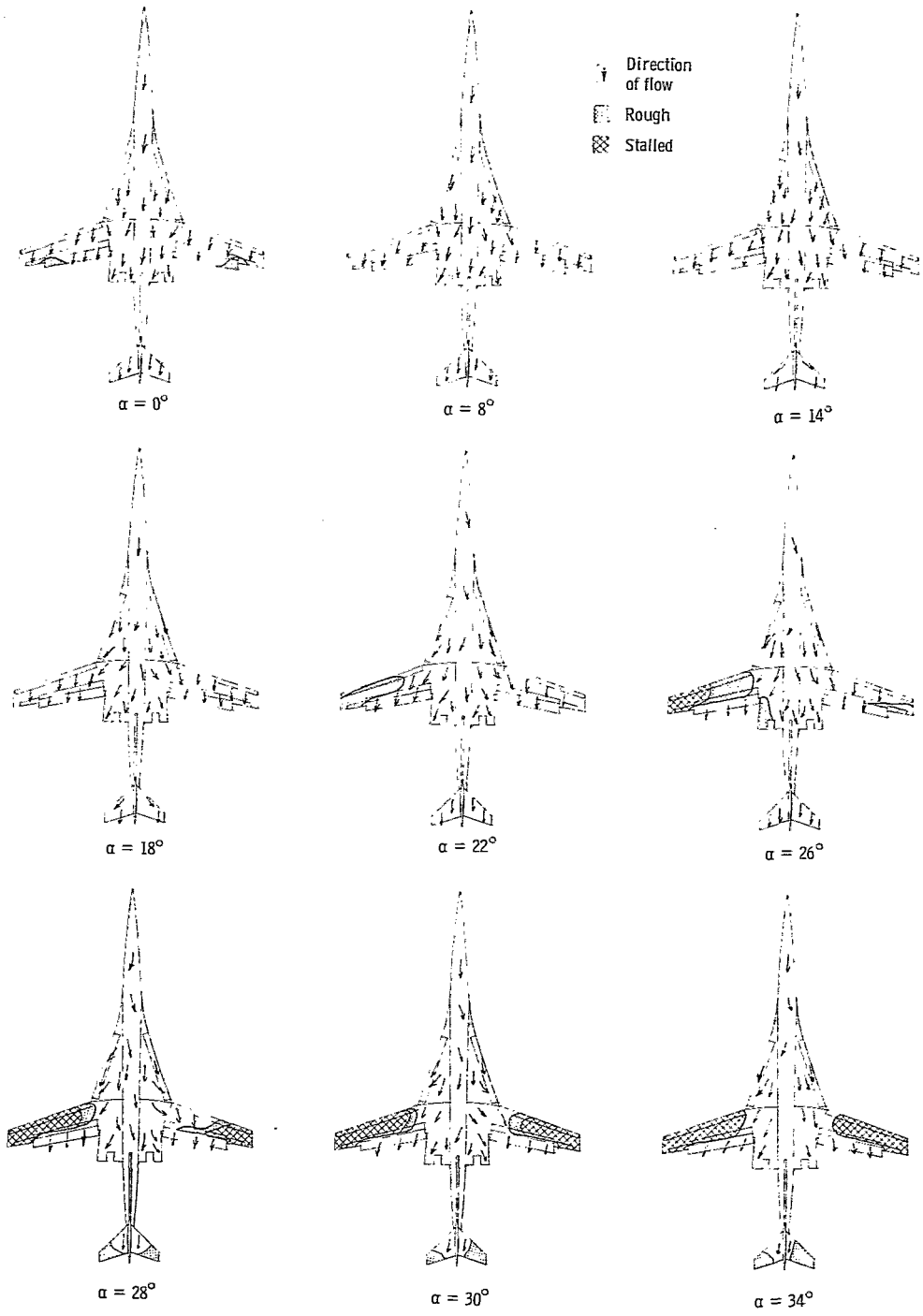

(c) $i_s = -10°$.

Figure 9.- Concluded.

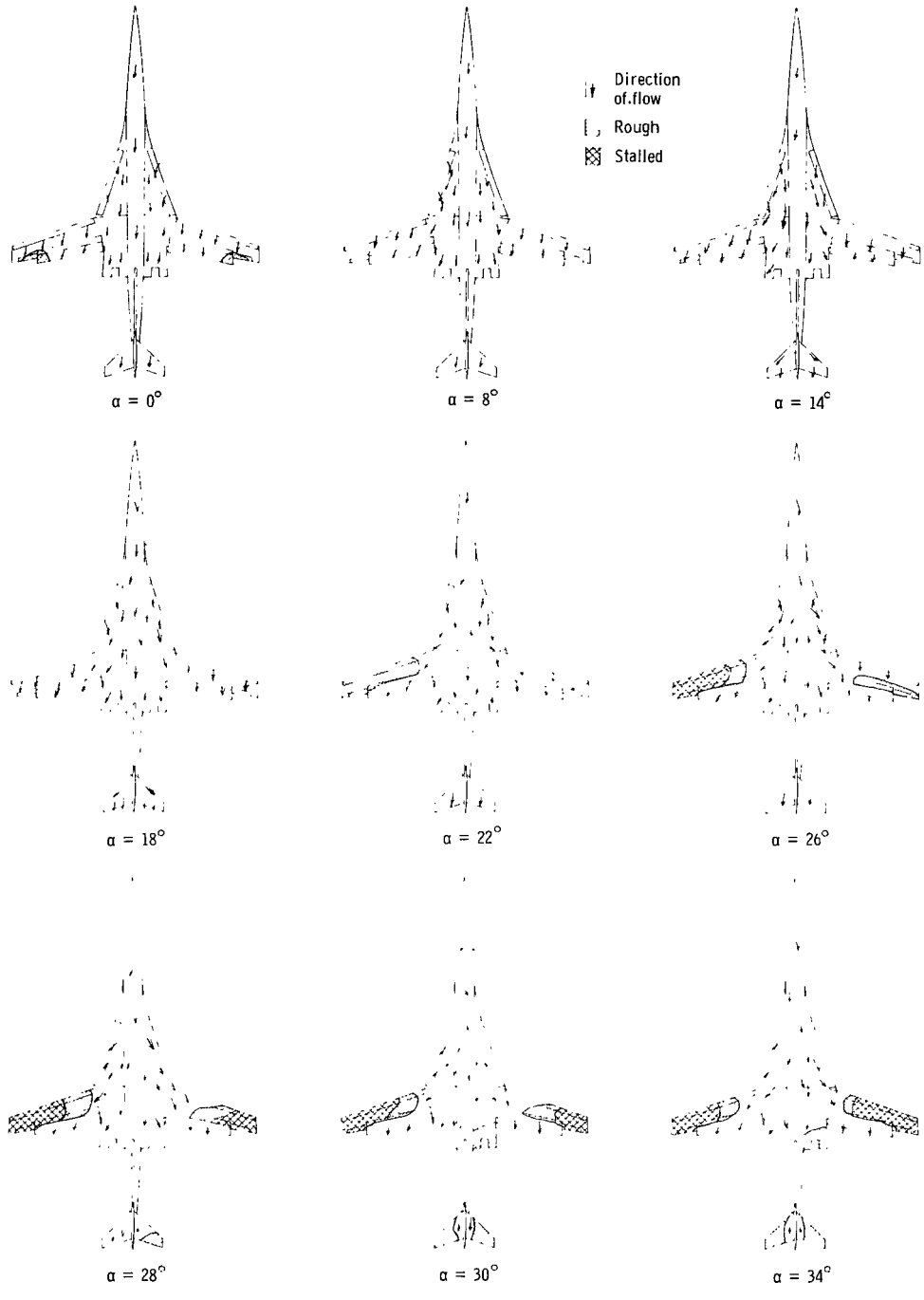

(a) $\delta_{s,le} = 30^{o}$.

Figure 10.- Airflow patterns with strake leading edge deflected. $\delta_{f,te} = 30^{o}/50^{o}$; $i_s = 0^{o}$; T-tail; $i_t = 0^{o}$; $\Lambda = 20^{o}$; $\beta = 0^{o}$.

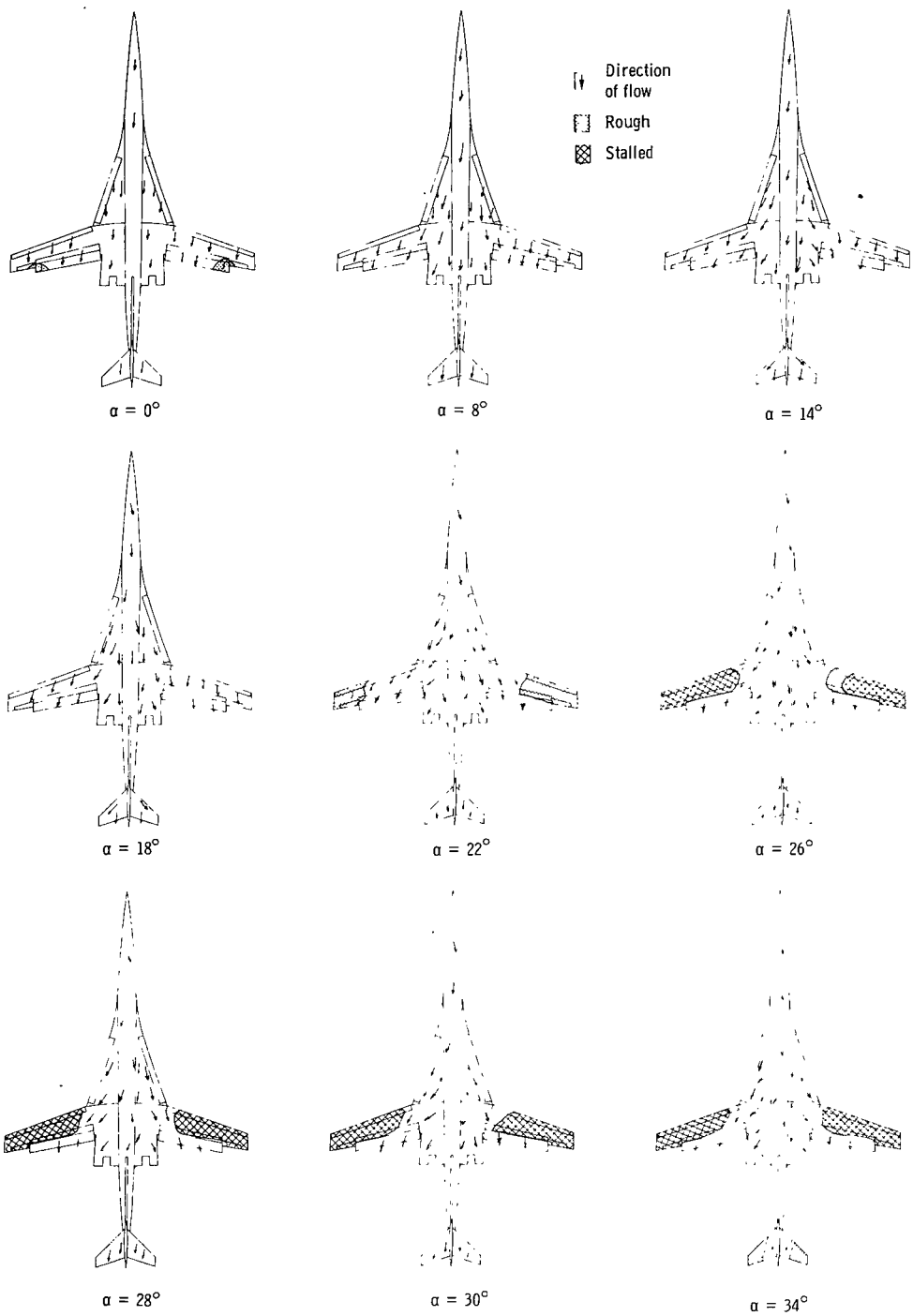

(b) $\delta_{s,le} = 60°$.

Figure 10.- Continued.

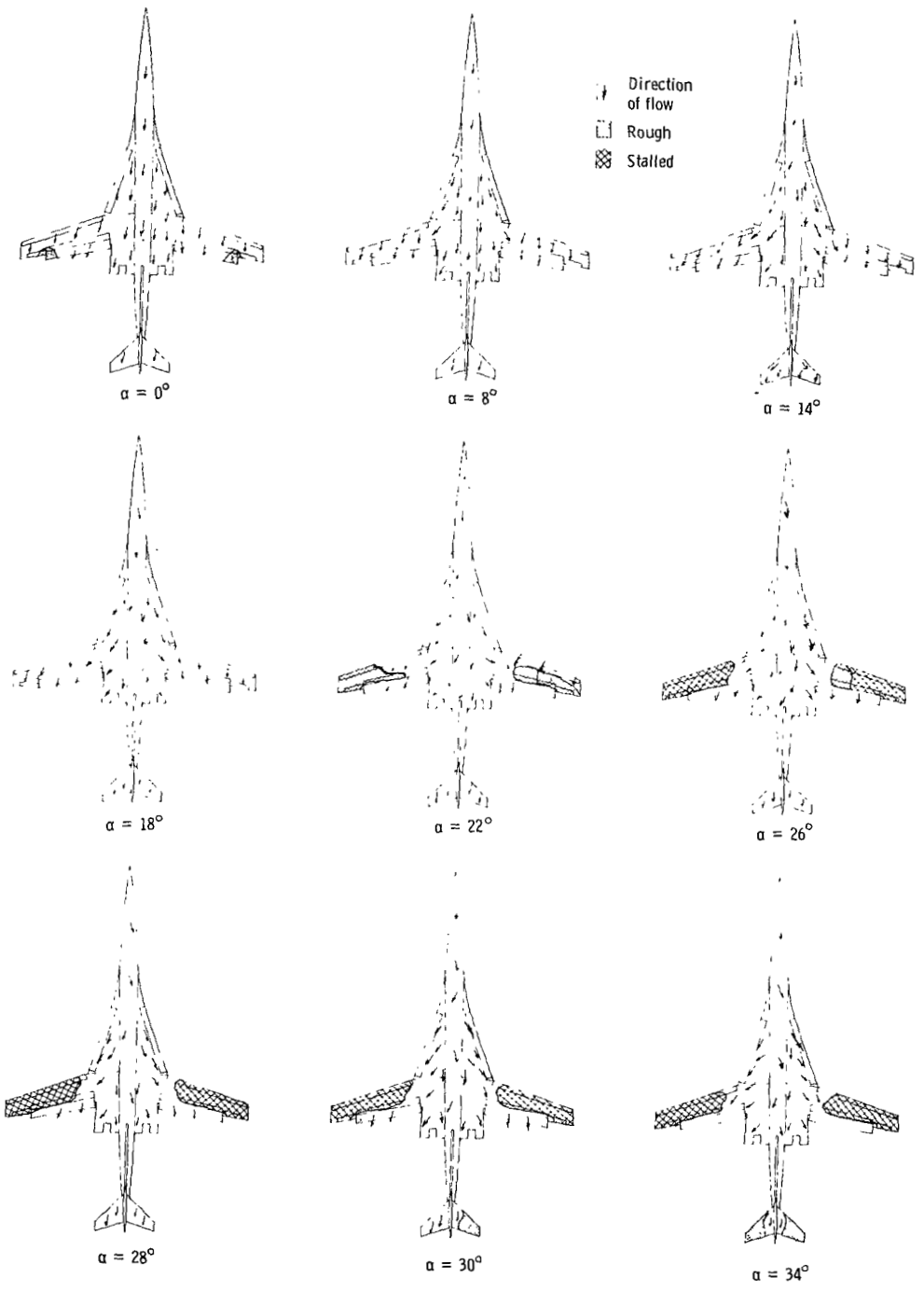

(c) $\delta_{s,le} = 90°$.

Figure 10.- Concluded.

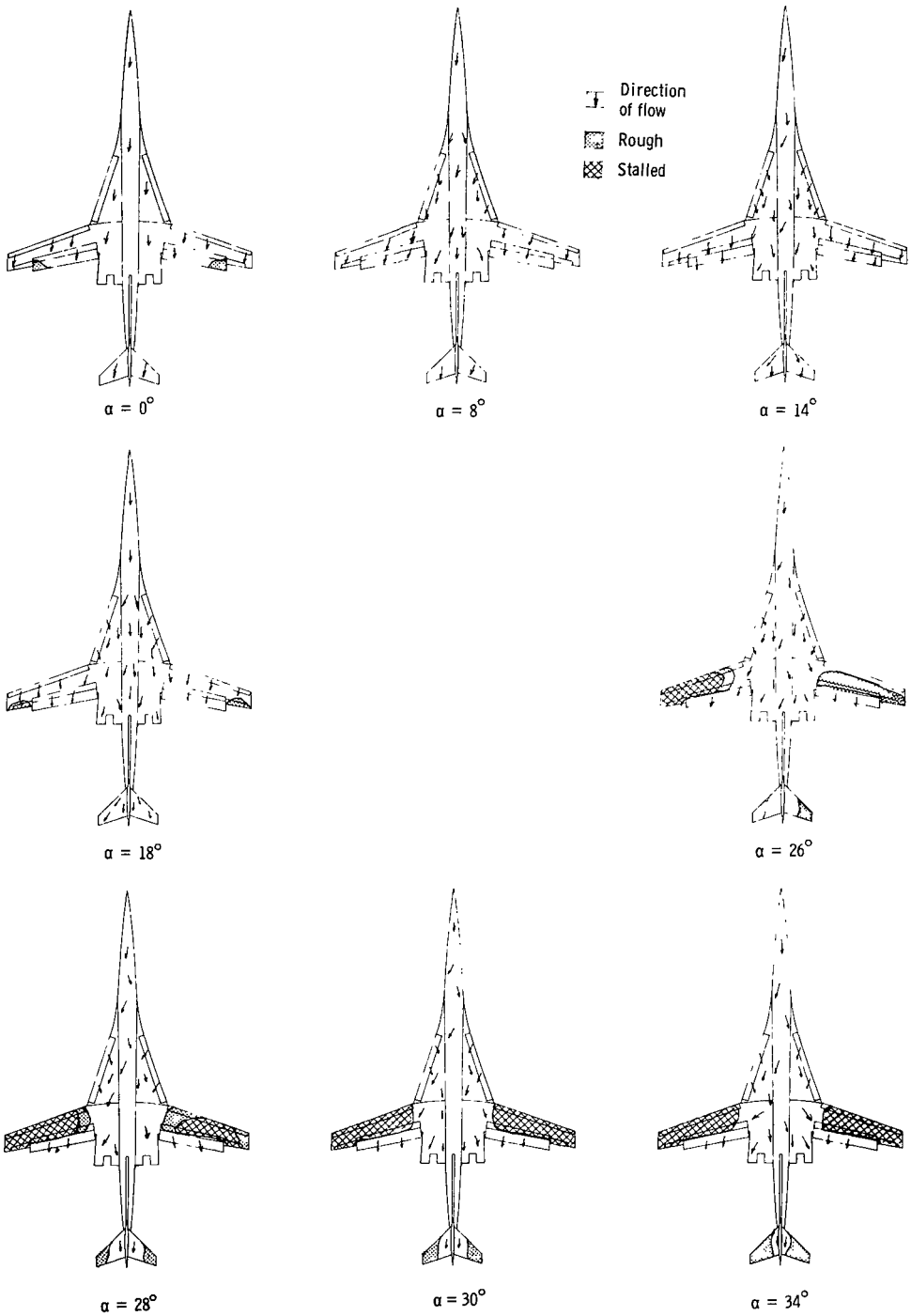

(a) $\beta = 0^{\circ}$.

Figure 11.- Airflow patterns with sideslip varied. Slatted strake; $\delta_{f,te} = 30^{\circ}/50^{\circ}$; $i_s = 0^{\circ}$; T-tail; $i_t = 0^{\circ}$; $\Lambda = 20^{\circ}$.

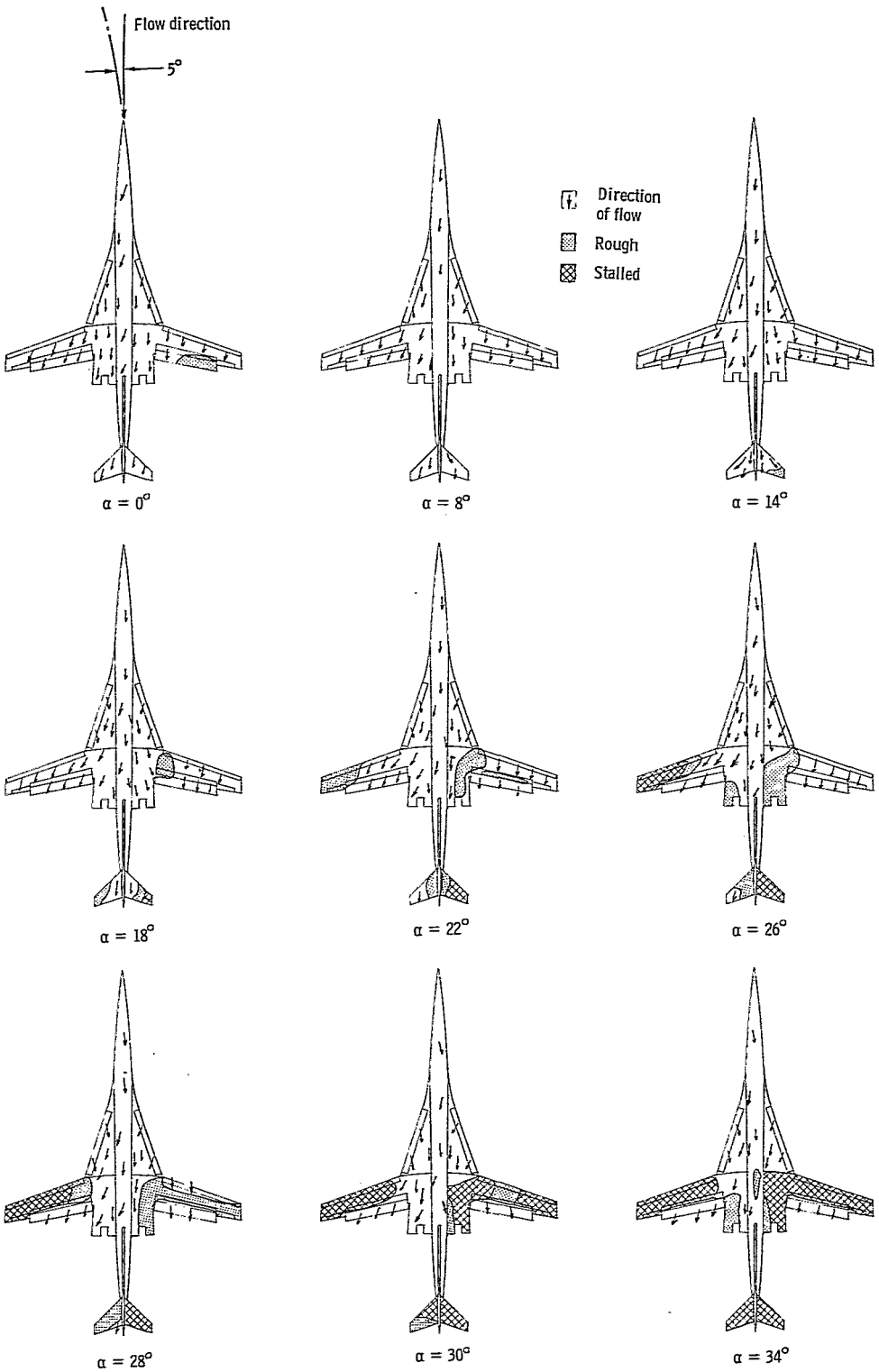

(b) $\beta = 5^{\circ}$.

Figure 11.- Continued.

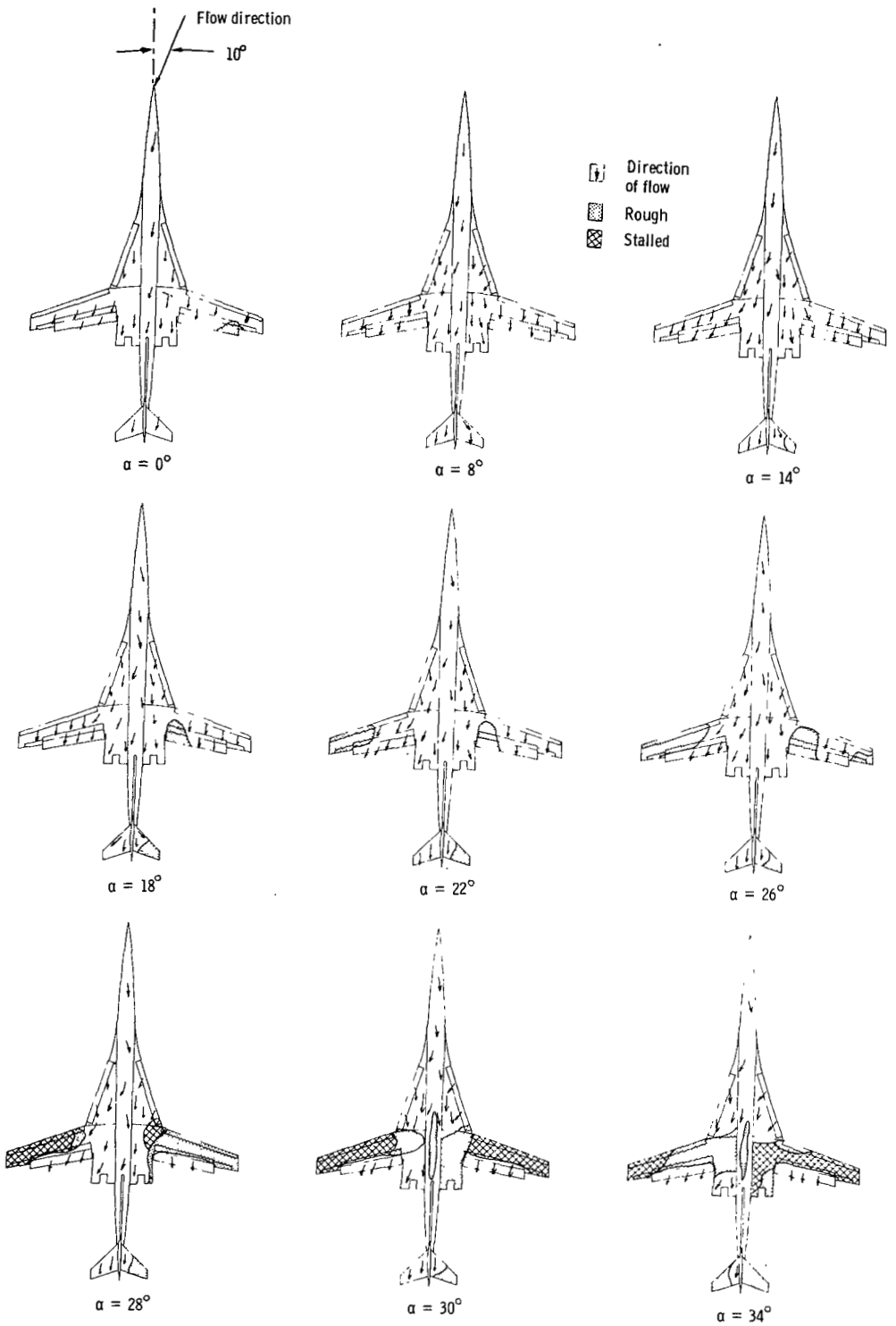

(c) $\beta = 10^{\circ}$.

Figure 11.- Concluded.

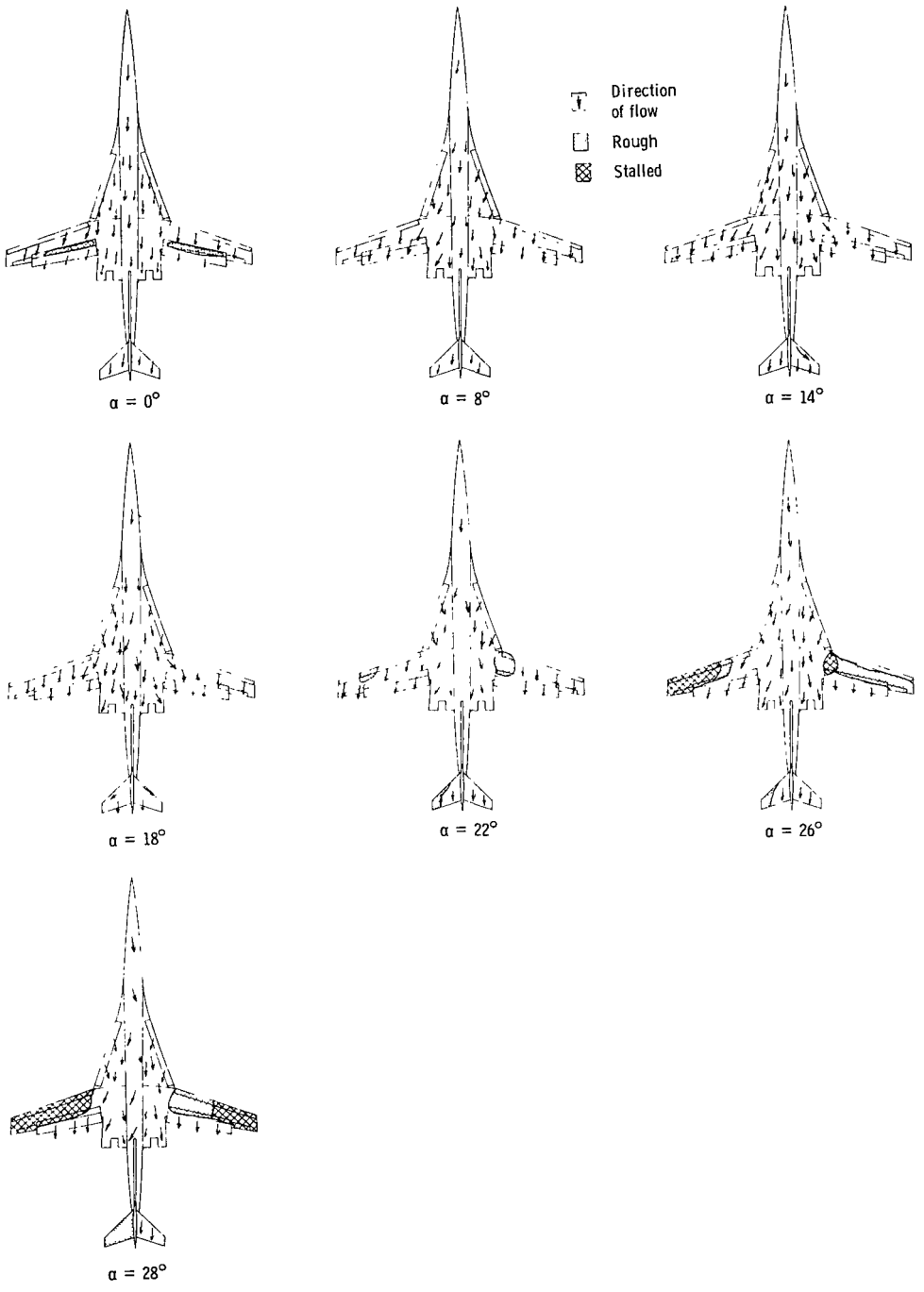

Figure 12.- Airflow patterns at increased speed (≈84 knots). Slatted strake; $\delta_{f,te} = 30°/50°$; $i_s = 0°$; T-tail; $i_t = 0°$; $\Lambda = 20°$; $\beta = 0°$. (Compare with patterns of fig. 11(a) (≈54 knots).)

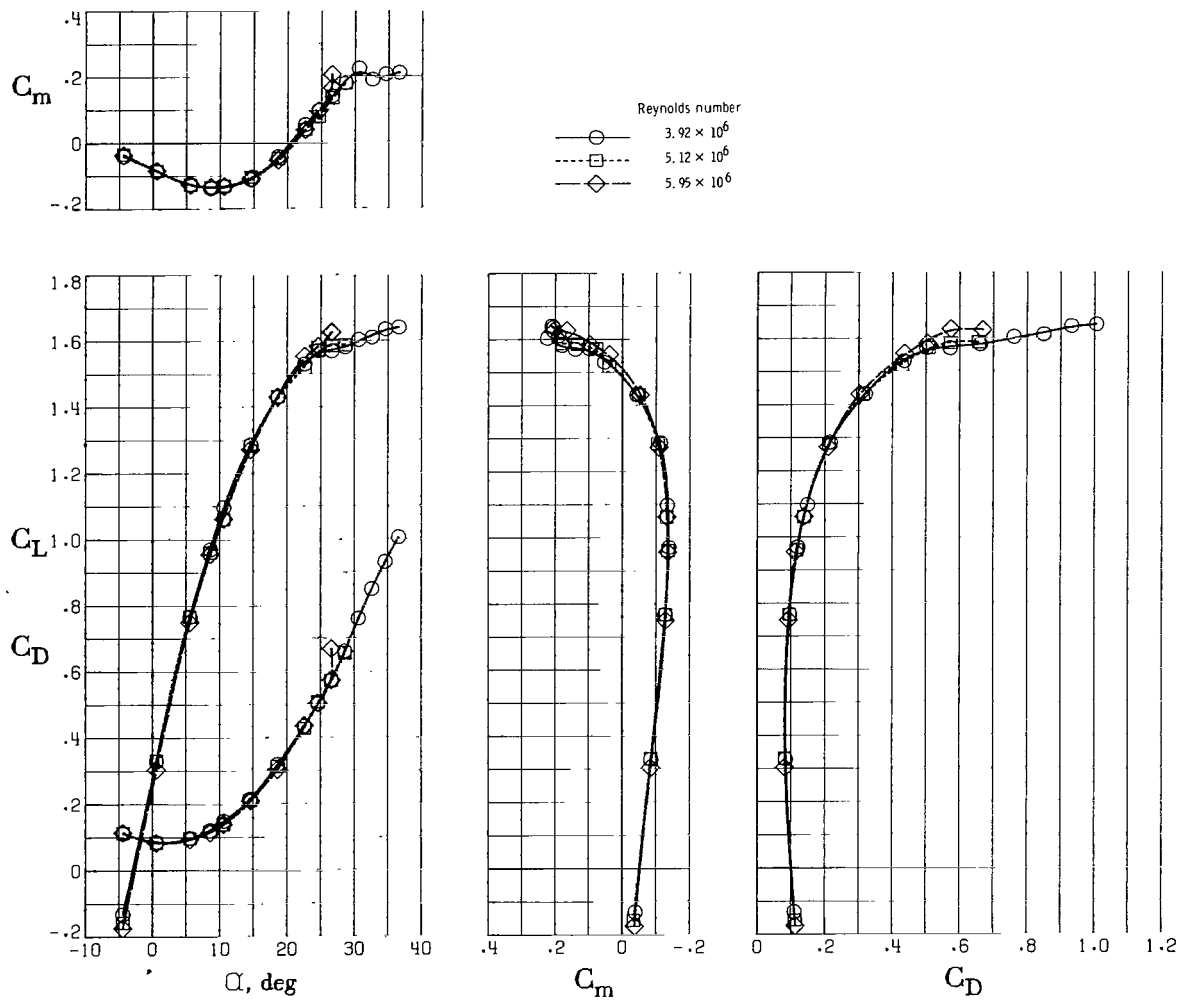

(a) Basic strake.

Figure 13.- Effect of Reynolds number for two strake arrangements. $\delta_{f,te}$ = 30°/50°; i_s = 0°; T-tail; i_t = 0°; Λ = 20°; β = 0°.

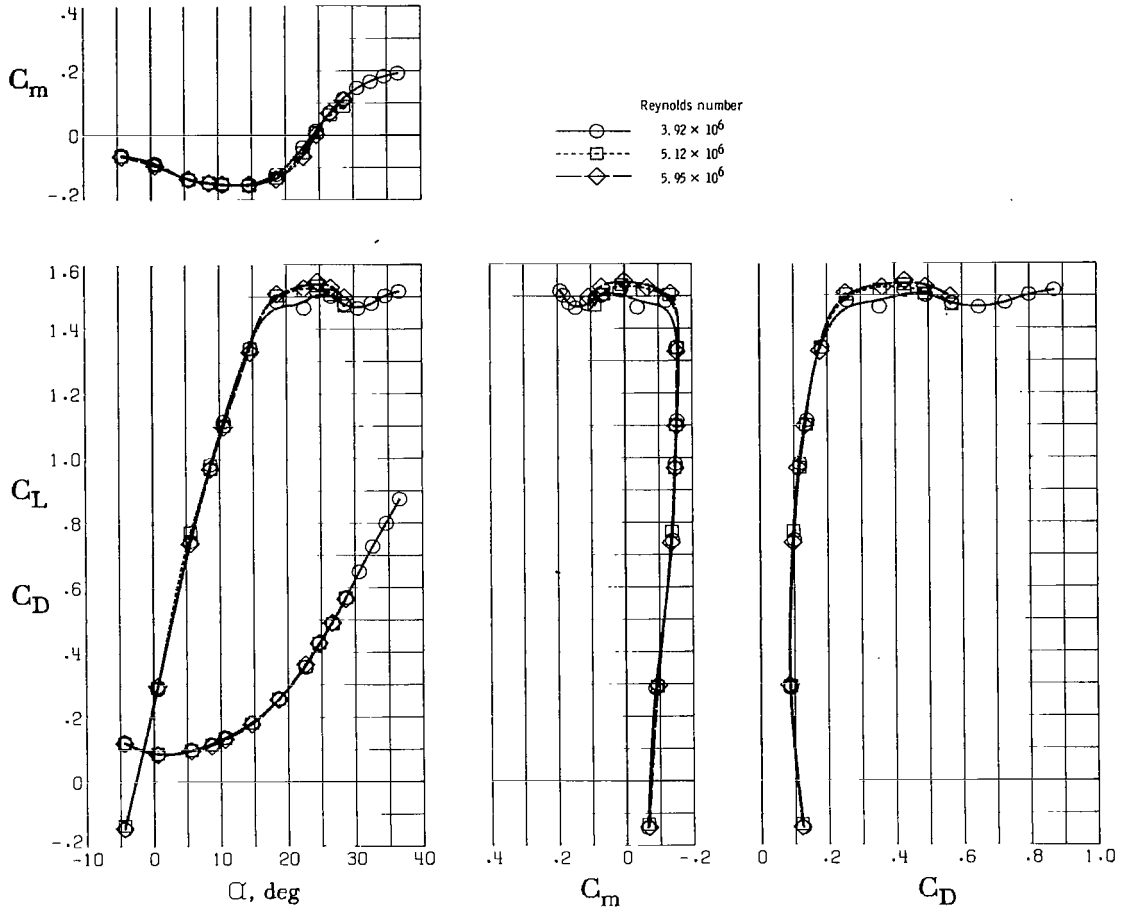

(b) Slatted strake.

Figure 13.- Concluded.

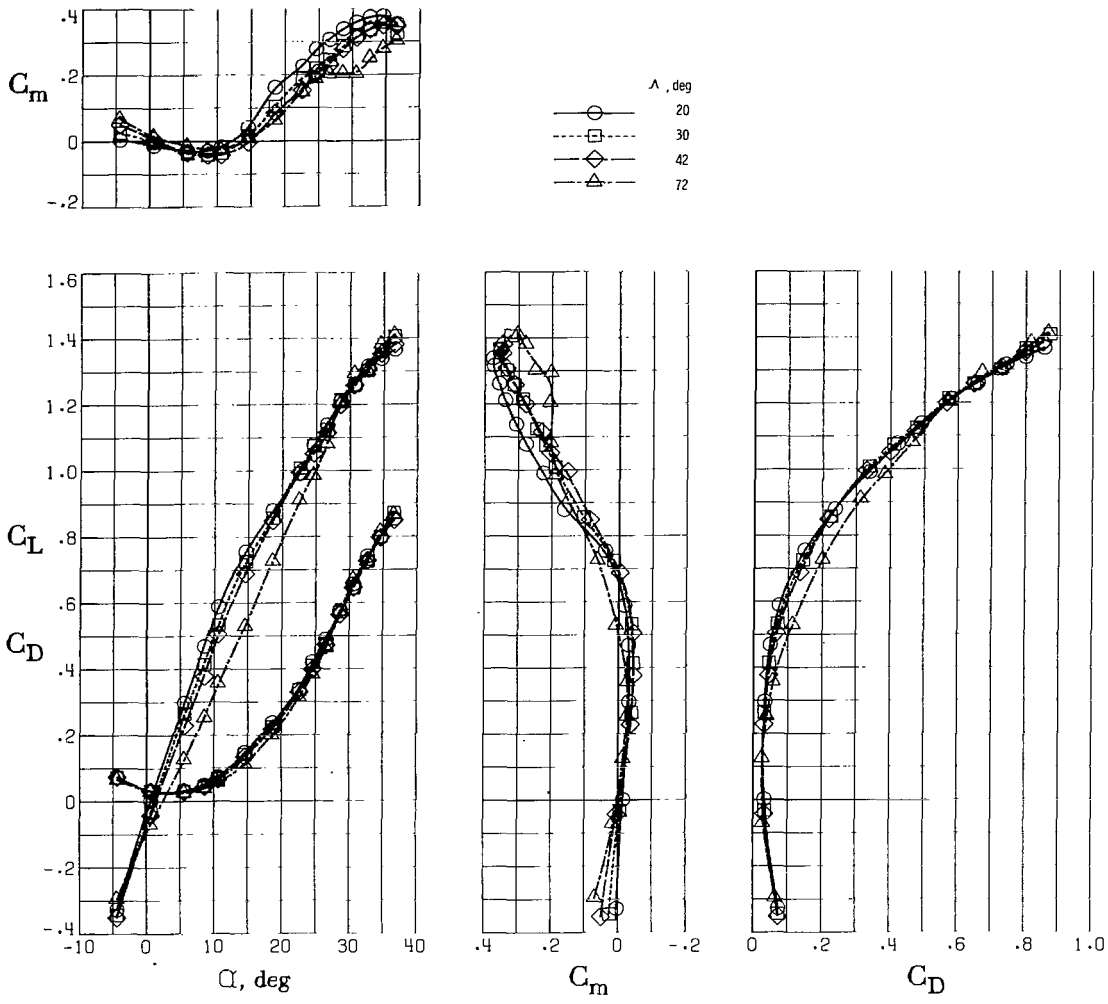

(a) T-tail.

Figure 14.- Effect of wing leading-edge sweep for two tail arrangements. Clean wing configuration; $i_t = 0^o$; $\beta = 0^o$; undrooped fuselage nose.

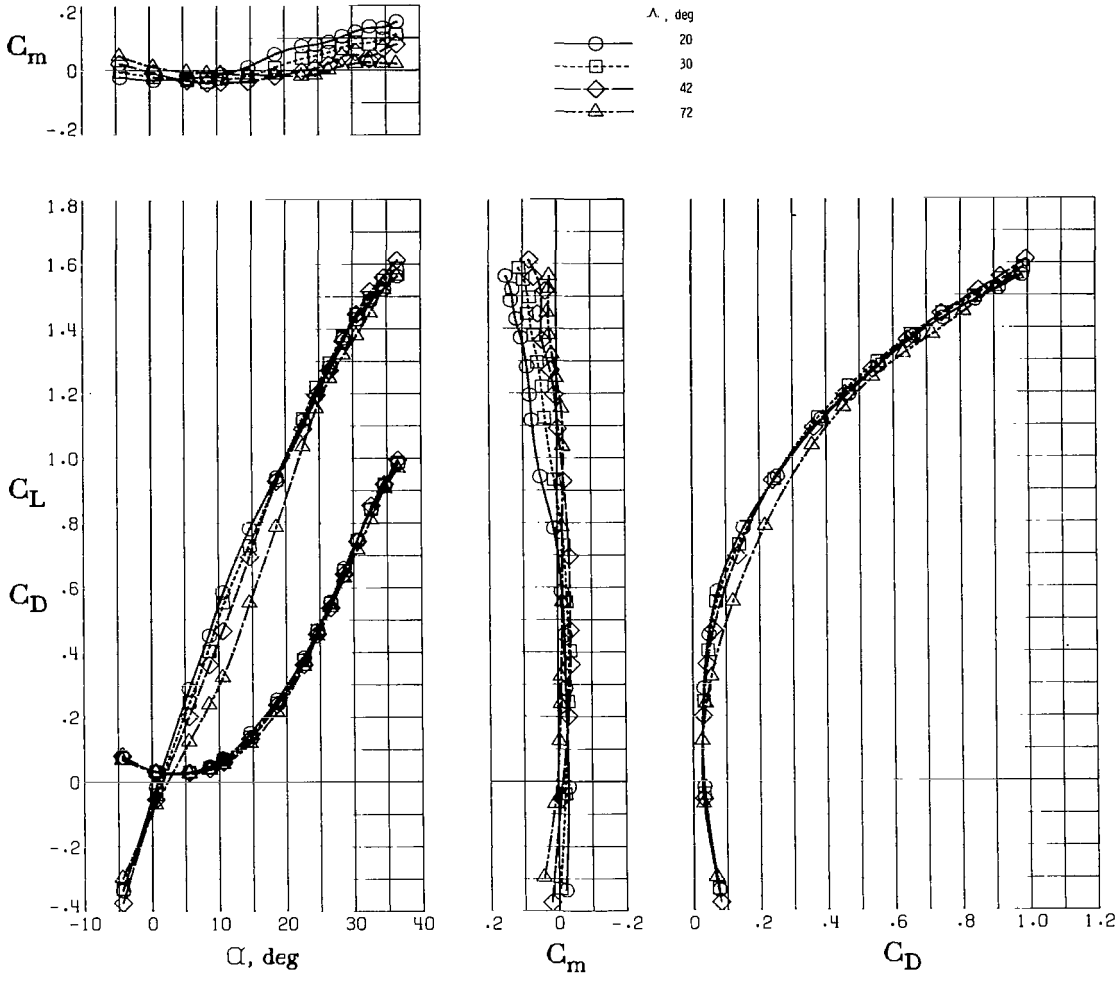

(b) Low tail.

Figure 14.- Concluded.

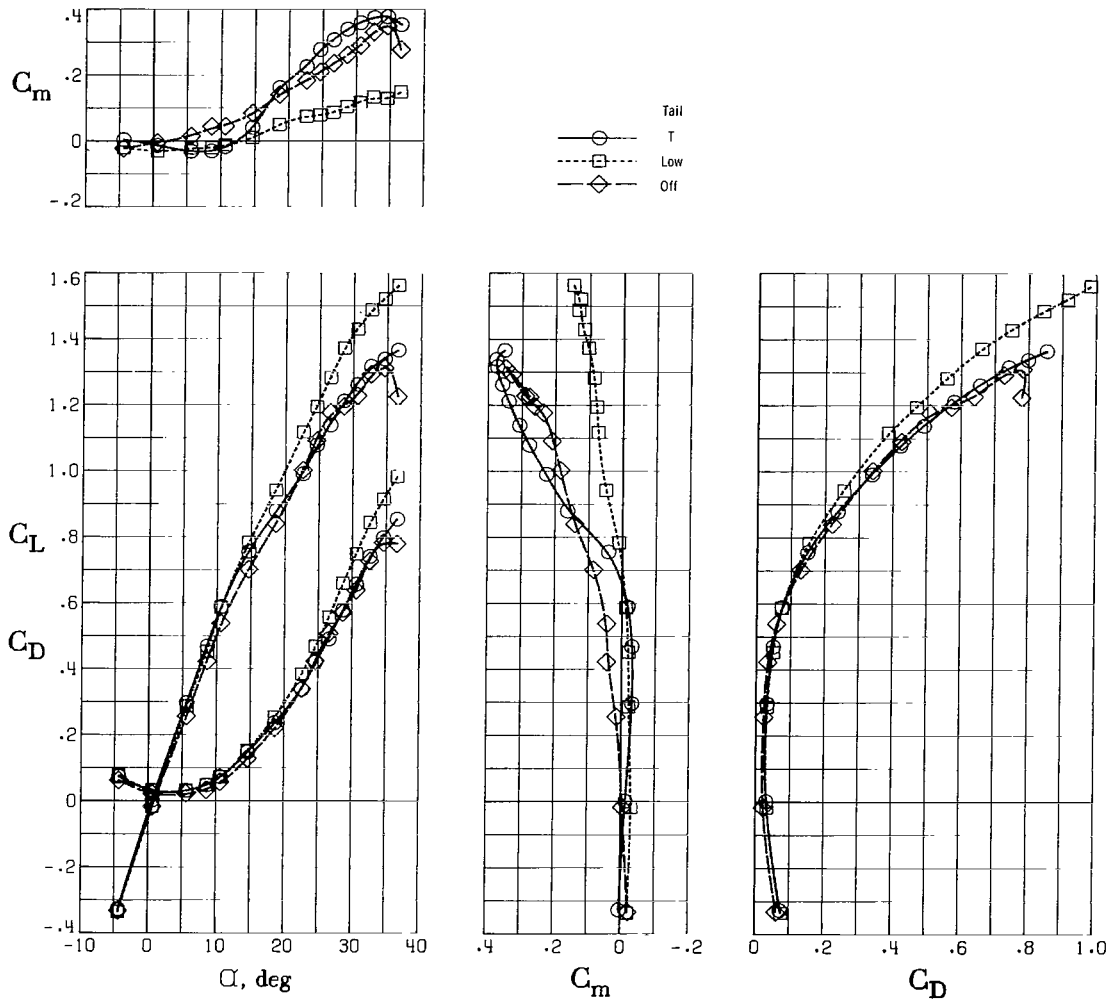

(a) $\Lambda = 20^{\circ}$.

Figure 15.- Effect of horizontal tail position for various wing-sweep angles. $\delta_{f,te} = 0^{\circ}$; $i_t = 0^{\circ}$; $\beta = 0^{\circ}$.

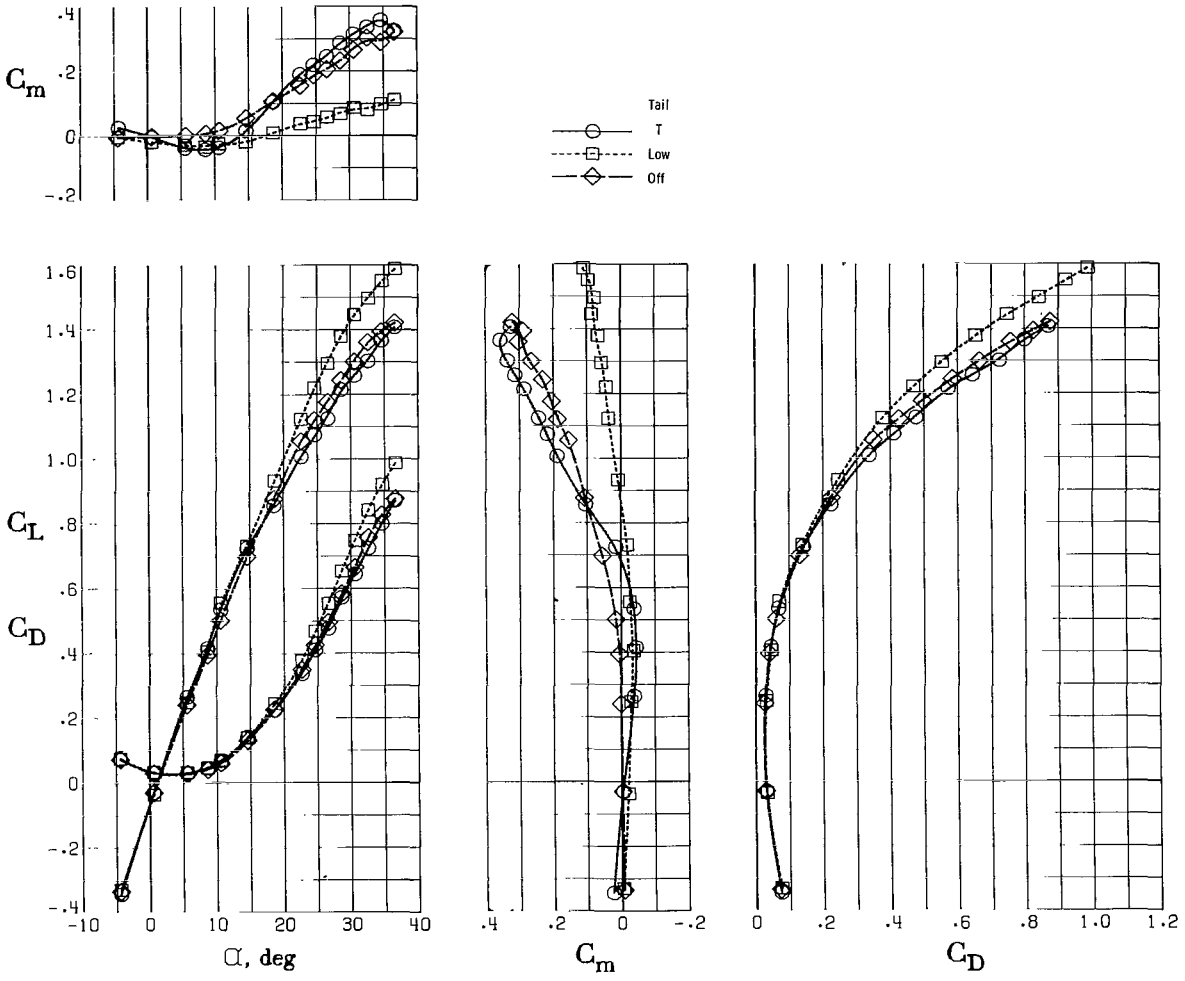

(b) $\Lambda = 30^{\circ}$.

Figure 15.- Continued.

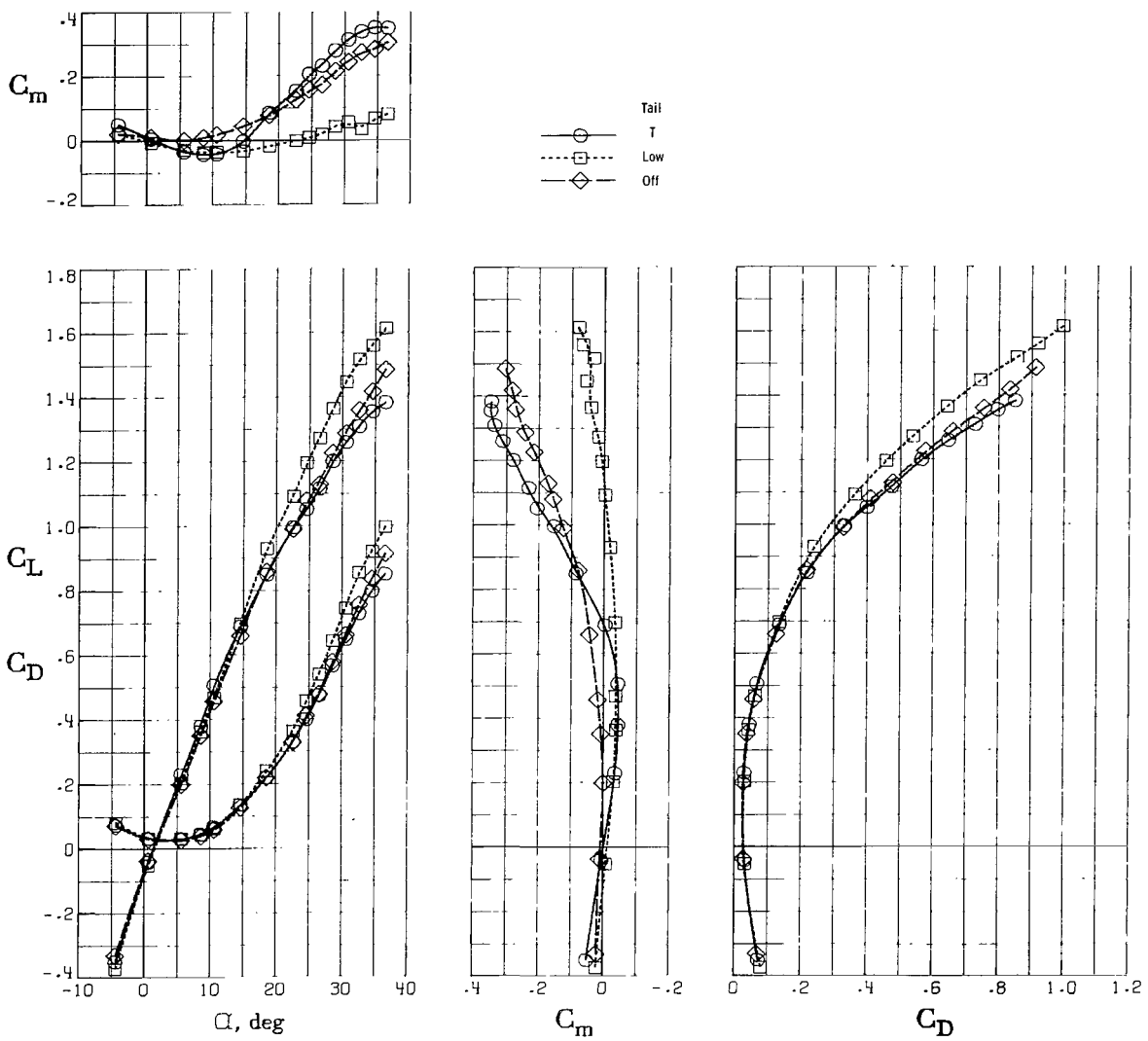

(c) Λ = 42°.

Figure 15.- Continued.

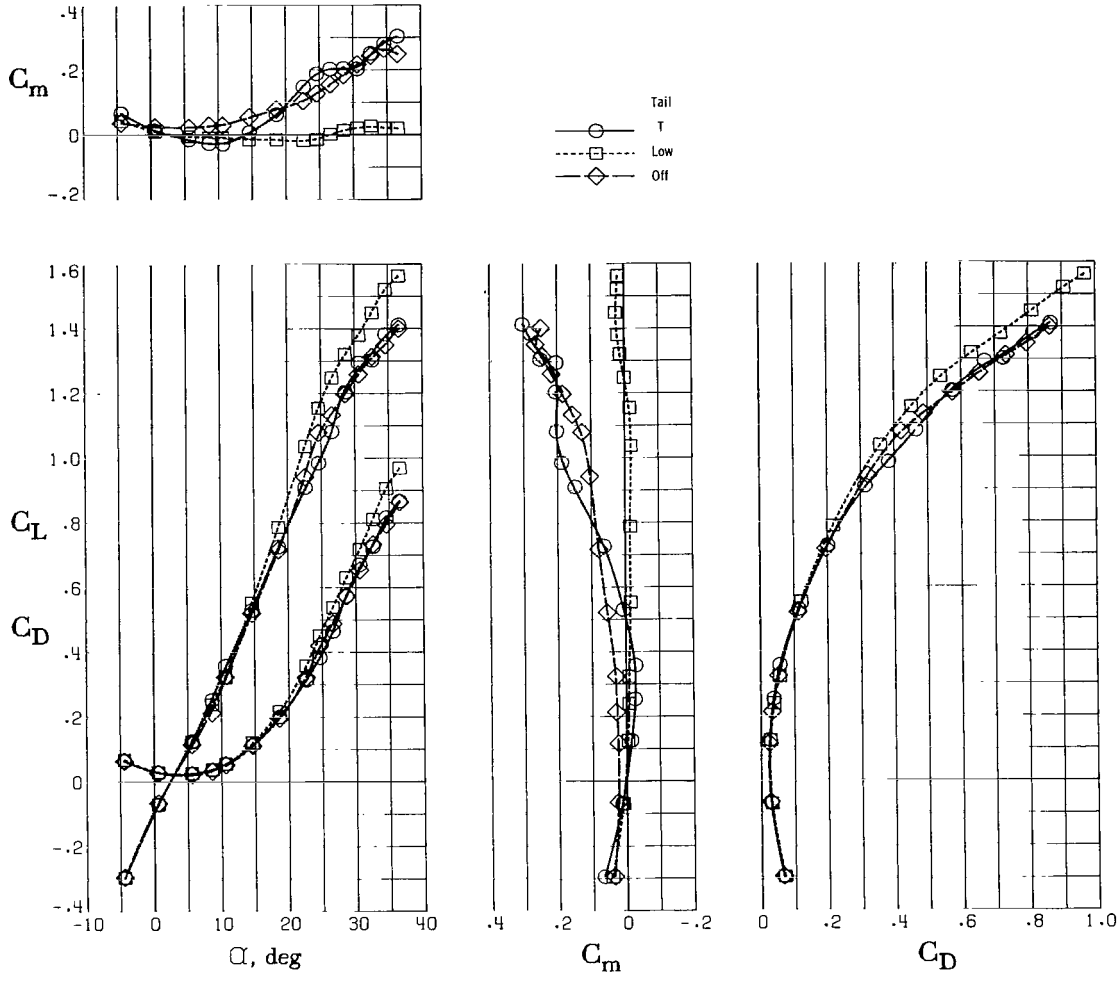

(d) $\Lambda = 72°$.

Figure 15.- Concluded.

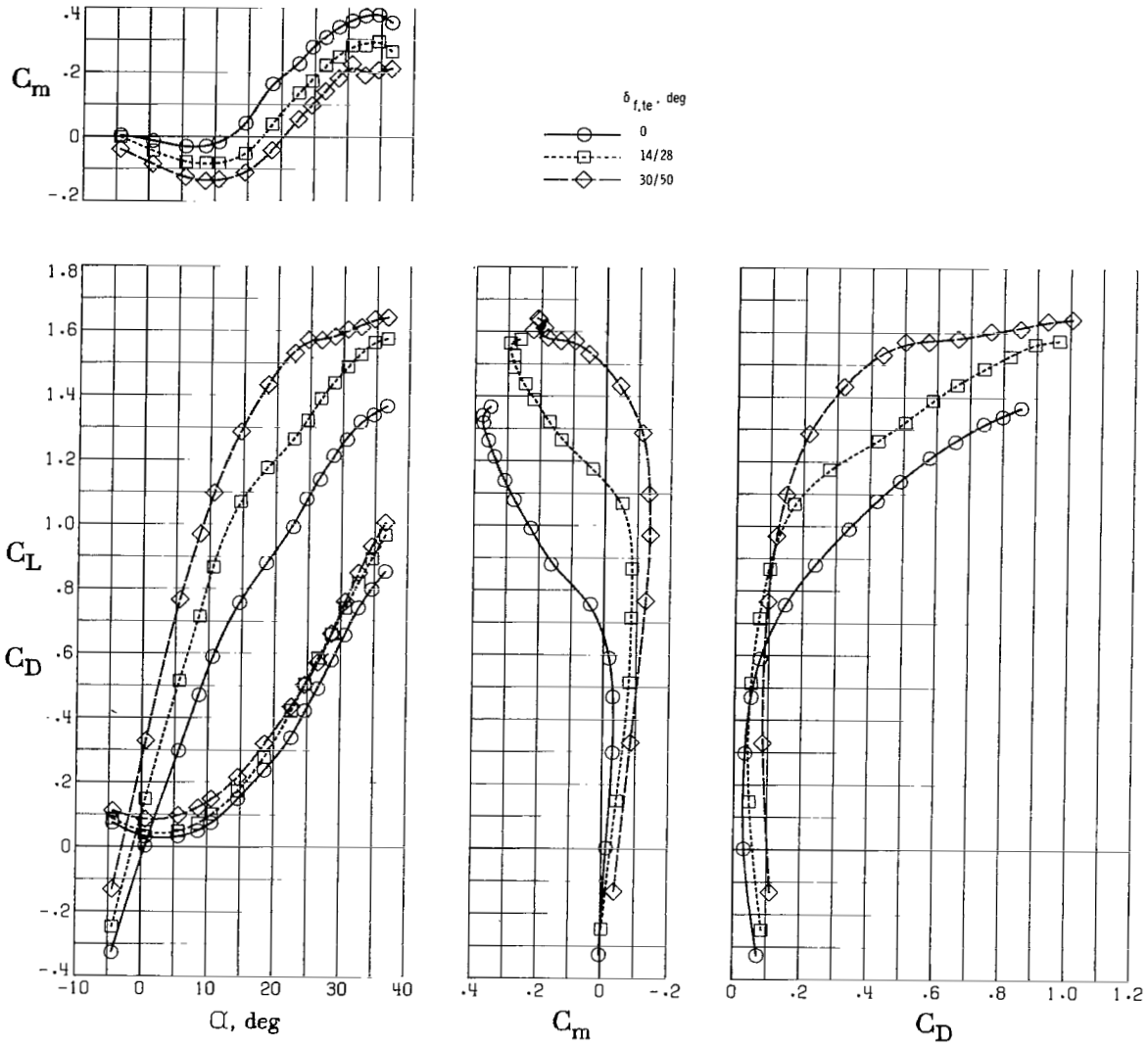

Figure 16.- Effect of high-lift devices for basic strake and T-tail. $i_t = 0^o$; $\Lambda = 20^o$; $\beta = 0^o$.

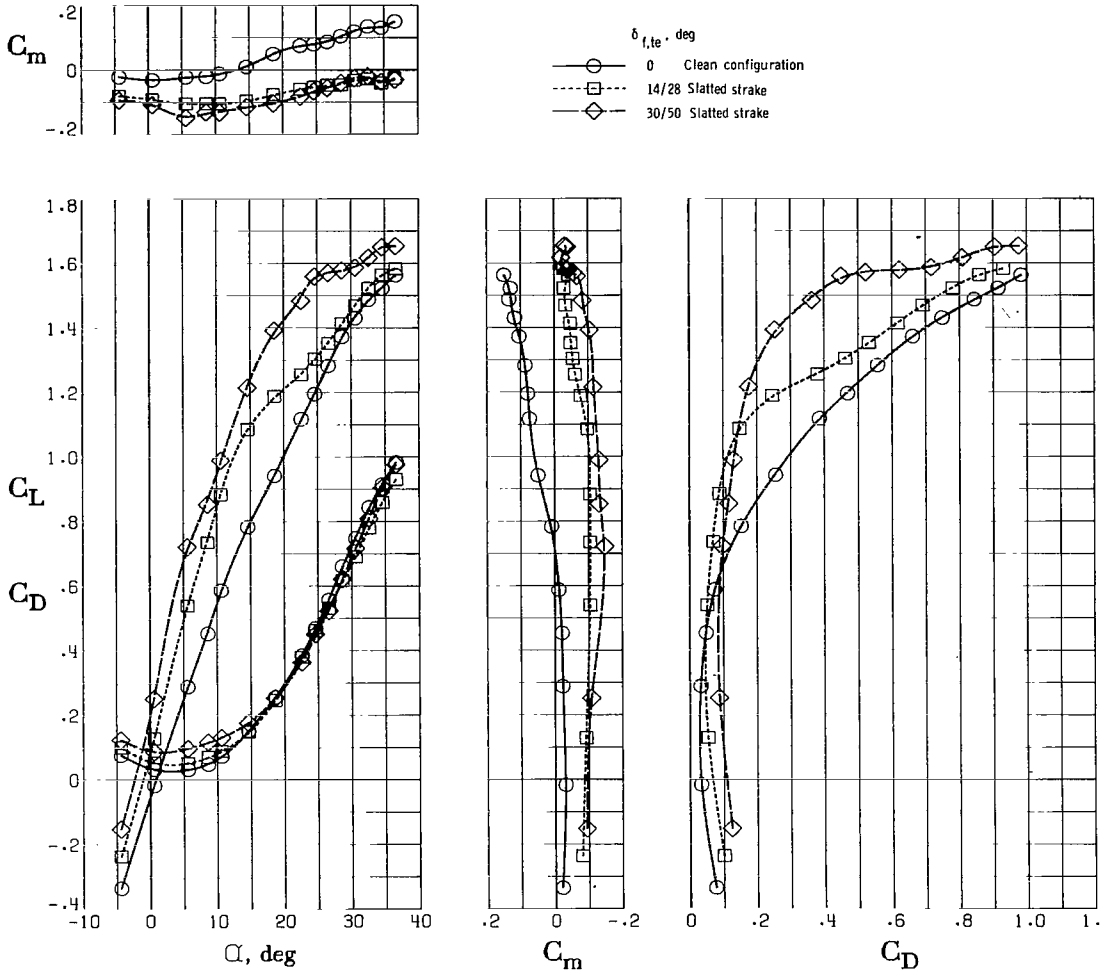

Figure 17.- Effect of high-lift devices for slatted strake and low tail. $i_t = 0^o$; $\Lambda = 20^o$; $\beta = 0^o$.

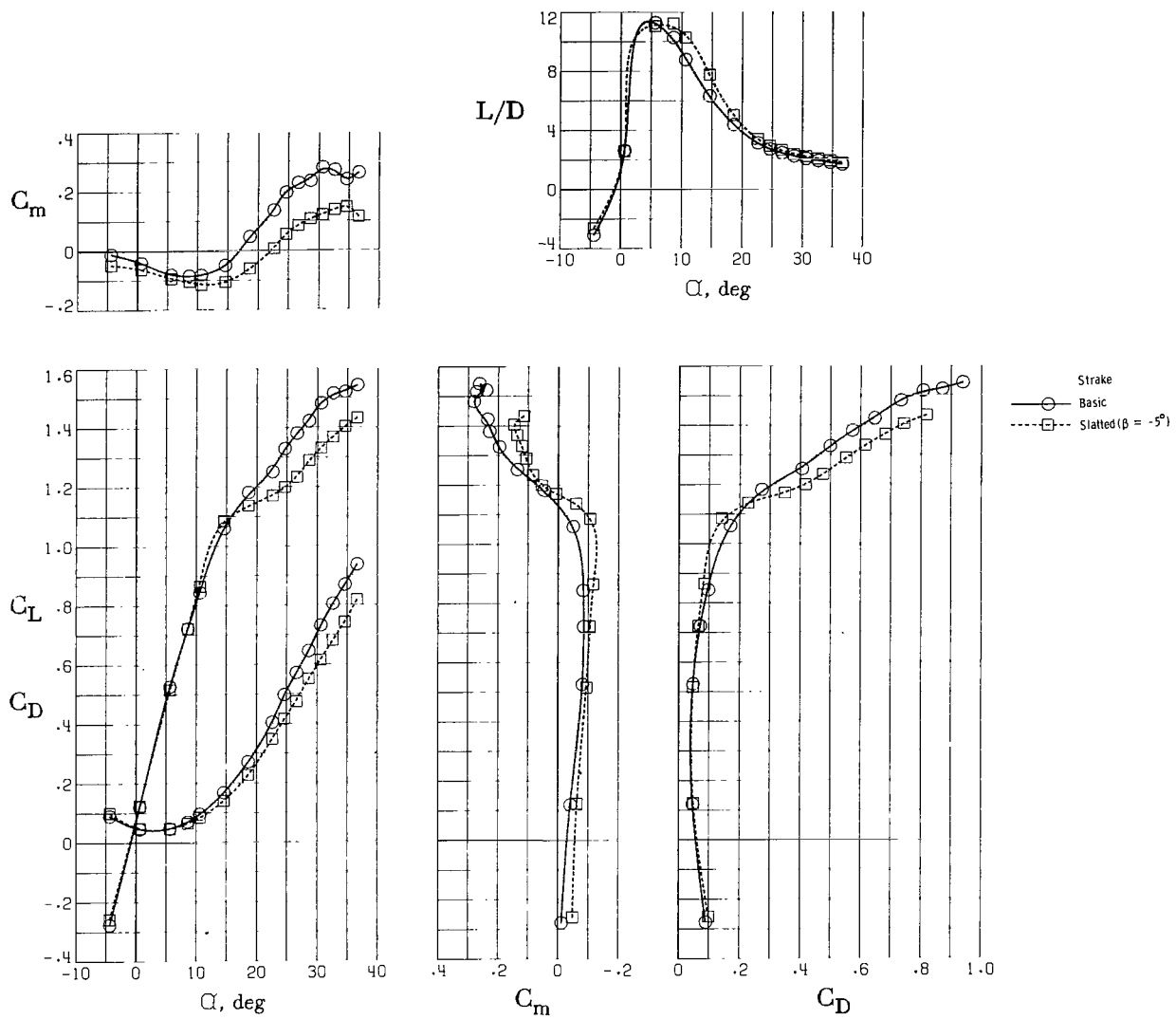

(a) T-tail; $\delta_{f,te}$ = 14°/28°.

Figure 18.- Effect of slatted strake. Λ = 20°; β = 0°.

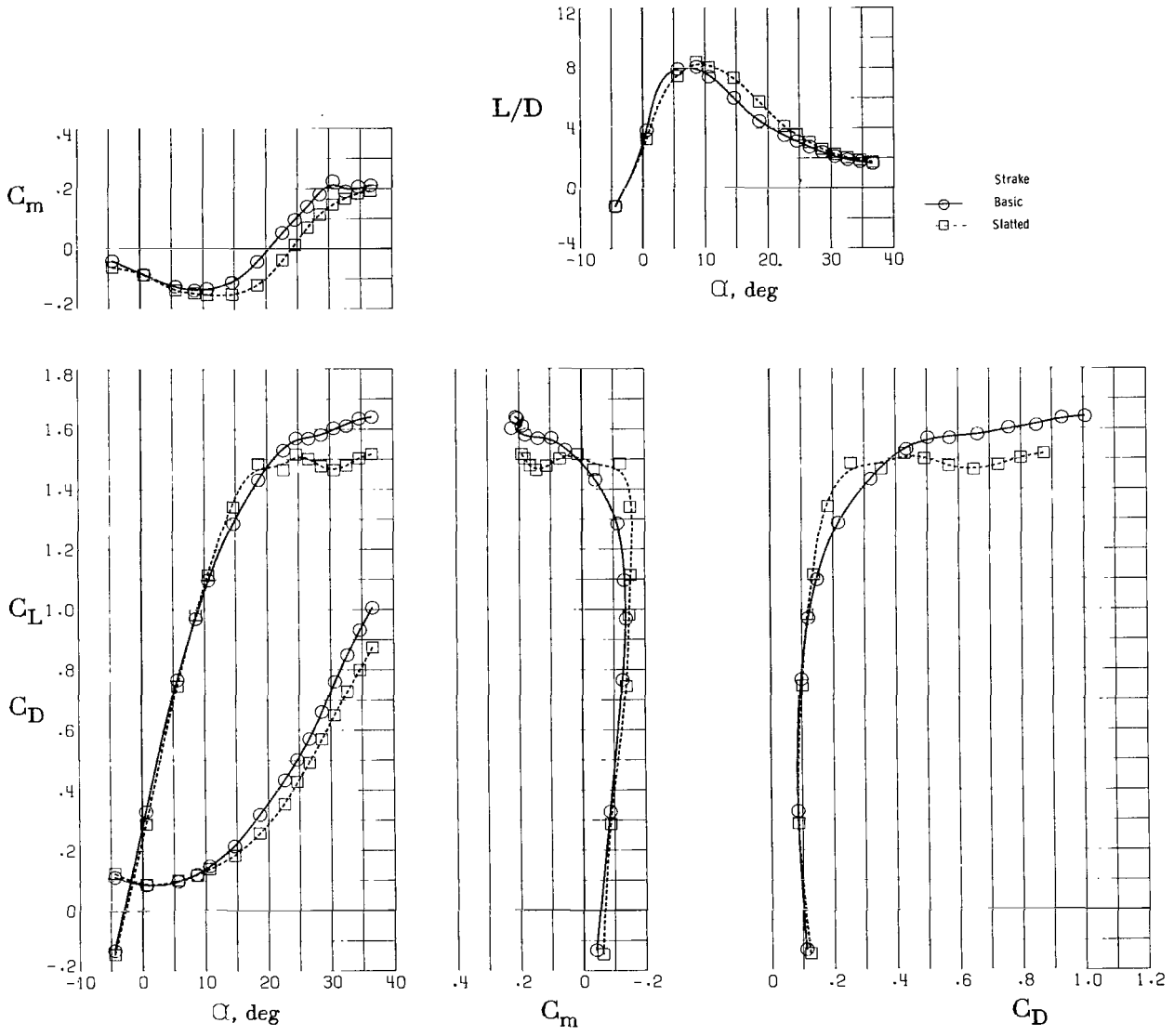

(b) T-tail; $\delta_{f,te}$ = 30°/50°.

Figure 18.- Concluded.

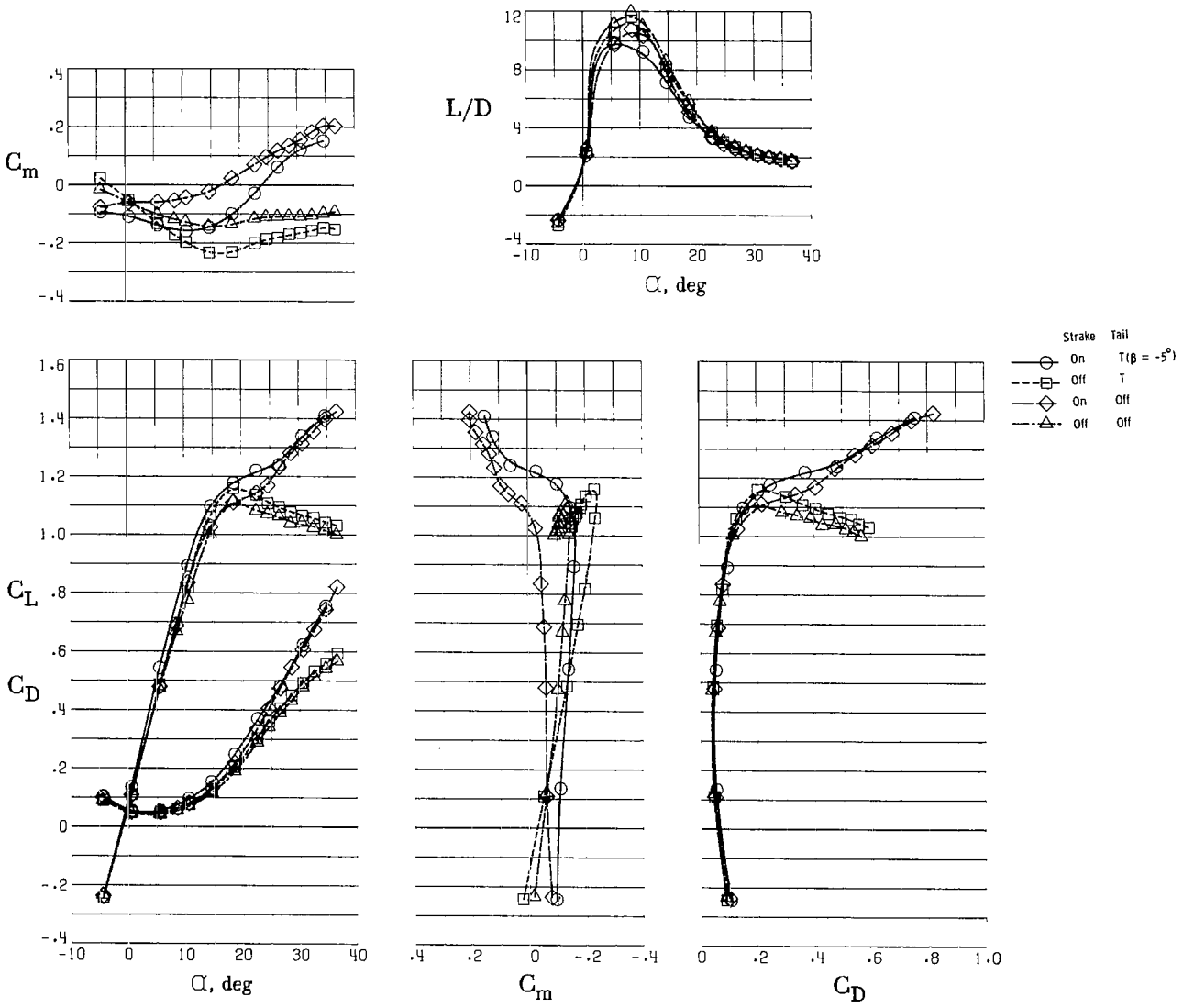

(a) $\delta_{f,te} = 14^o/28^o$.

Figure 19.- Effect of removing slatted strake. $i_t = 0^o$; $\Lambda = 20^o$; $\beta = 0^o$.

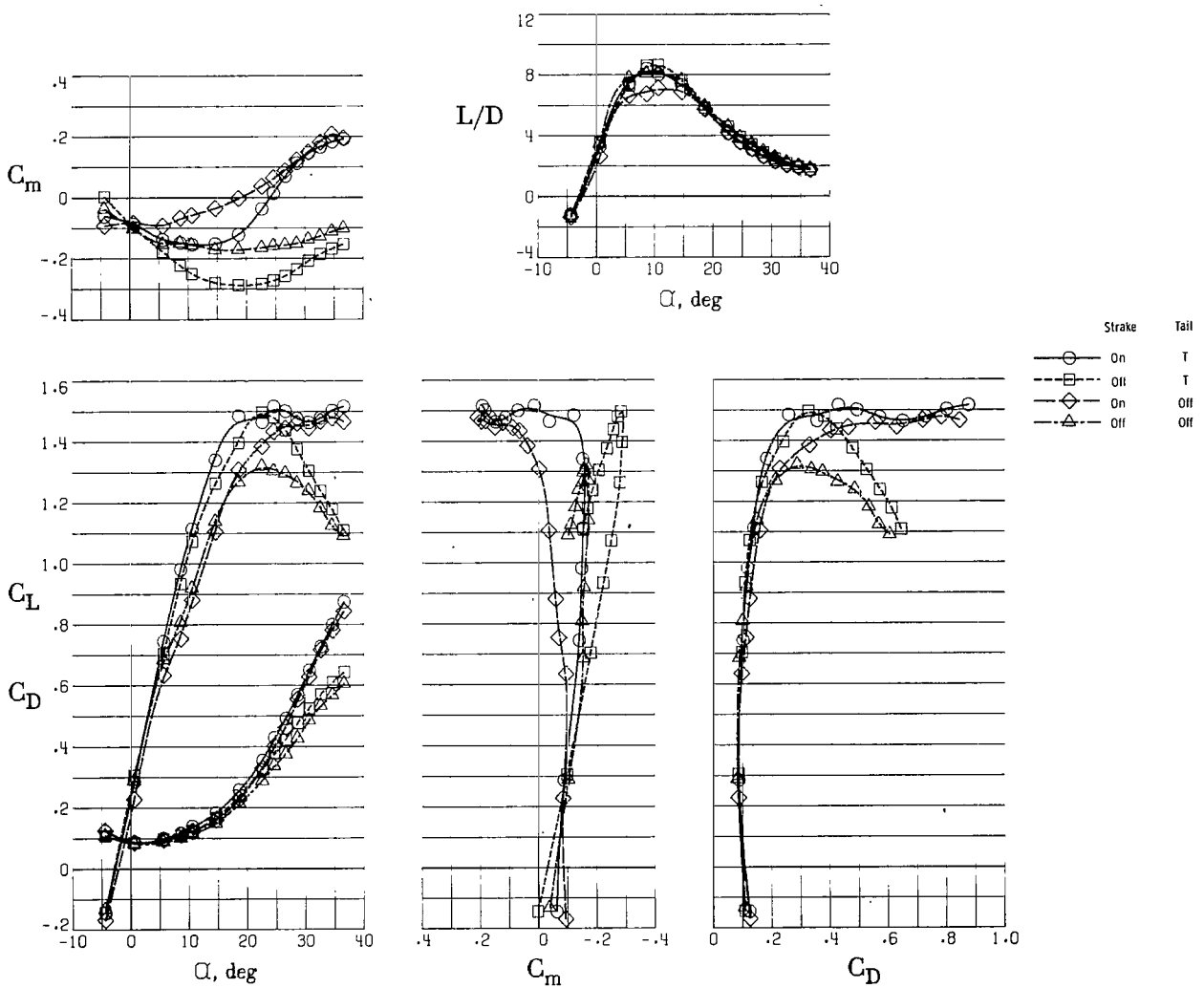

(b) $\delta_{f,te}$ = 30°/50°.

Figure 19.- Concluded.

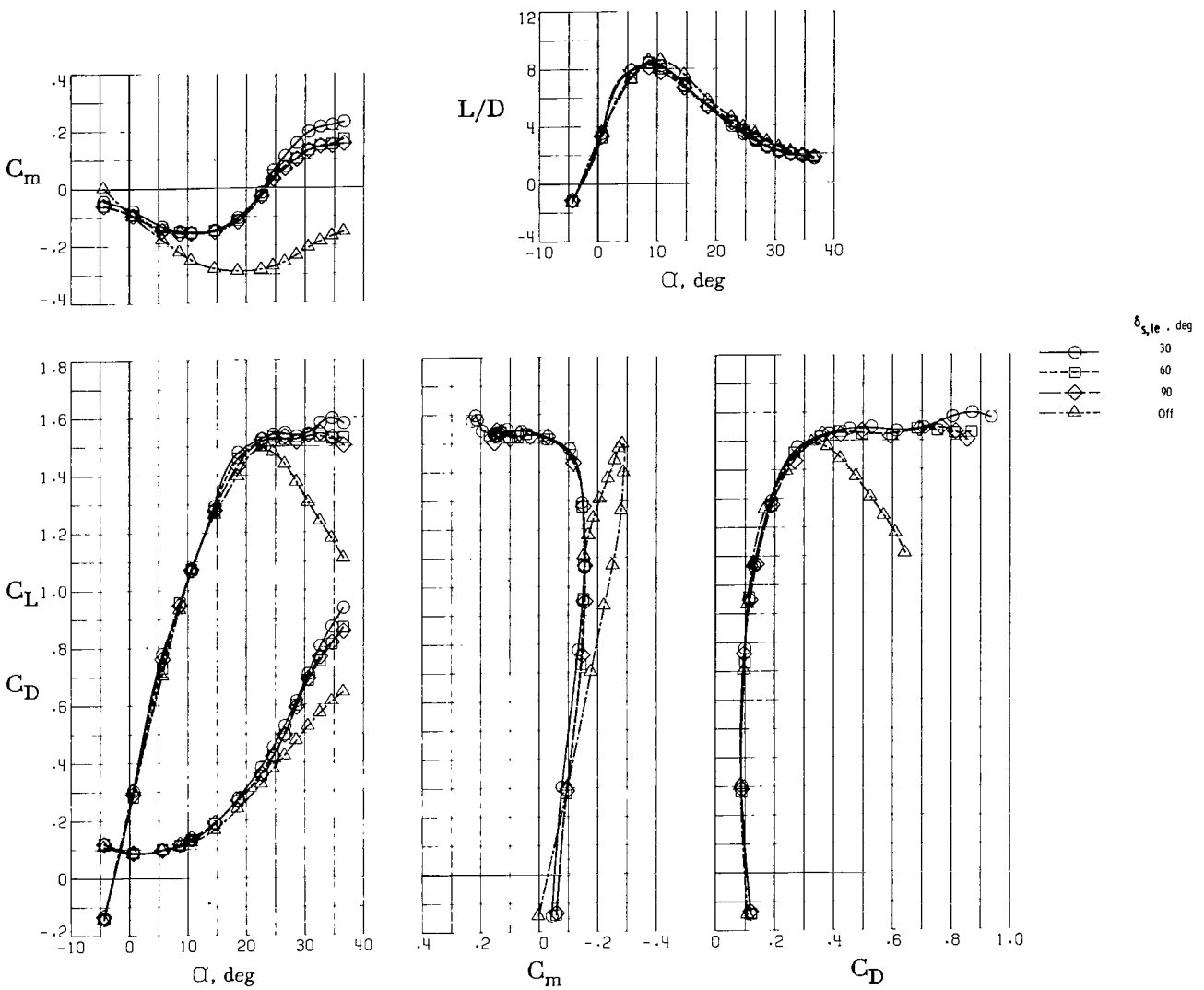

Figure 20.- Effect of strake leading-edge droop. $\delta_{f,te}$ = 30°/50°; T-tail; i_t = 0°; Λ = 20°; β = 0°.

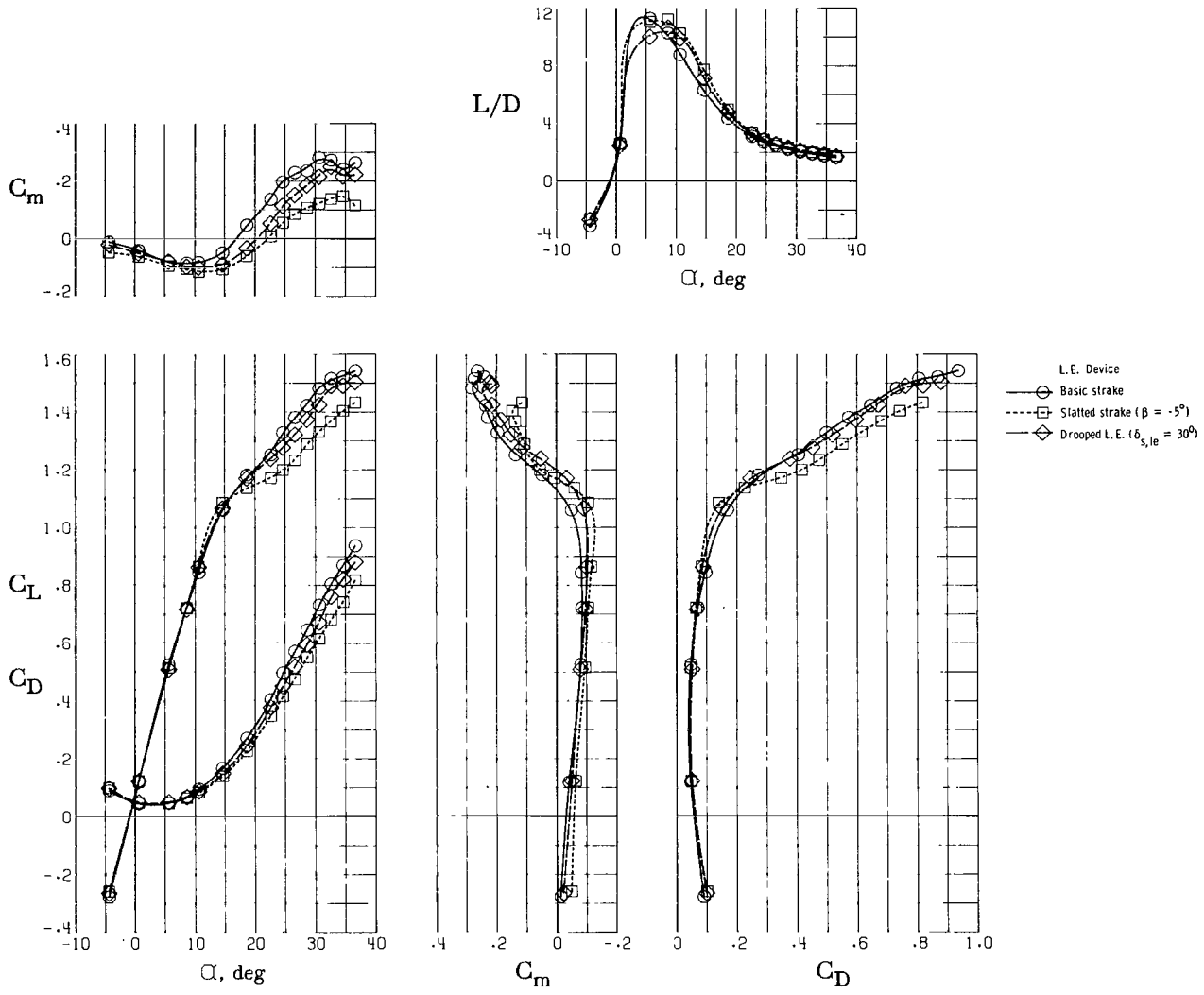

(a) $\delta_{f,te}$ = 14°/28°.

Figure 21.- Effect of strake leading-edge devices. T-tail; i_t = 0°; Λ = 20°; β = 0°.

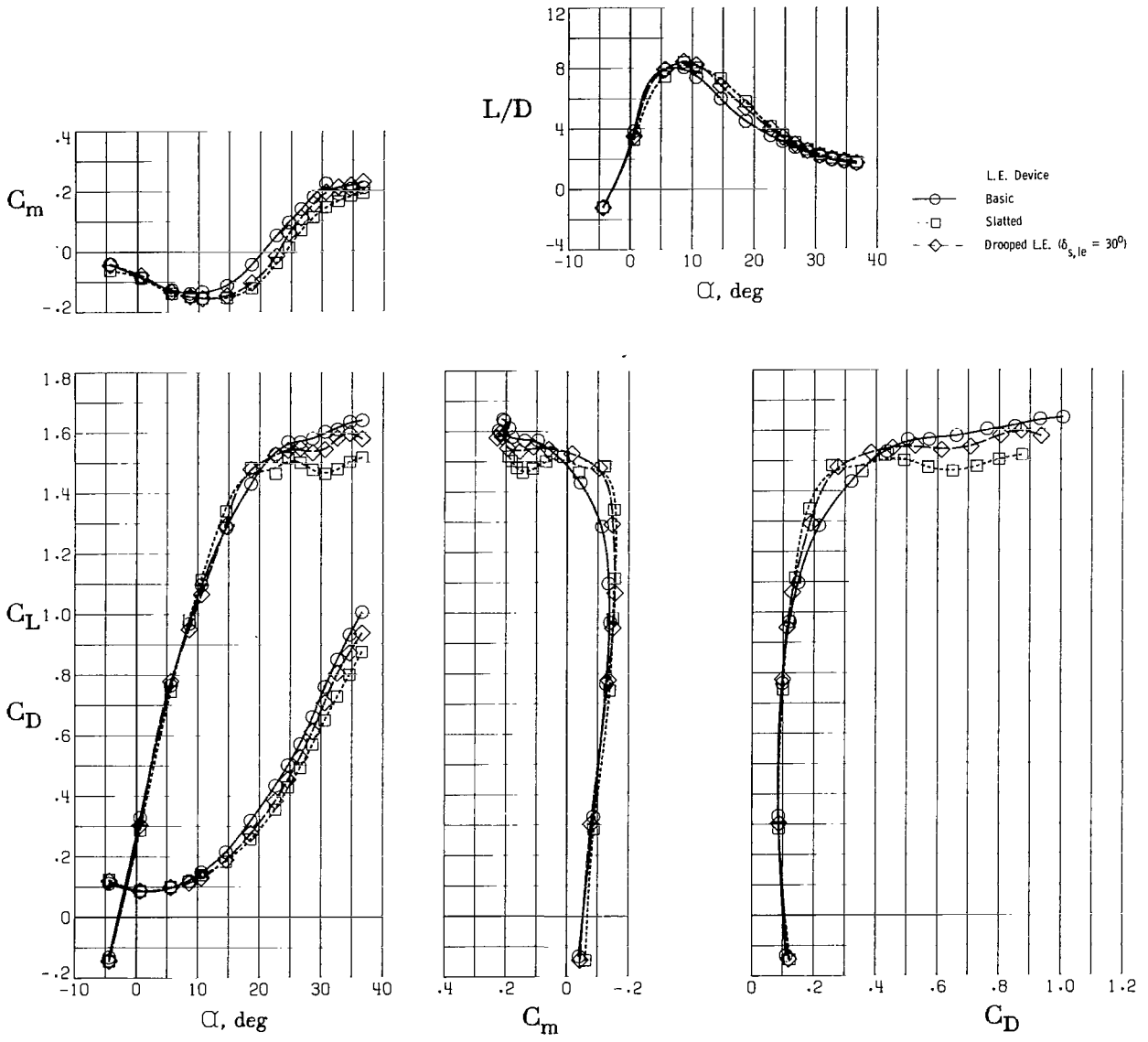

(b) $\delta_{f,te}$ = 30°/50°.

Figure 21.- Concluded.

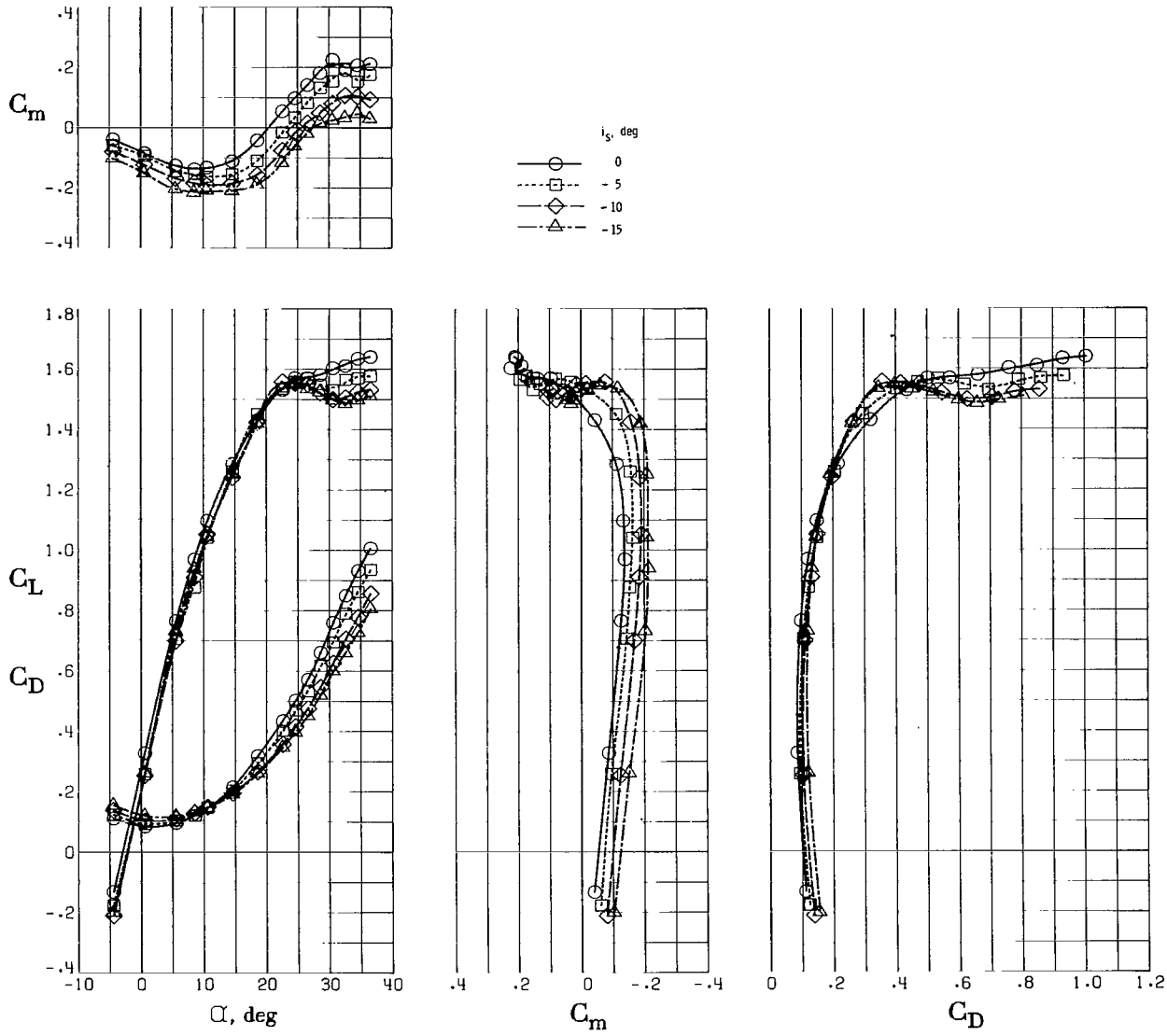

Figure 22.- Effect of strake incidence. $\delta_{f,te}$ = 30°/50°; T-tail; i_t = 0°; Λ = 20°; β = 0°.

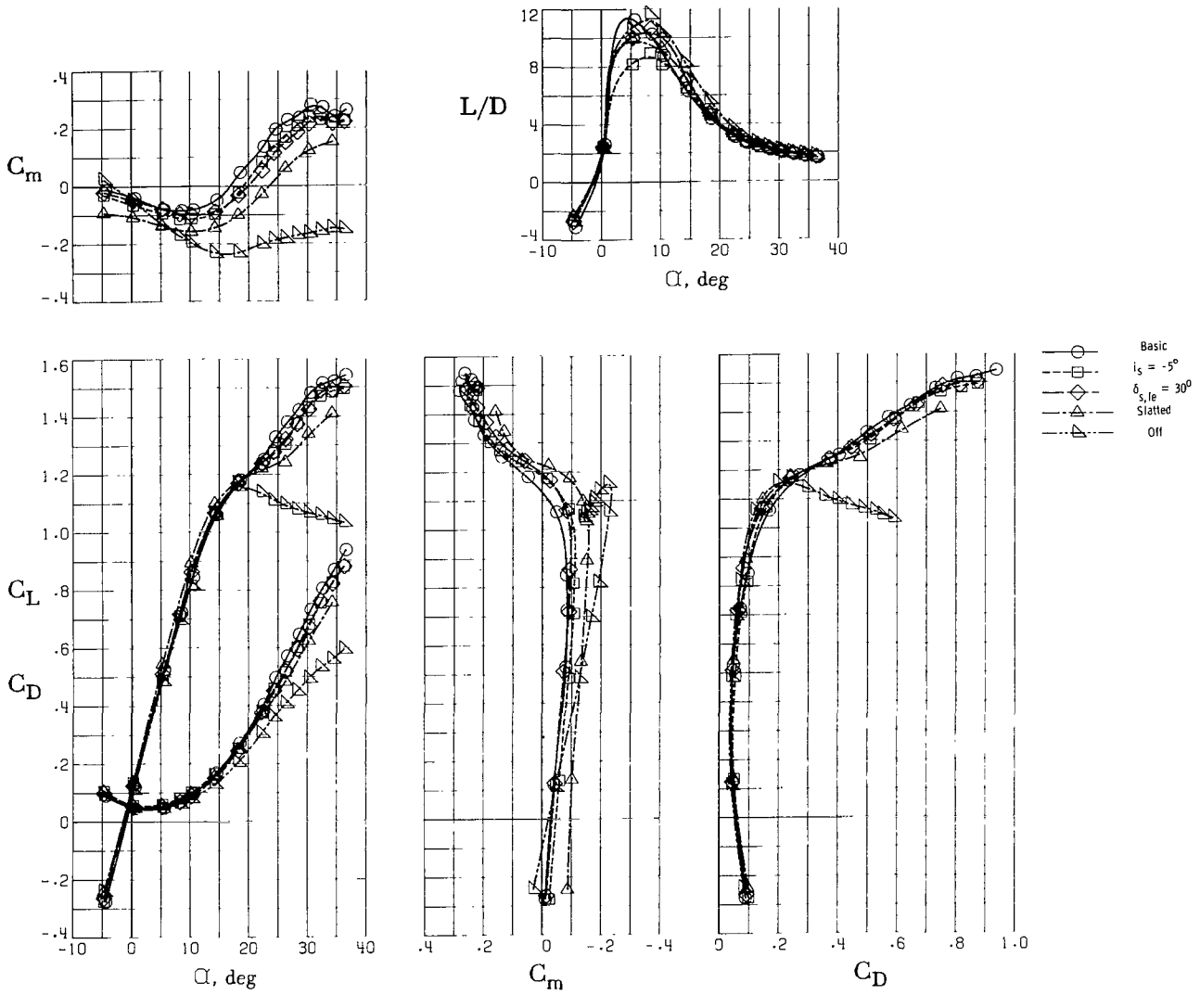

Figure 23.- Effect of strake leading-edge arrangement. $\delta_{f,te}$ = 14°/28°; T-tail; i_t = 0°; Λ = 20°; β = 0°.

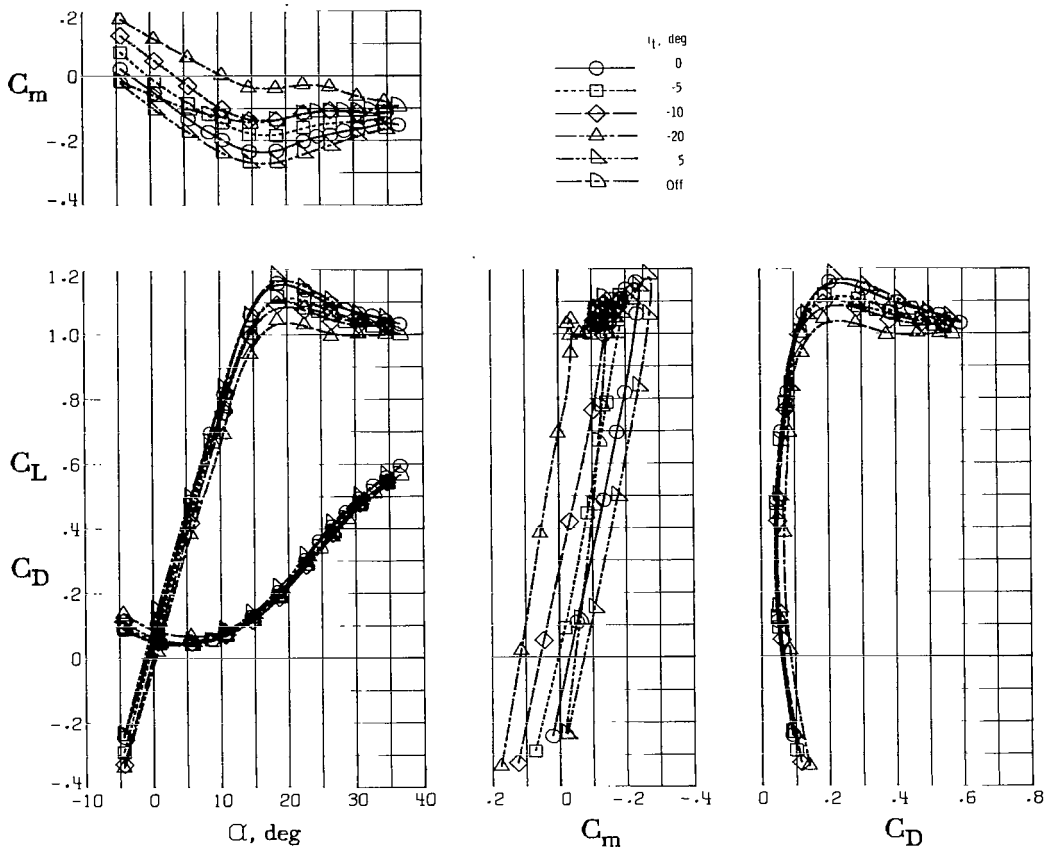

(a) $\delta_{f,te} = 14^o/28^o$.

Figure 24.- Effect of horizontal tail incidence with strake removed. T-tail; $\Lambda = 20^o$; $\beta = 0^o$.

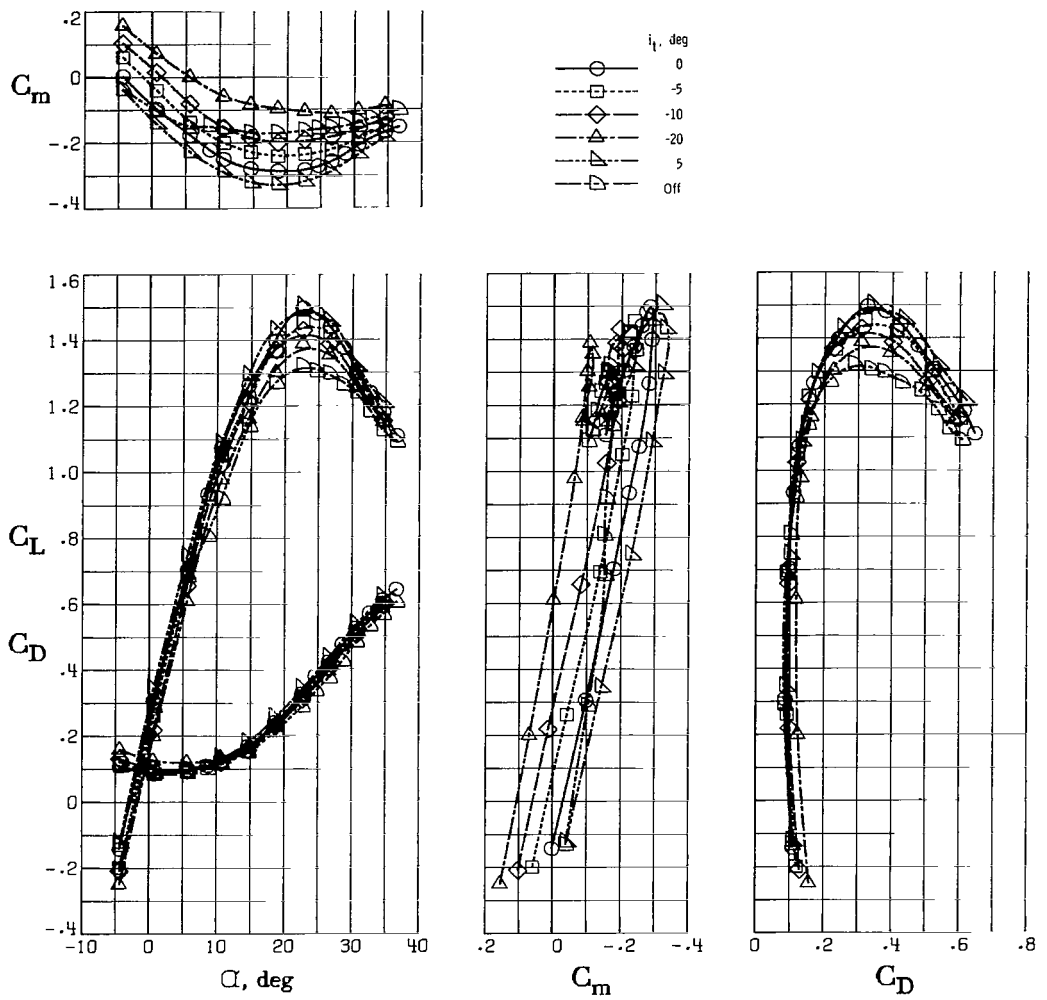

(b) $\delta_{f,te}$ = 30°/50°.

Figure 24.- Concluded.

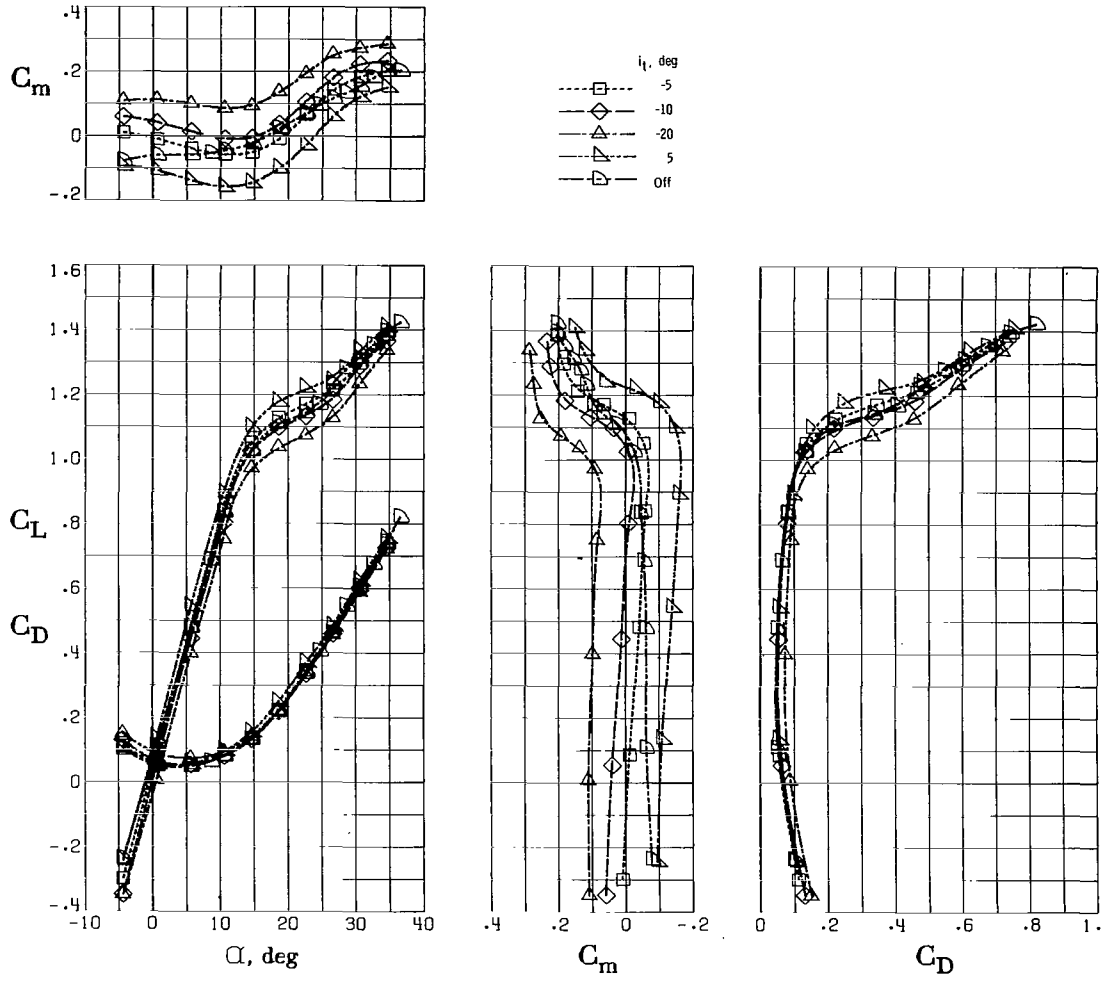

(a) $\delta_{f,te}$ = 14°/28°.

Figure 25.- Effect of horizontal tail incidence with slatted strake and T-tail. Λ = 20°; β = 0°.

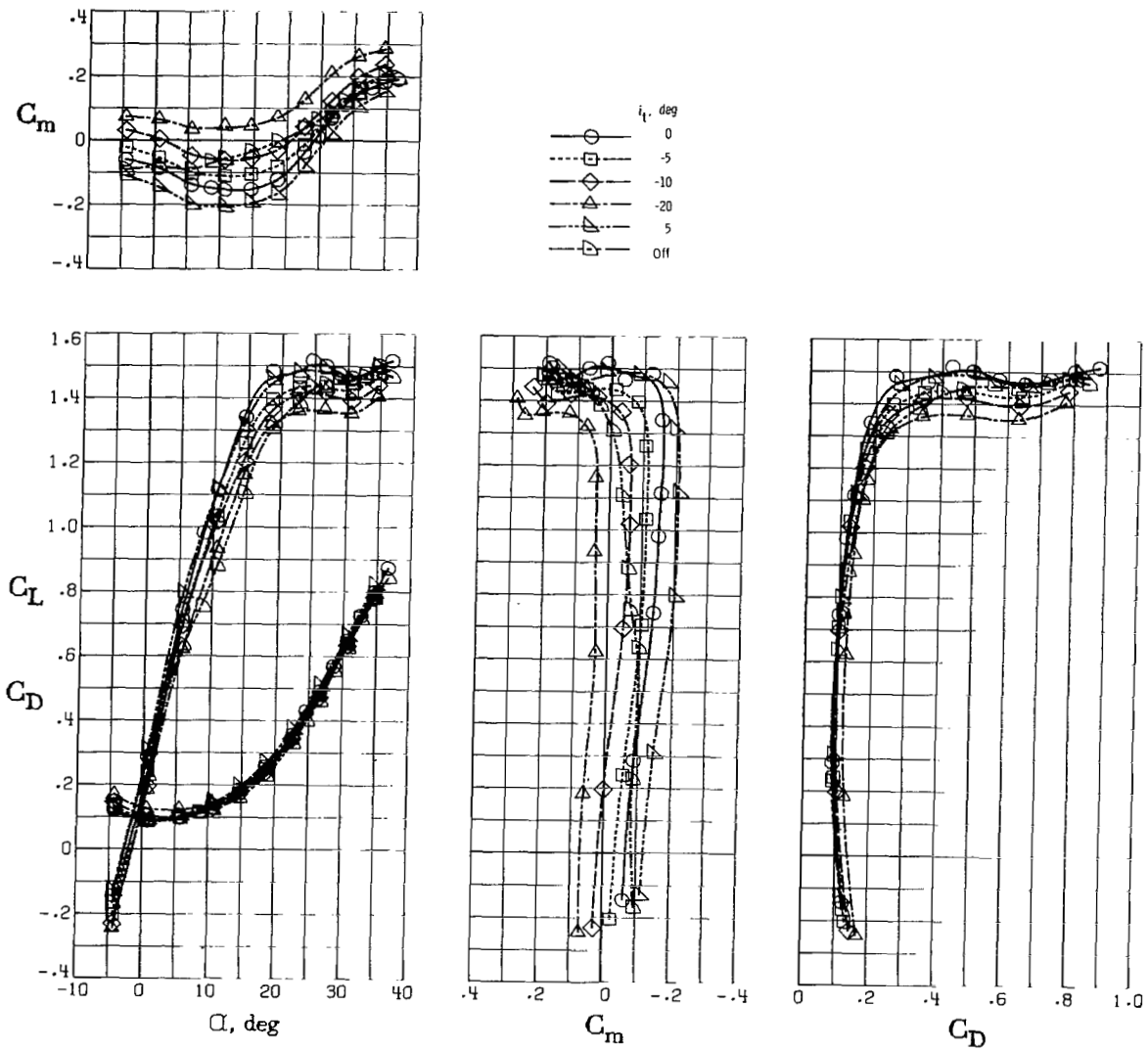

(b) $\delta_{f,te}$ = 30°/50°.

Figure 25.- Concluded.

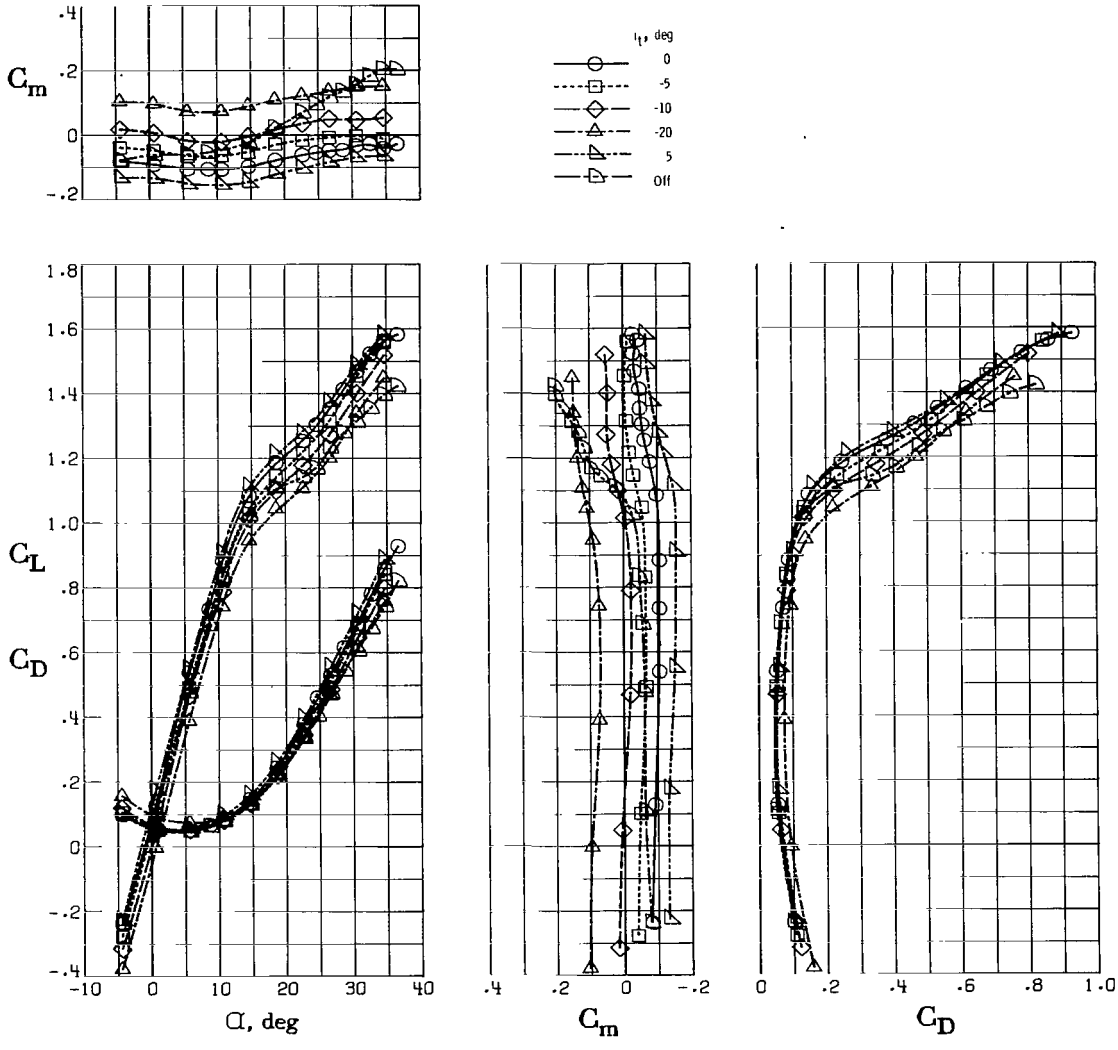

(a) $\delta_{f,te} = 14^o/28^o$.

Figure 26.- Effect of horizontal tail incidence with slatted strake and low tail. $\Lambda = 20^o$; $\beta = 0^o$.

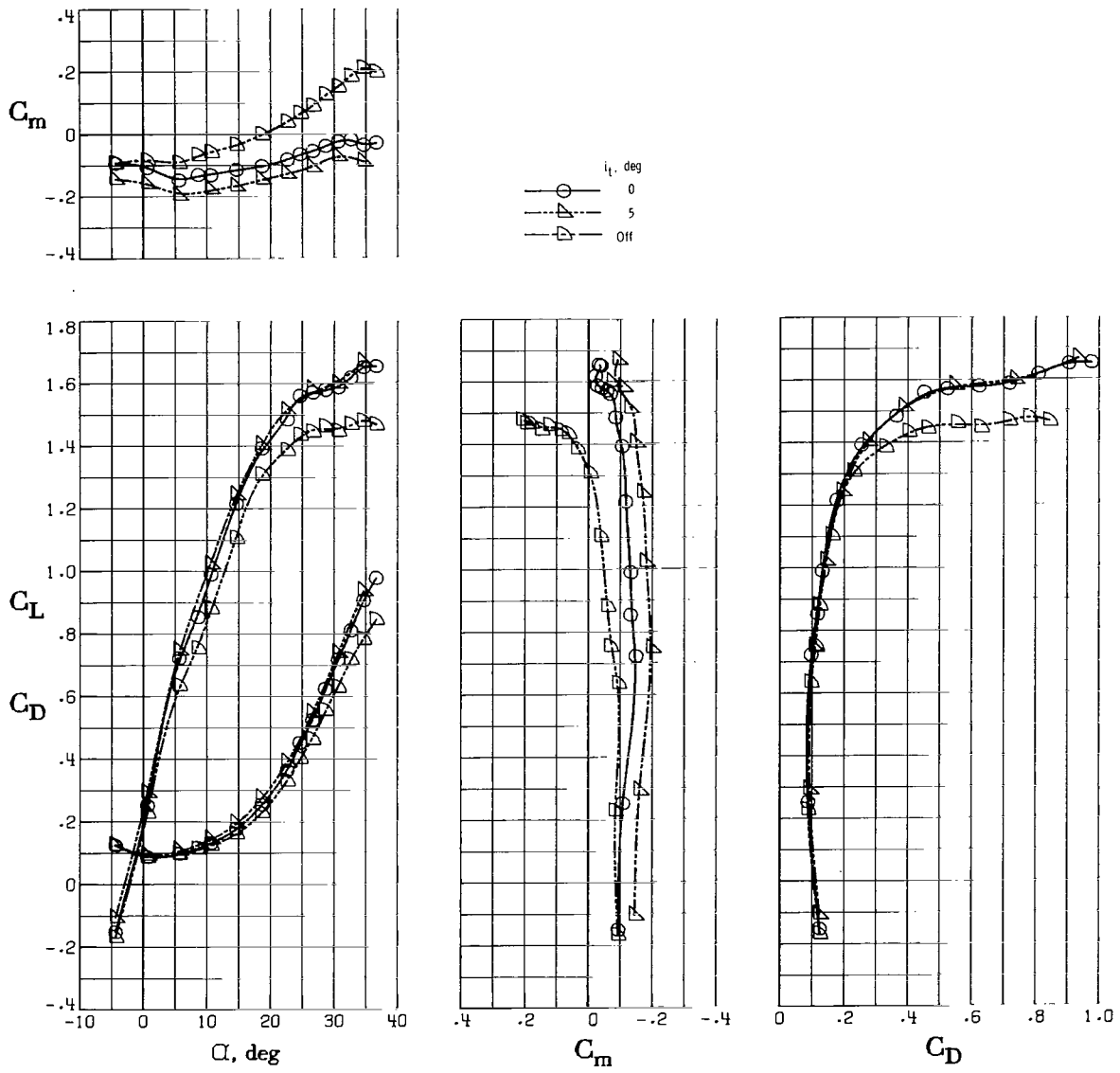

(b) $\delta_{f,te} = 30^o/50^o$.

Figure 26.- Concluded.

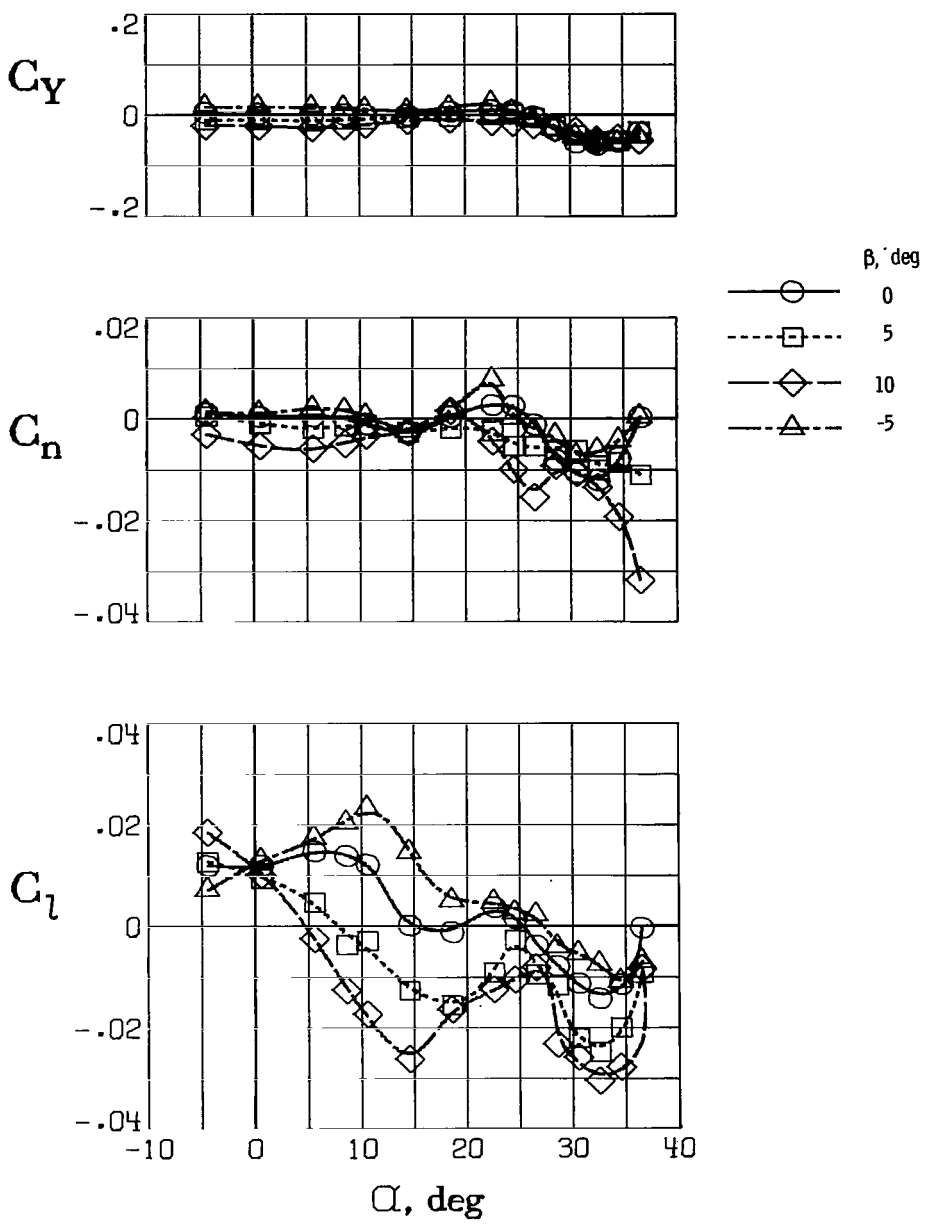

(a) $\Lambda = 20^{\circ}$.

Figure 27.- Lateral-directional characteristics of clean wing configuration with horizontal tail removed.

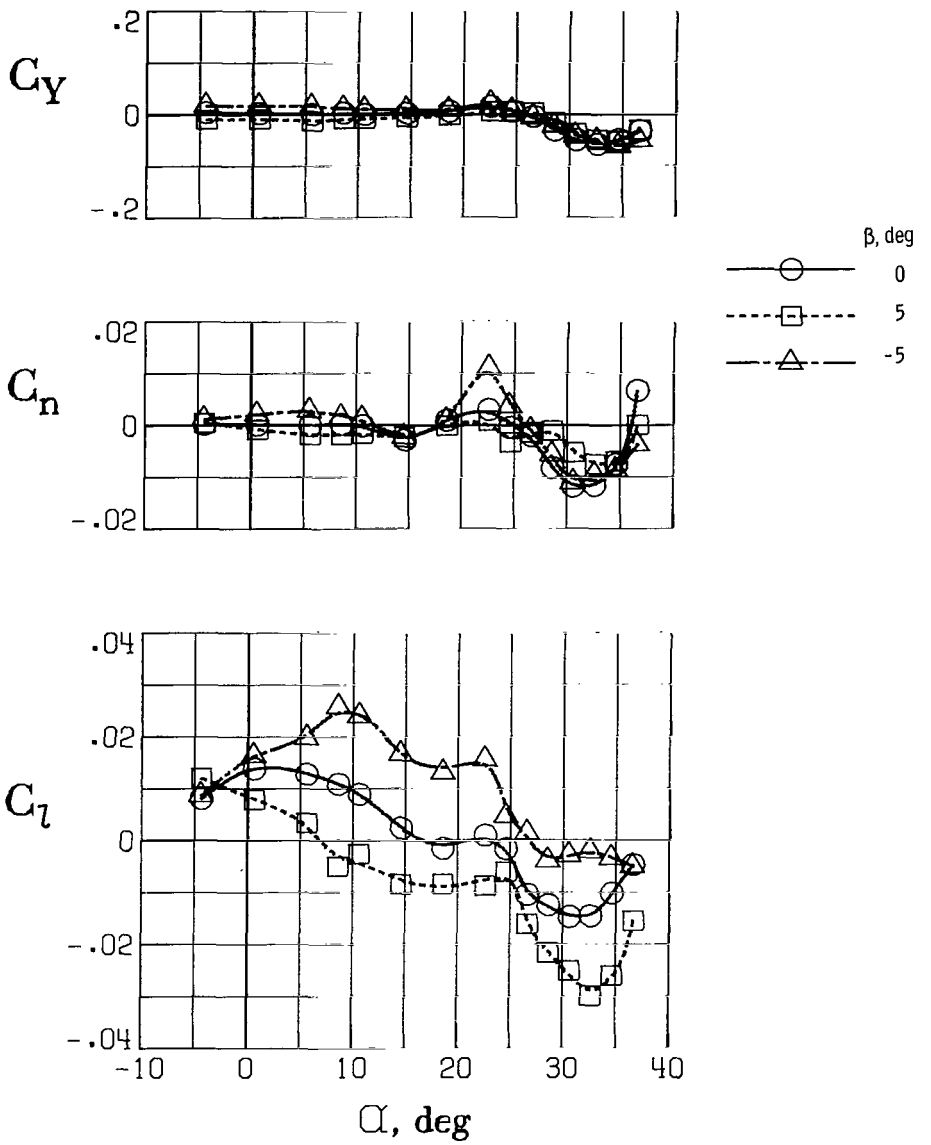

(b) $\Lambda = 30^{\circ}$.

Figure 27.- Continued.

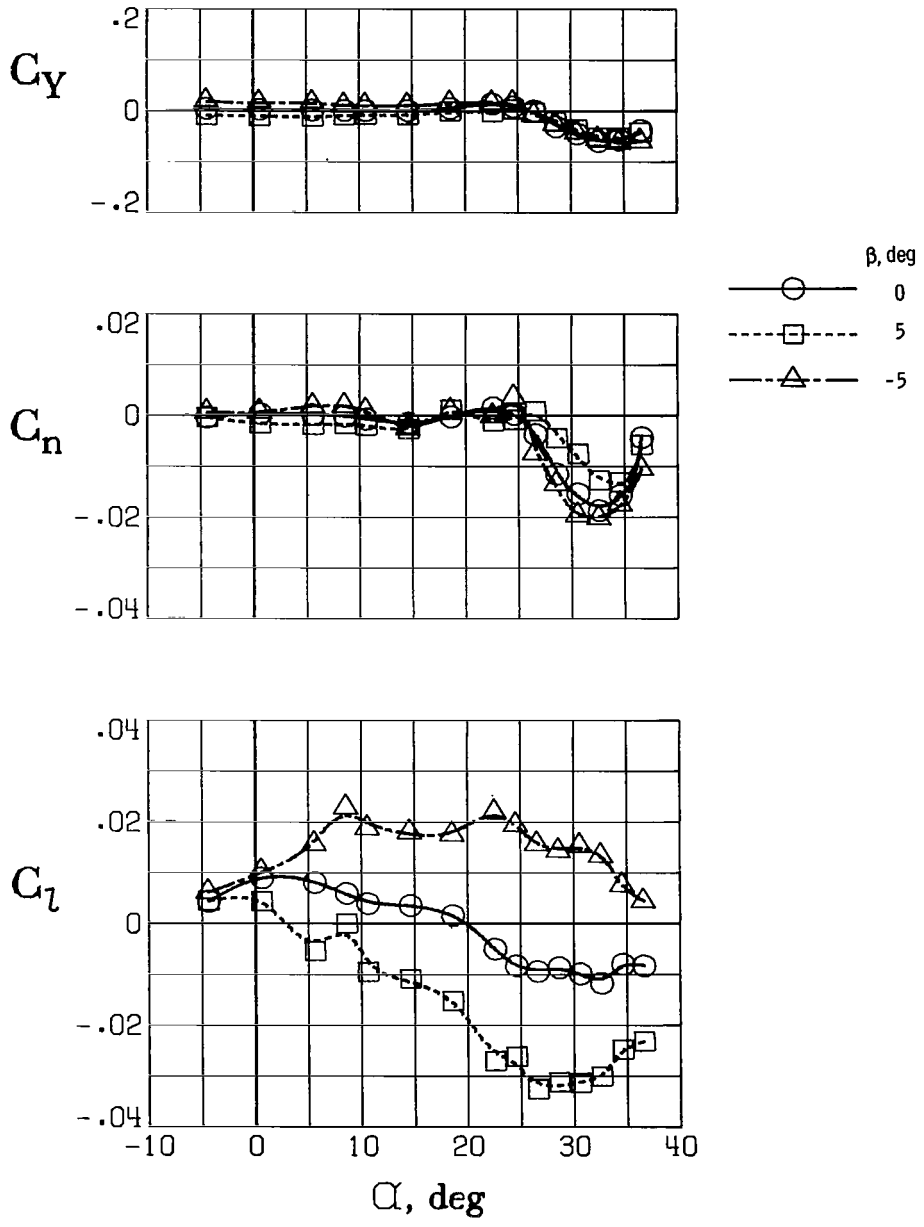

(c) $\Lambda = 42^{\circ}$.

Figure 27.- Continued.

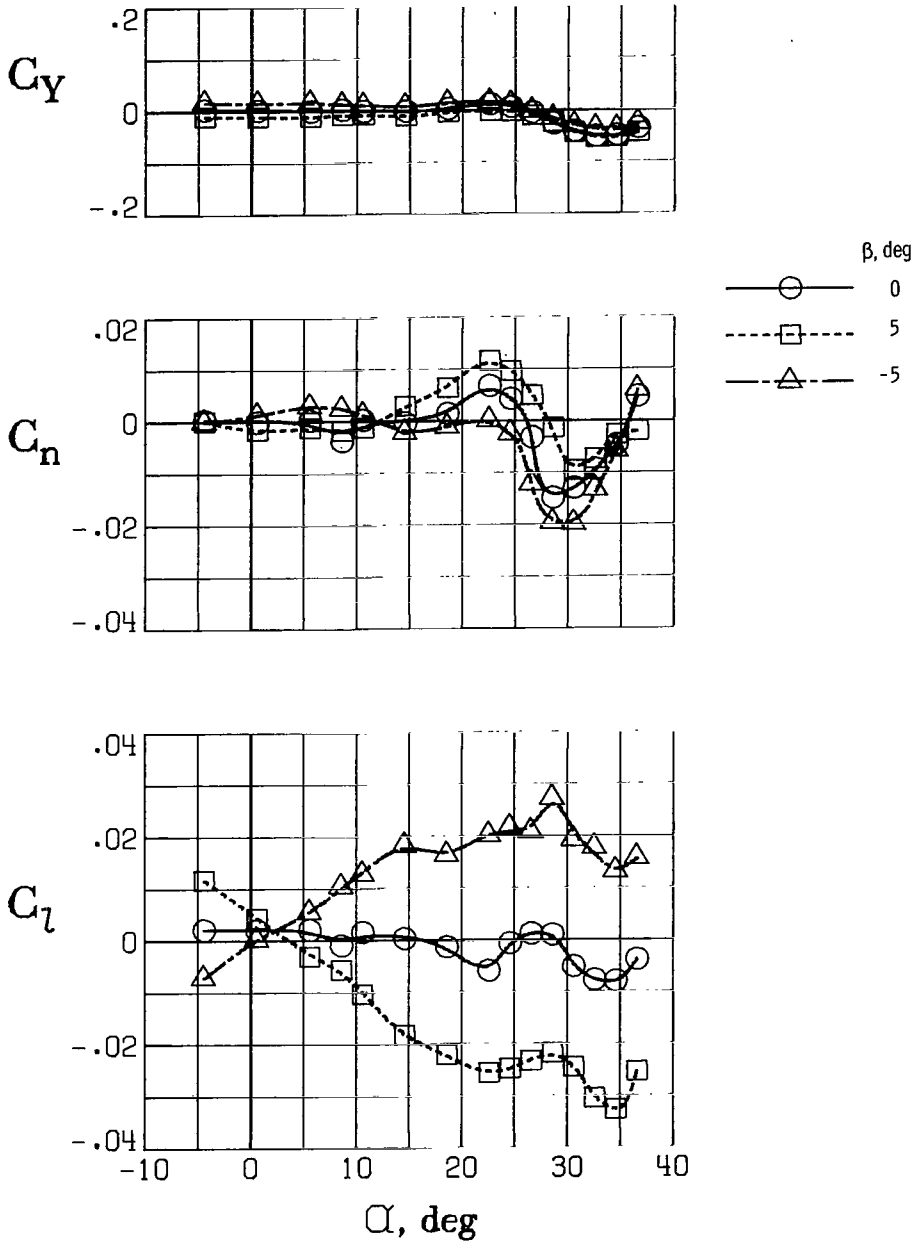

(d) $\Lambda = 72^{\circ}$.

Figure 27.- Concluded.

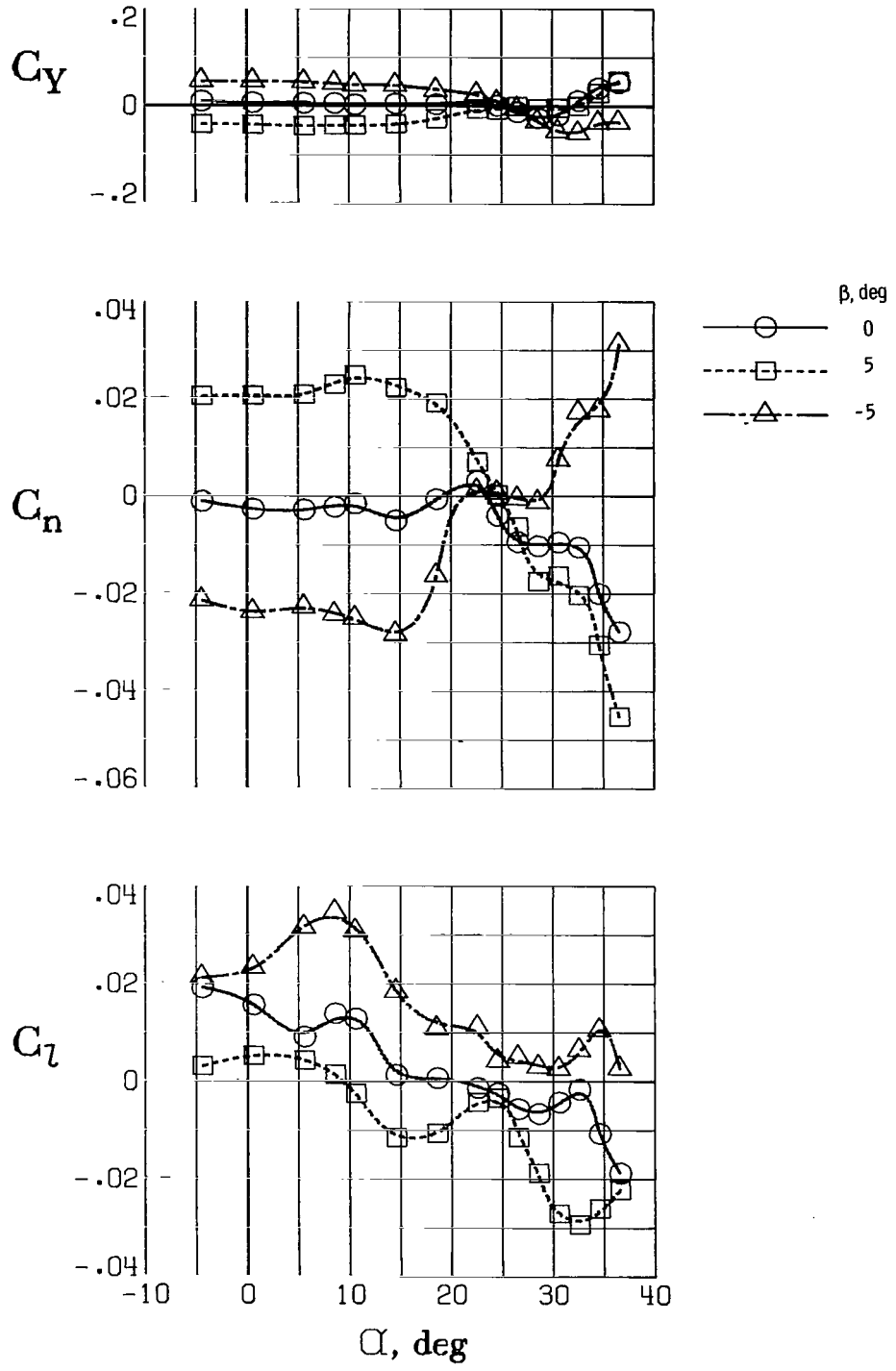

(a) $\Lambda = 20^{\circ}$.

Figure 28.- Lateral-directional characteristics of clean wing configuration with T-tail. $i_t = 0^{\circ}$.

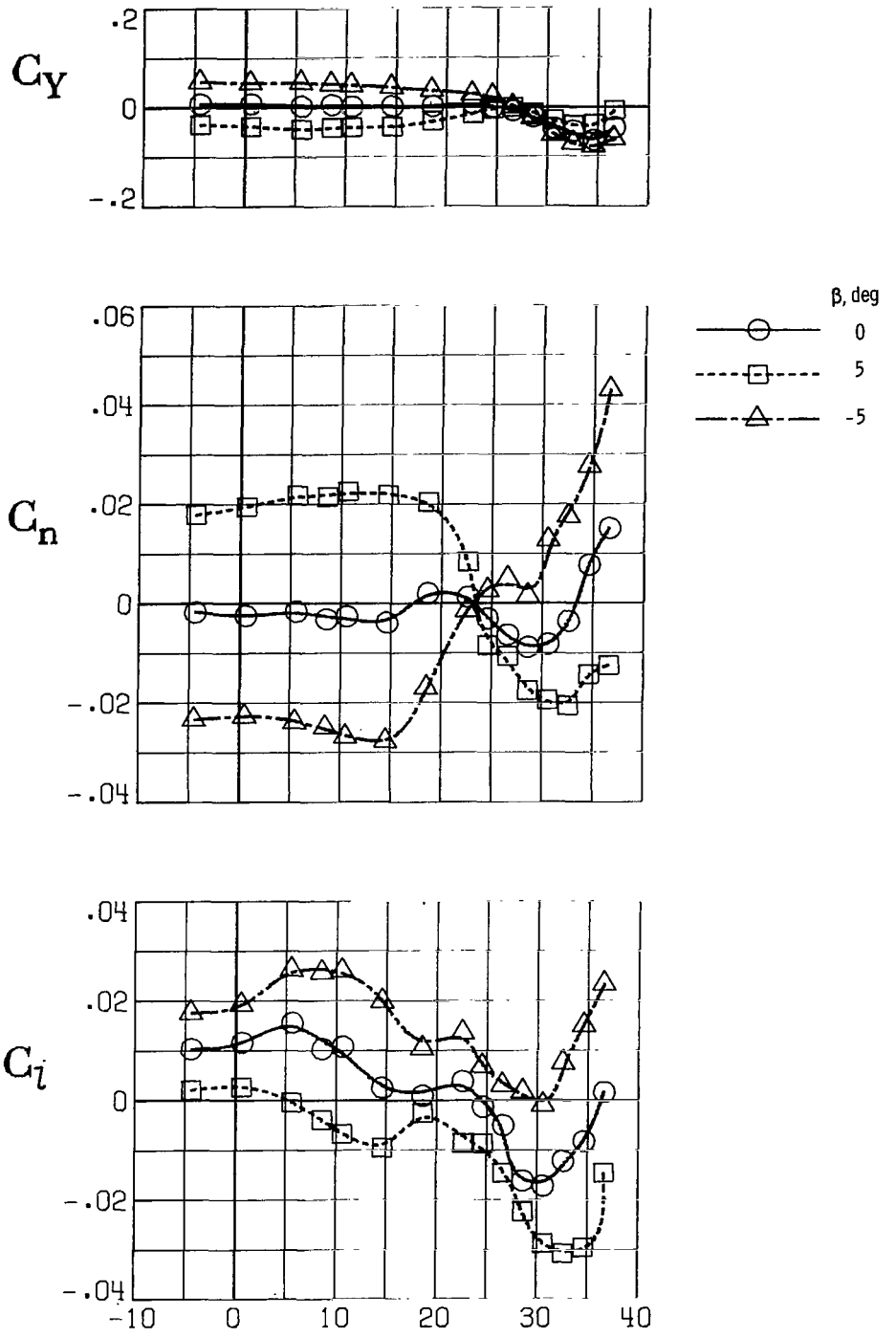

(b) $\Lambda = 30°$.

Figure 28.- Continued.

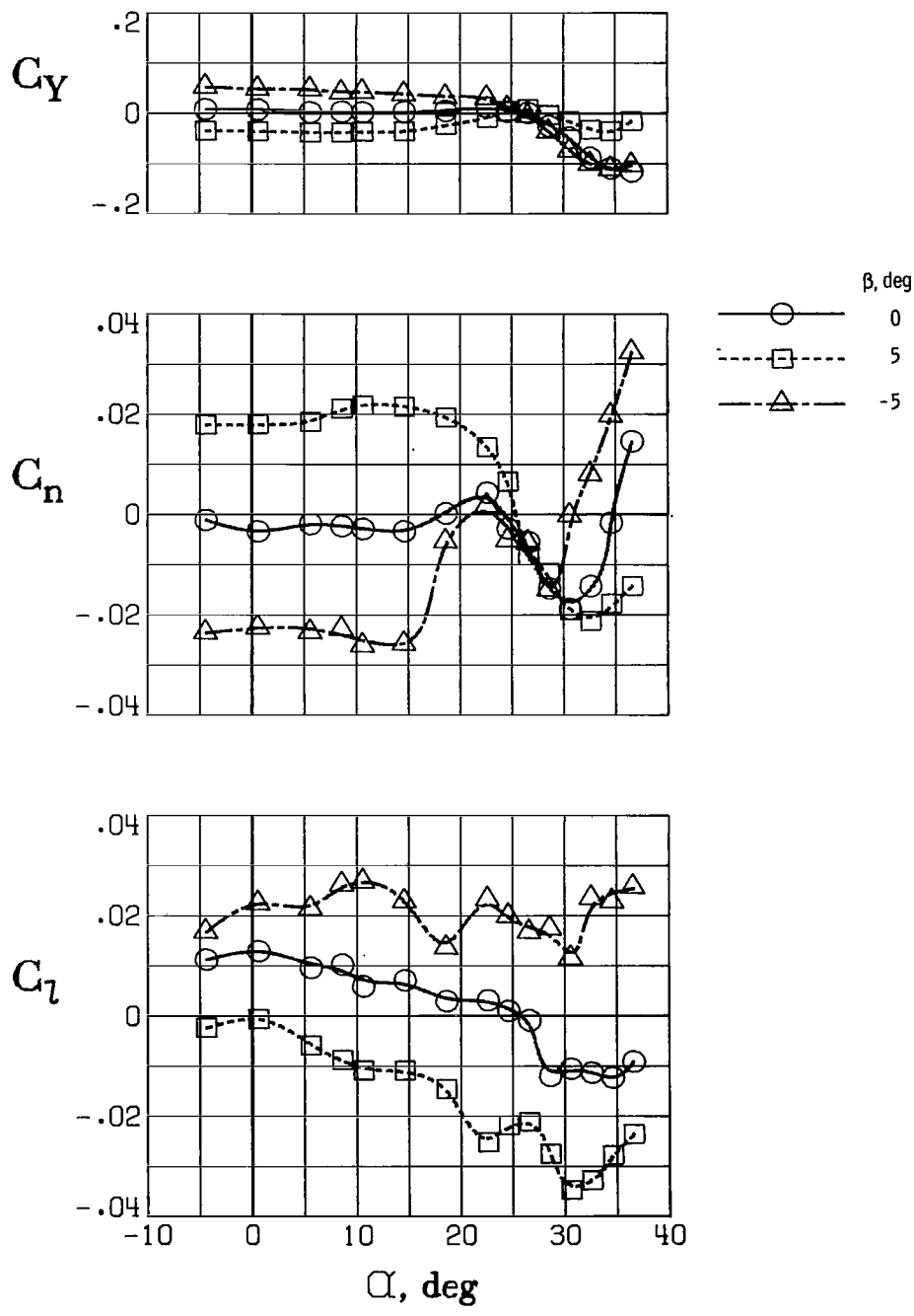

(c) $\Lambda = 42^{\circ}$.

Figure 28.- Continued.

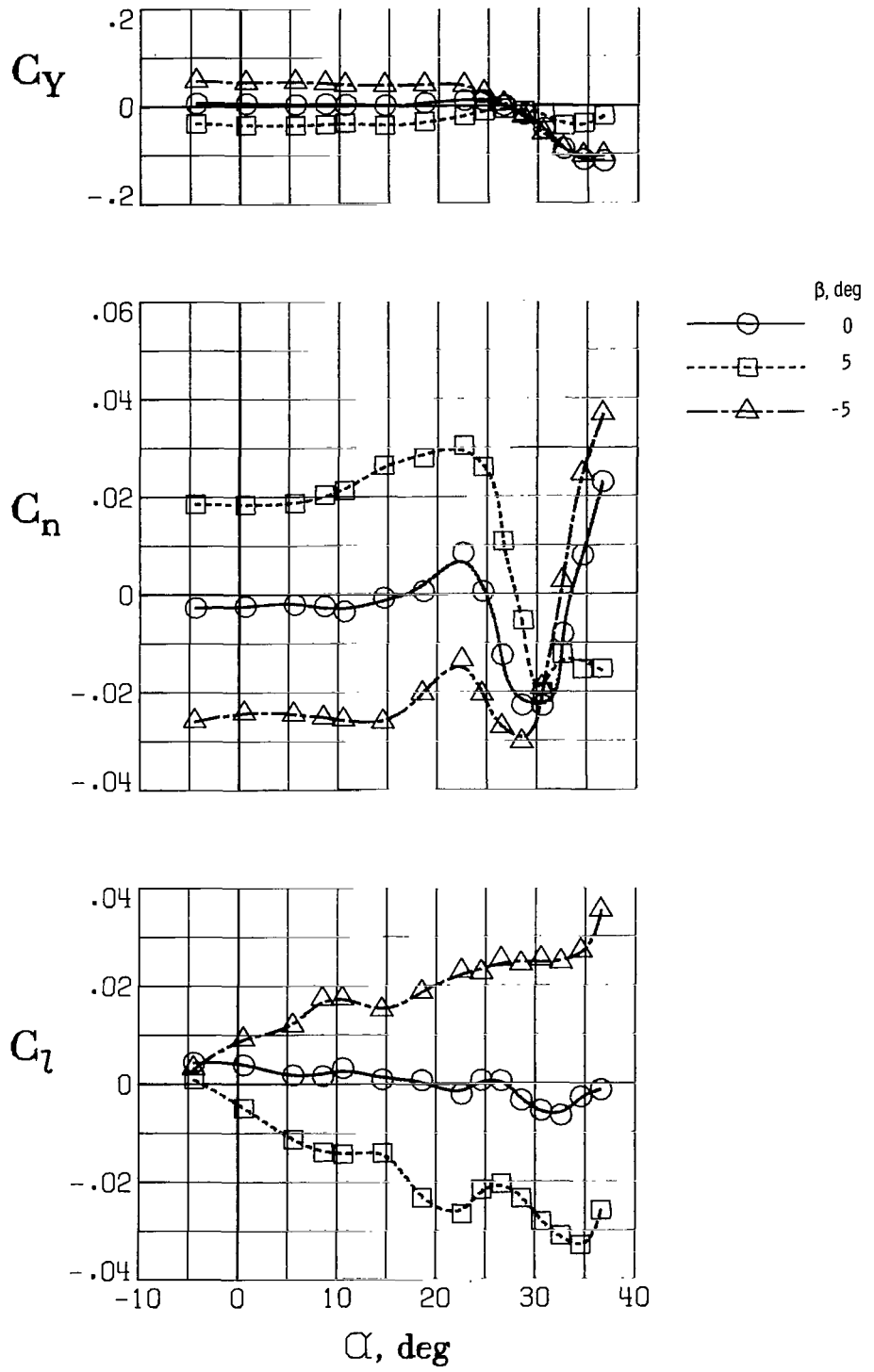

(d) $\Lambda = 72^{\circ}$.

Figure 28.- Concluded.

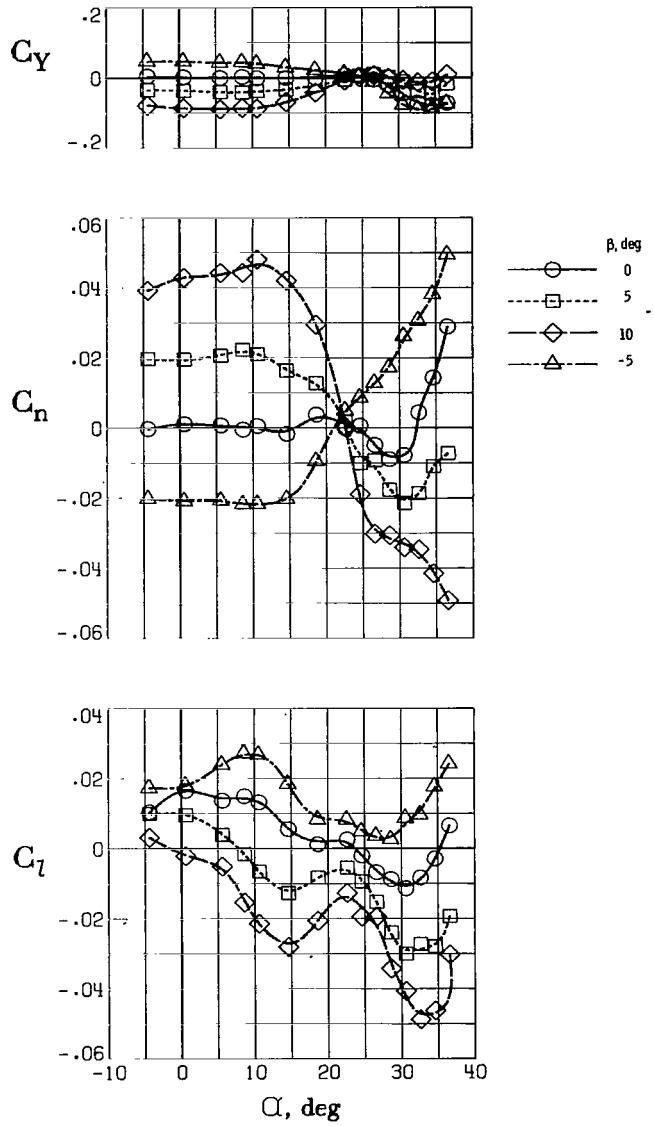

(a) $\Lambda = 20^{\circ}$.

Figure 29.- Lateral-directional characteristics of clean wing configuration with low tail. $i_t = 0^{\circ}$.

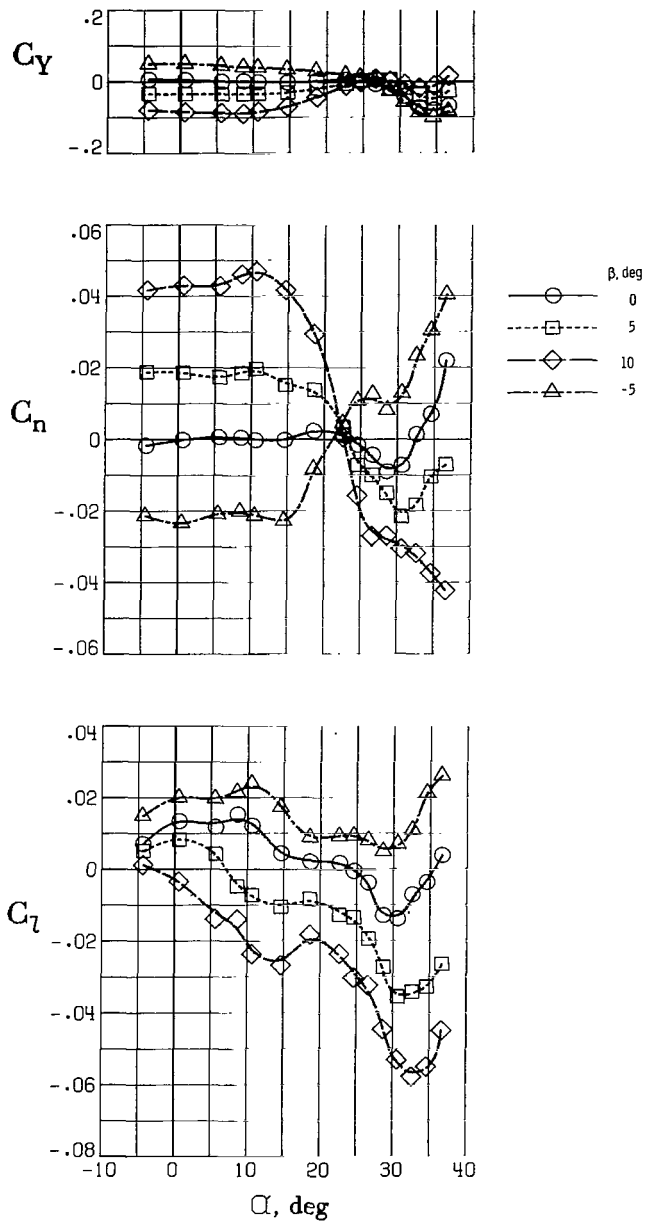

(b) $\Lambda = 30^\circ$.

Figure 29.- Continued.

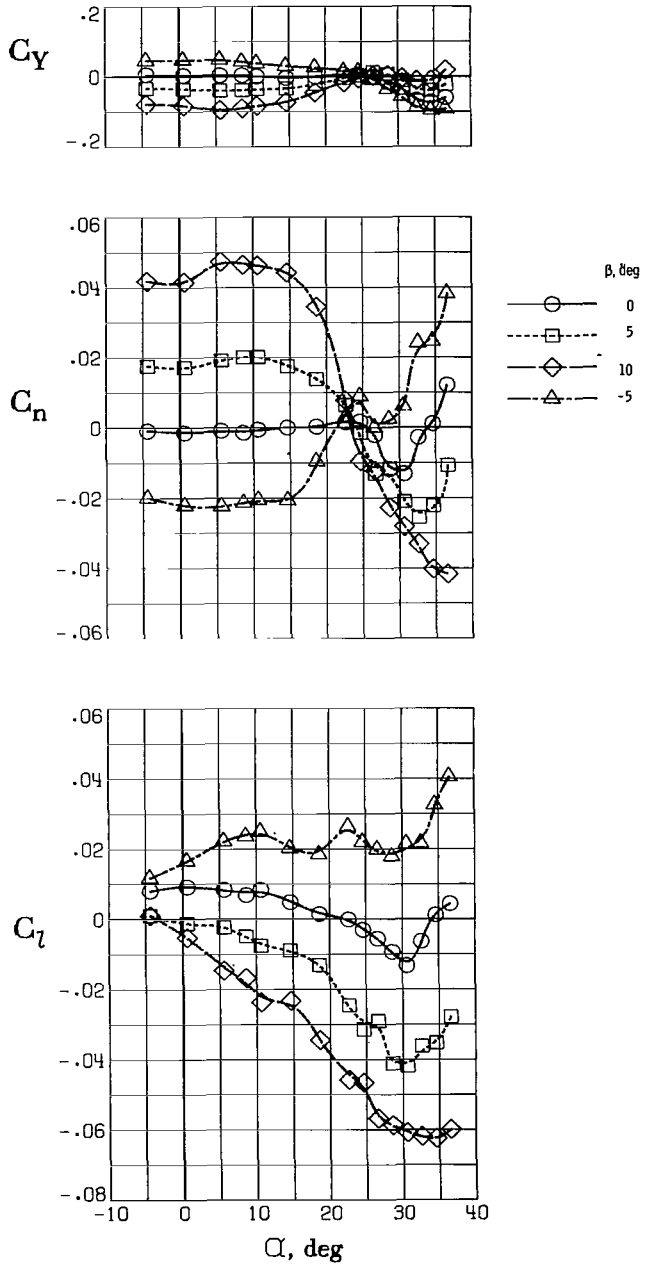

(c) $\Lambda = 42^{\circ}$.

Figure 29.- Continued.

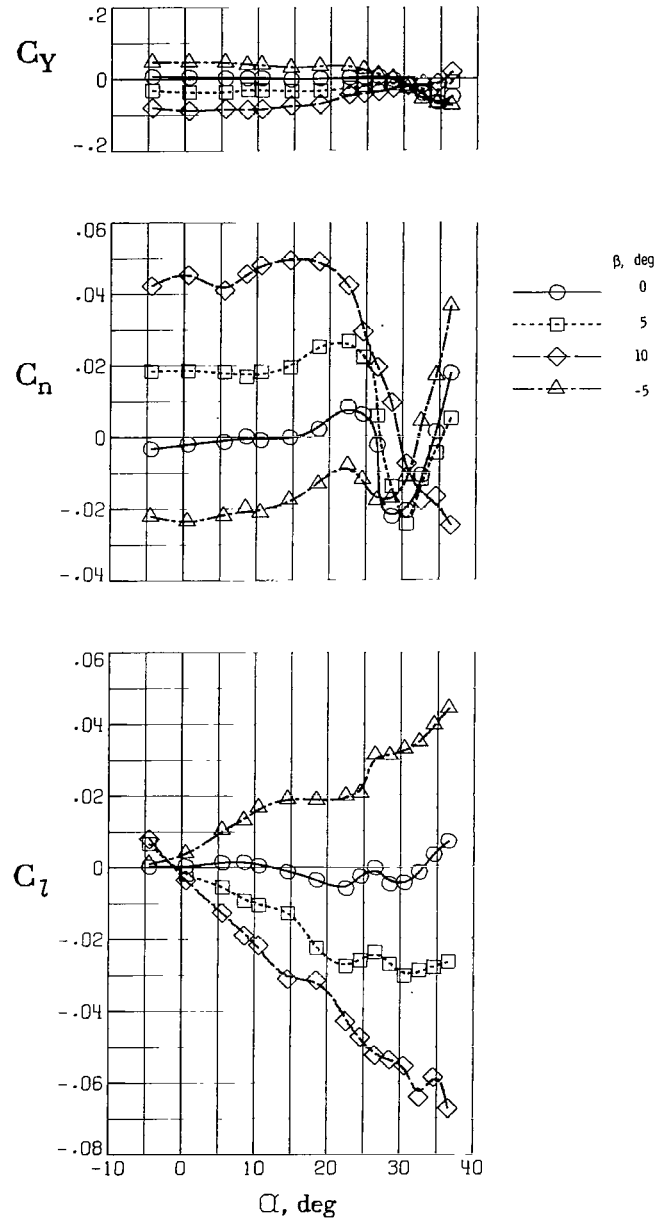

(d) $\Lambda = 72^{\circ}$.

Figure 29.- Concluded.

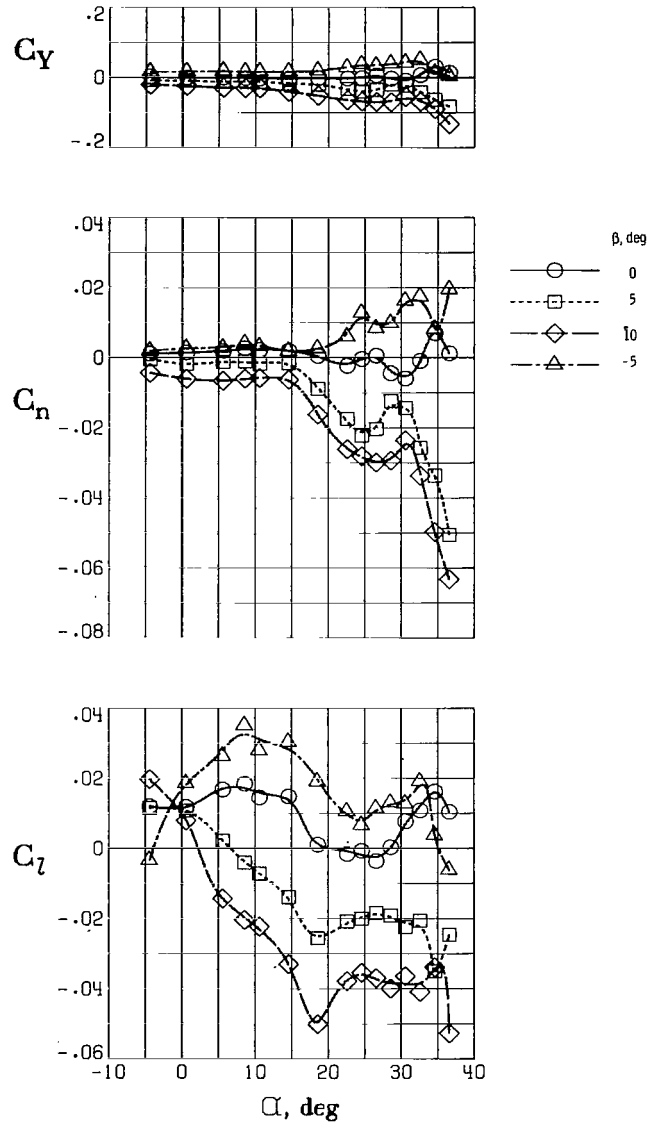

Figure 30.- Lateral-directional characteristics of configuration with basic strake. $\delta_{f,te} = 14^o/28^o$; tail removed; $\Lambda = 20^o$.

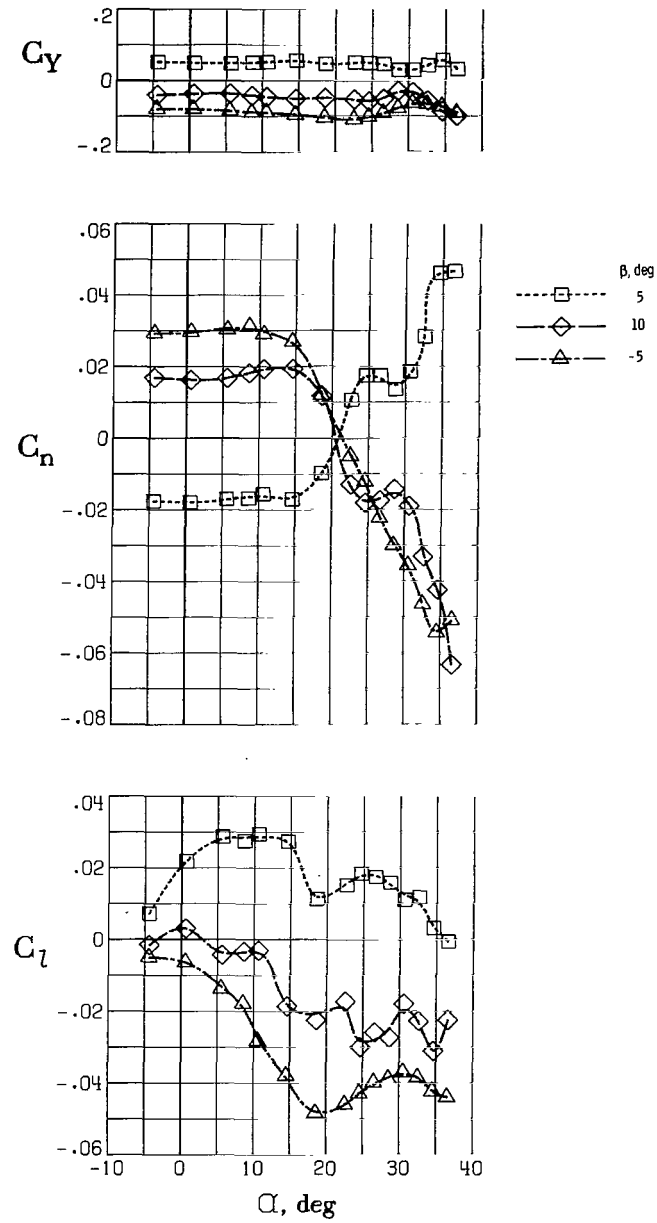

(a) $\Lambda = 20^\circ$.

Figure 31.- Lateral-directional characteristics of configuration with slatted strake. $\delta_{f,te} = 14^\circ/28^\circ$; T-tail; $i_t = 0^\circ$.

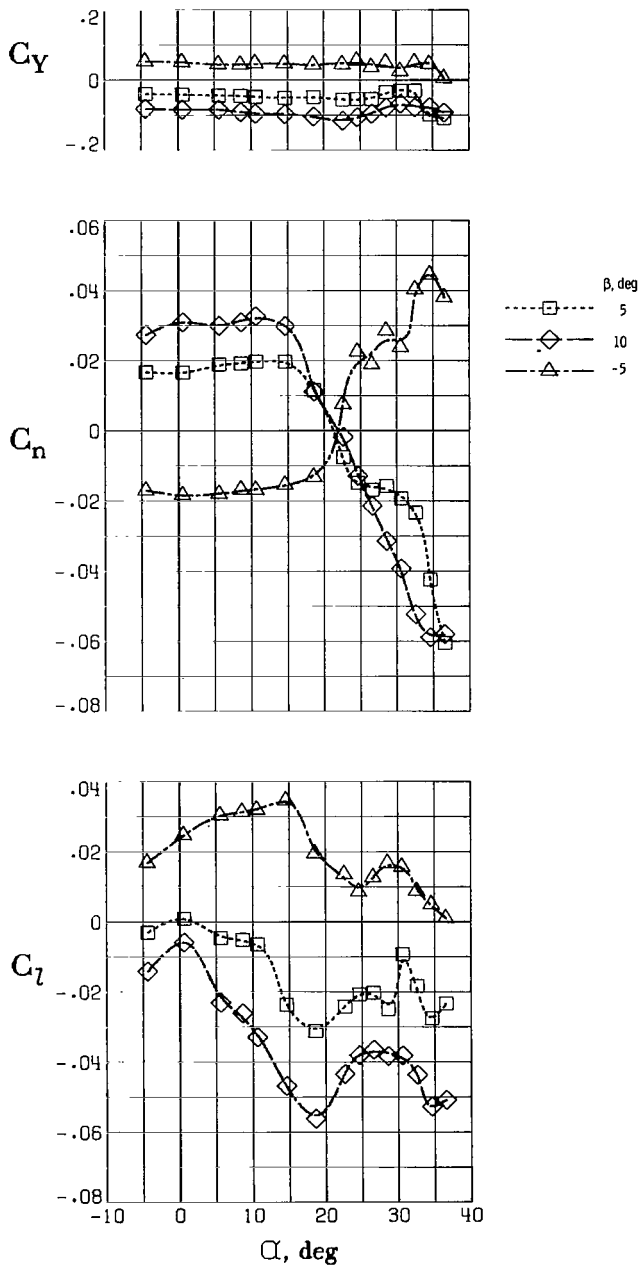

(b) $\Lambda = 30^{\circ}$.

Figure 31.- Concluded.

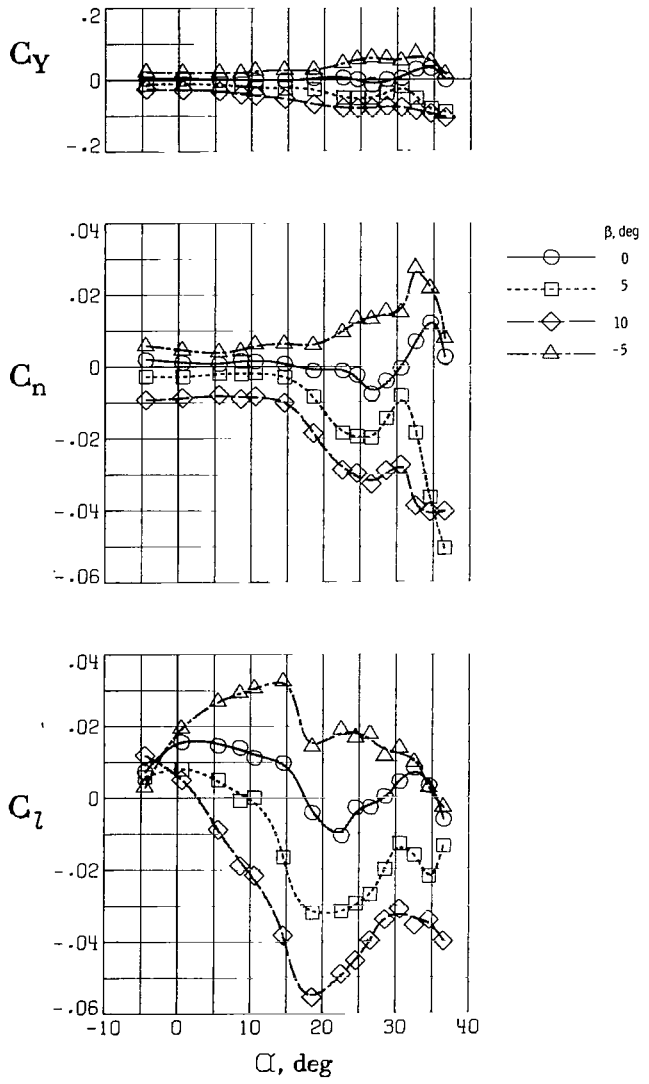

(a) Tail off.

Figure 32.- Lateral-directional characteristics for three tail arrangements, slatted strake, and $\delta_{f,te} = 14^o/28^o$. $\Lambda = 20^o$.

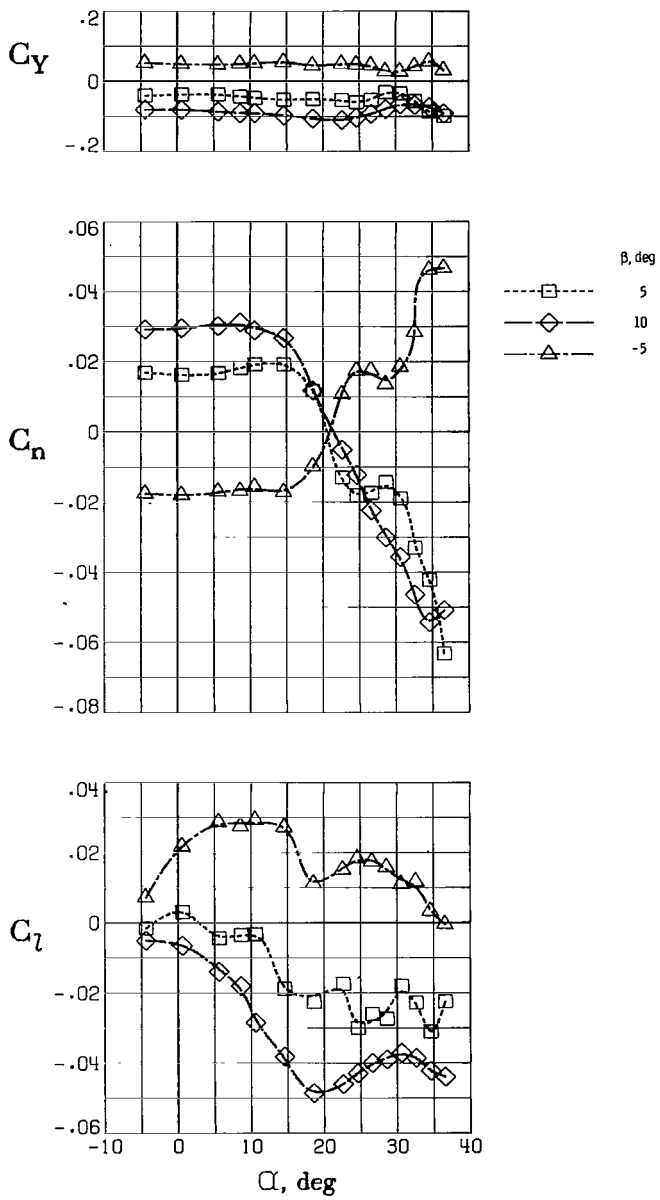

(b) T-tail.

Figure 32.- Continued.

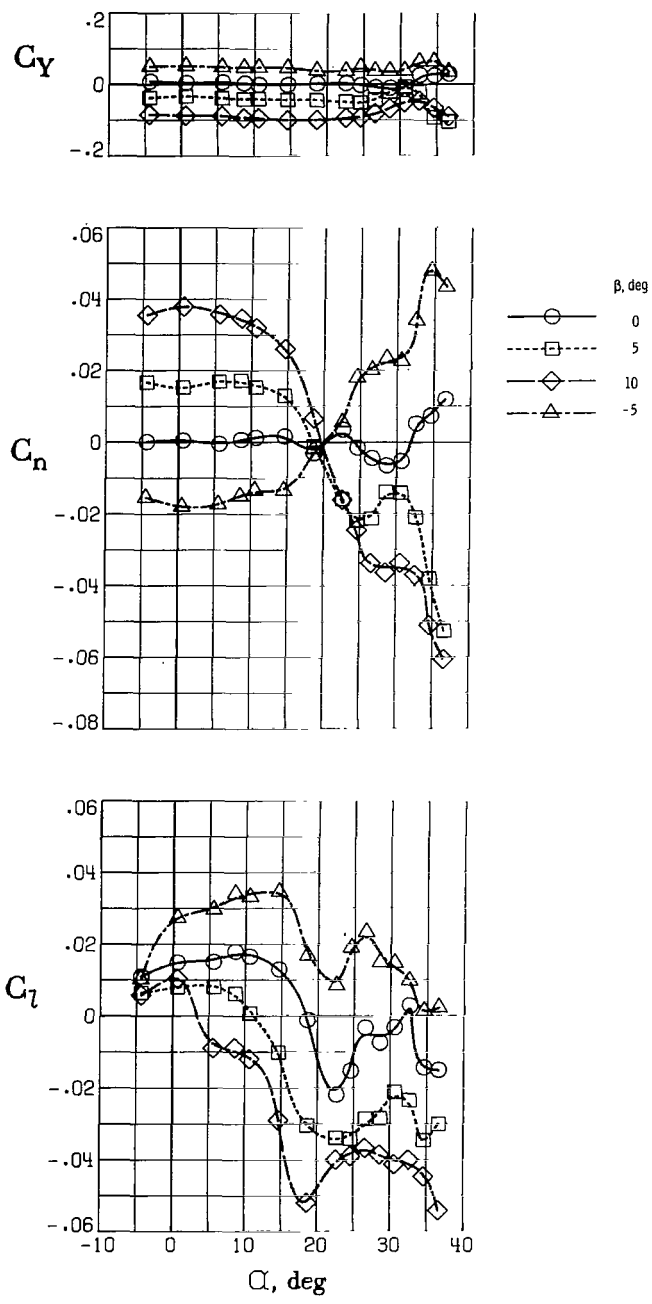

(c) Low-tail.

Figure 32.- Concluded.

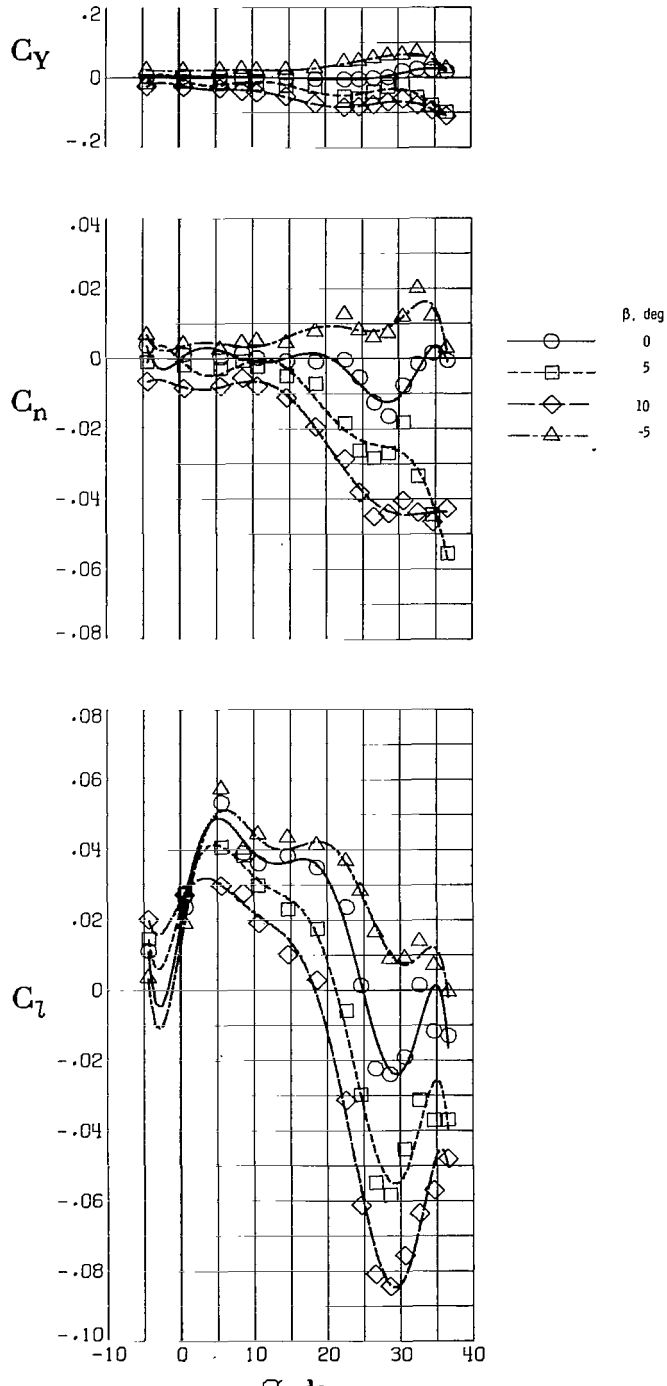

(a) Tail off.

Figure 33.- Lateral-directional characteristics for three tail arrangements, slatted strake, and $\delta_{f,te} = 30^o/50^o$. $\Lambda = 20^o$.

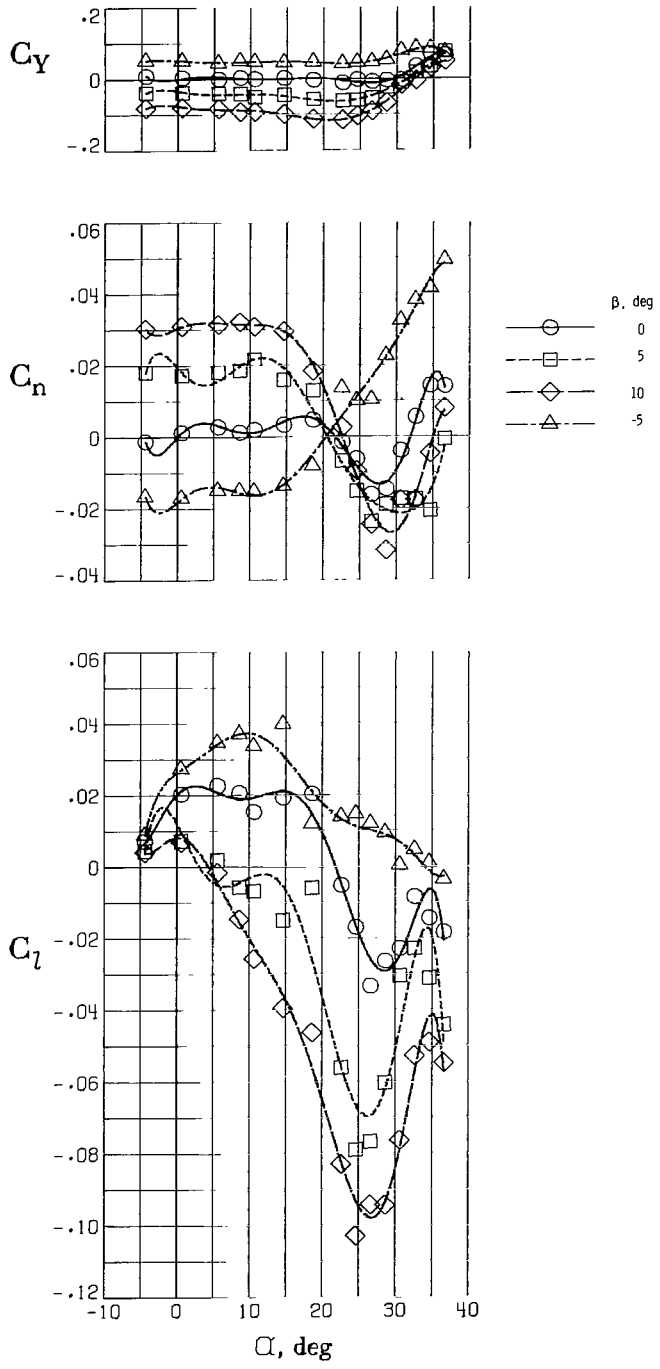

(b) T-tail.

Figure 33.- Continued.

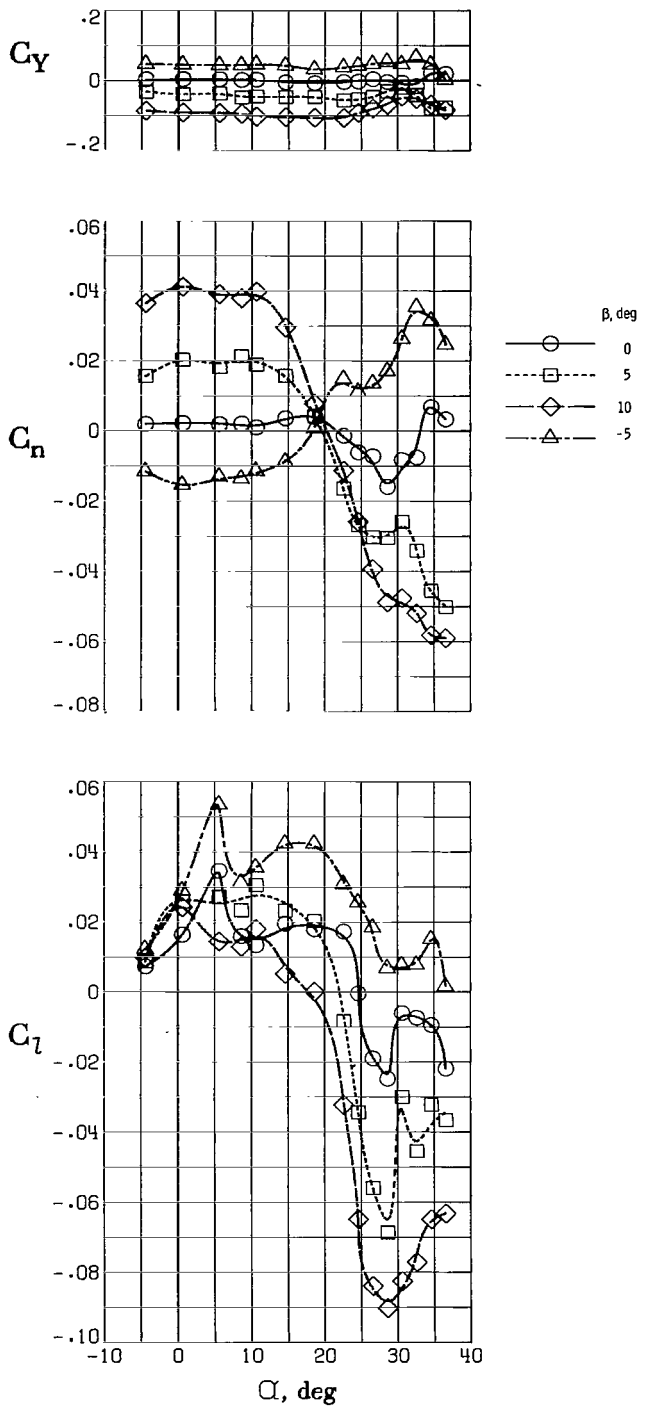

(c) Low-tail.

Figure 33.- Concluded.

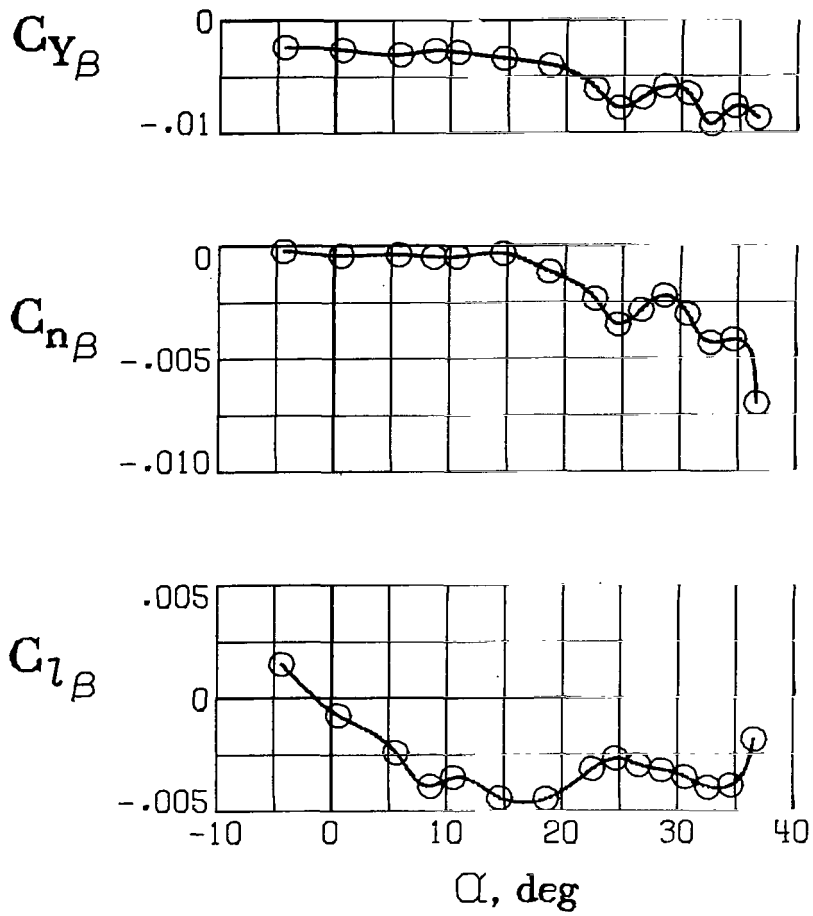

Figure 34.- Lateral-directional stability derivatives for configuration with basic strake and tail off. $\Lambda = 20^\circ$. $\delta_{f,te} = 14^\circ/28^\circ$.

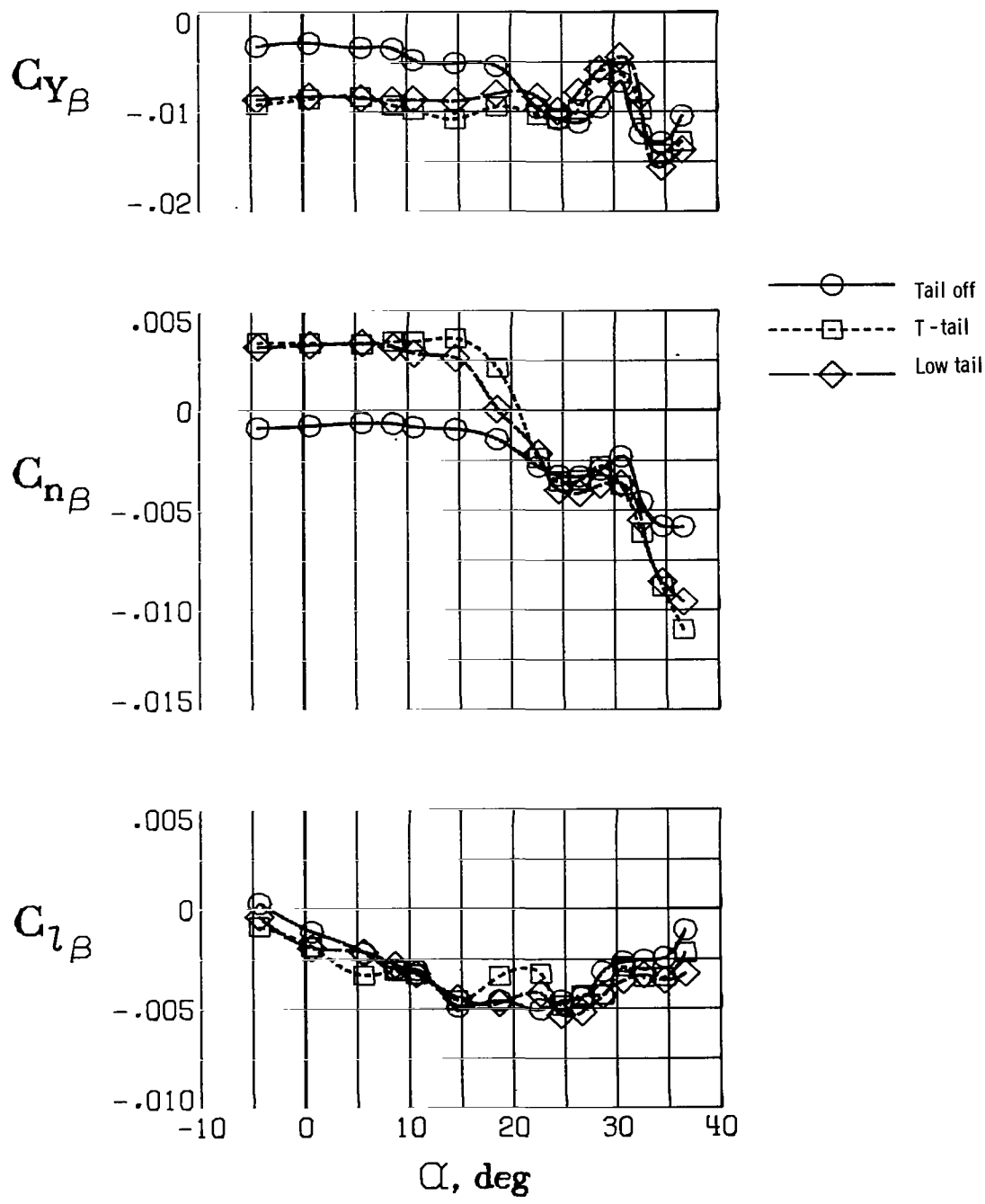

(a) $\delta_{f,te} = 14^o/28^o$.

Figure 35.- Lateral-directional stability derivatives of configuration with slatted strake. $\Lambda = 20^o$.

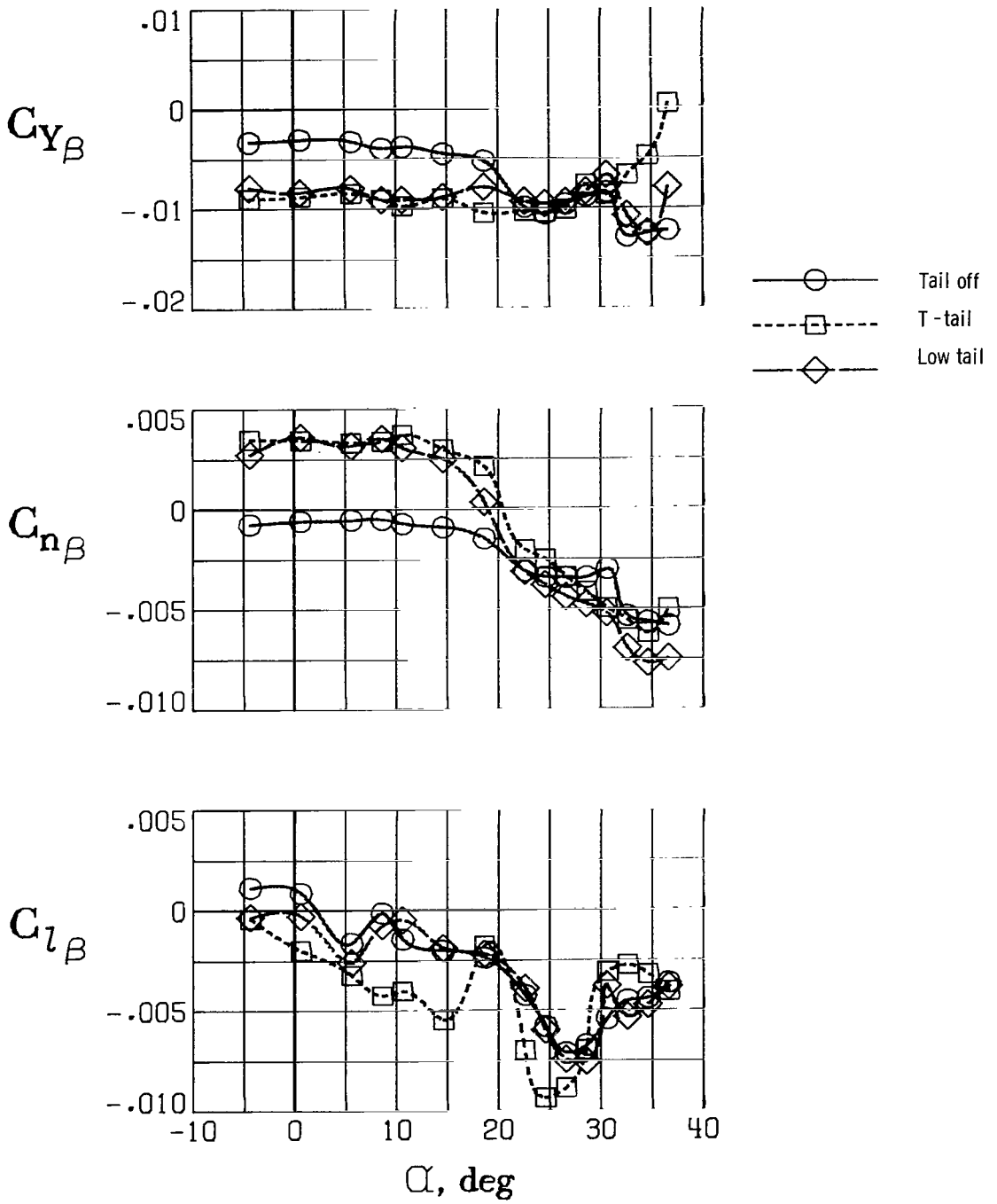

(b) $\delta_{f,te}$ = 30°/50°.

Figure 35.- Concluded.

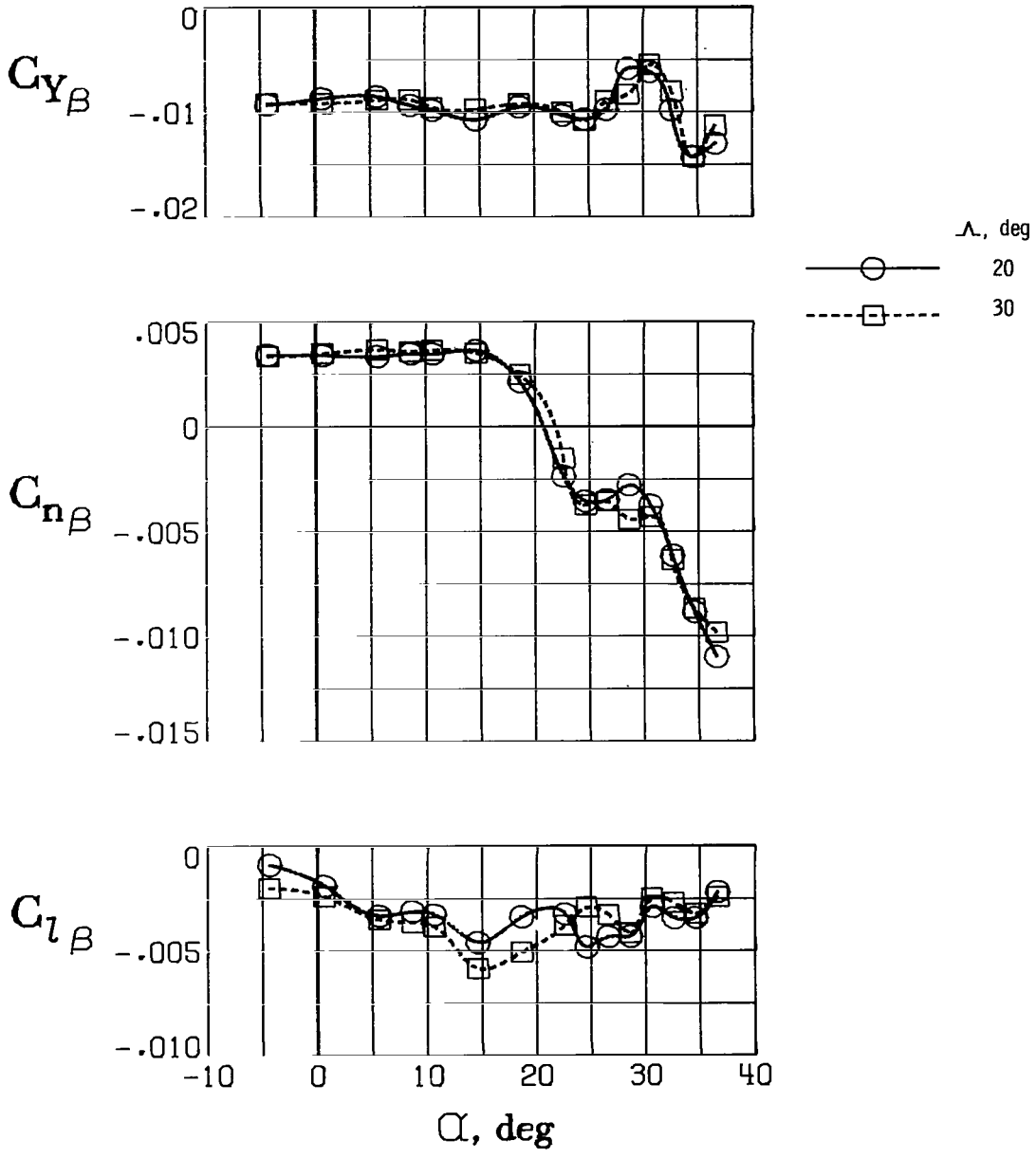

Figure 36.- Lateral-directional stability derivatives of configuration with slatted strake for two wing-sweep angles. $\delta_{f,te} = 14^o/28^o$.

"The aeronautical and space activities of the United States shall be conducted so as to contribute . . . to the expansion of human knowledge of phenomena in the atmosphere and space. The Administration shall provide for the widest practicable and appropriate dissemination of information concerning its activities and the results thereof."

—NATIONAL AERONAUTICS AND SPACE ACT OF 1958

NASA SCIENTIFIC AND TECHNICAL PUBLICATIONS

TECHNICAL REPORTS: Scientific and technical information considered important, complete, and a lasting contribution to existing knowledge.

TECHNICAL NOTES: Information less broad in scope but nevertheless of importance as a contribution to existing knowledge.

TECHNICAL MEMORANDUMS: Information receiving limited distribution because of preliminary data, security classification, or other reasons. Also includes conference proceedings with either limited or unlimited distribution.

CONTRACTOR REPORTS: Scientific and technical information generated under a NASA contract or grant and considered an important contribution to existing knowledge.

TECHNICAL TRANSLATIONS: Information published in a foreign language considered to merit NASA distribution in English.

SPECIAL PUBLICATIONS: Information derived from or of value to NASA activities. Publications include final reports of major projects, monographs, data compilations, handbooks, sourcebooks, and special bibliographies.

TECHNOLOGY UTILIZATION PUBLICATIONS: Information on technology used by NASA that may be of particular interest in commercial and other non-aerospace applications. Publications include Tech Briefs, Technology Utilization Reports and Technology Surveys.

Details on the availability of these publications may be obtained from:

SCIENTIFIC AND TECHNICAL INFORMATION OFFICE

NATIONAL AERONAUTICS AND SPACE ADMINISTRATION

Washington, D.C. 20546